AD-A043 341 MCDONNELL AIRCRAFT CO ST LOUIS MO F/G 17/5
FOVEAL LENS FEASIBILITY STUDY, 8 TO 14 MICRON SPECTRAL REGION.(U)
MAY 77 R W FISCHER, R D HELMICK, G LICIS N00014-76-C-0699
UNCLASSIFIED ONR-CR213-129-1-1F NL

OF
AD
A043 341

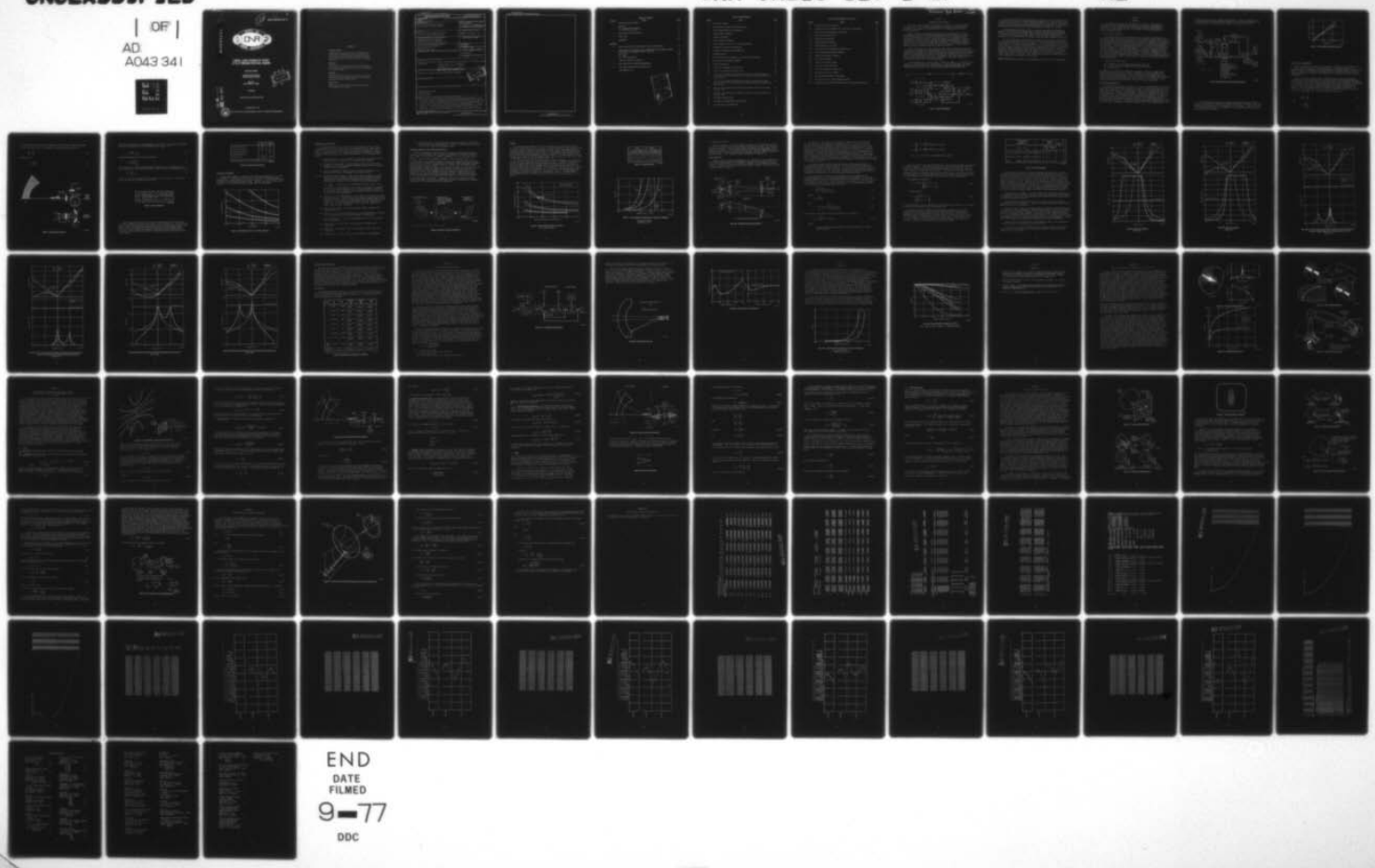

END
DATE FILMED
9-77
DDC

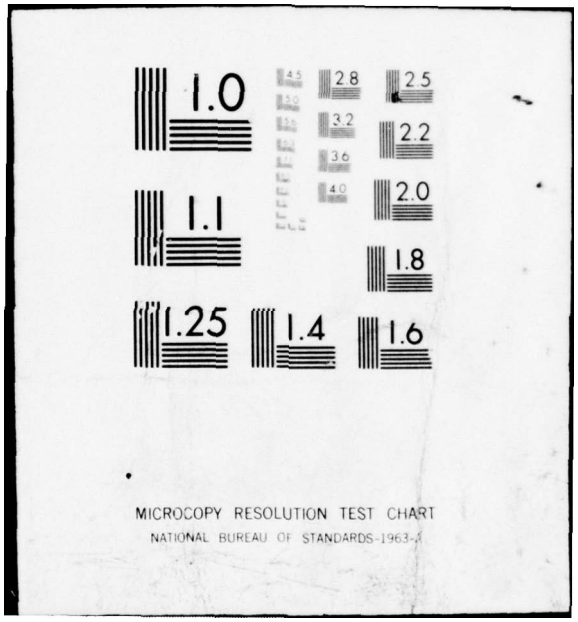
1.0
1.1
1.25
1.4
1.6
1.8
2.0
2.2
2.5
2.8
3.2
3.6
4.0
4.5
5.0
5.6
MICROCOPY RESOLUTION TEST CHART
NATIONAL BUREAU OF STANDARDS-1963-A

(12)

REPORT ONR-CR213-129-1-1F

FOVEAL LENS FEASIBILITY STUDY, 8 TO 14 MICRON SPECTRAL REGION

RALPH W. FISHER

McDonnell Aircraft Company
McDonnell Douglas Corporation

May 1977
Contract N00014-76-C-0699

Final Report

PREPARED FOR THE

OFFICE OF NAVAL RESEARCH ● 800 N. QUINCY ST. ● ARLINGTON ● VA ● 22217

NOTICES

Change of Address

Organizations receiving reports on the initial distribution list should confirm correct address. This list is located at the end of the report. Any change of address or distribution should be conveyed to the Office of Naval Research, Code 221, Arlington, Virginia 22217.

Disposition

When this report is no longer needed, it may be transmitted to other authorized organizations. Do not return it to the originator or the monitoring office.

Disclaimer

The findings in this report are not to be construed as an official Department of Defense or Military Department position unless so designated by other official documents.

Reproduction

UNCLASSIFIED

SECURITY CLASSIFICATION OF THIS PAGE (When Data Entered)

REPORT DOCUMENTATION PAGE		READ INSTRUCTIONS BEFORE COMPLETING FORM
1. REPORT NUMBER ONR-CR213-129-1-1F	2. GOVT ACCESSION NO.	3. RECIPIENT'S CATALOG NUMBER
4. TITLE (and Subtitle) FOVEAL LENS FEASIBILITY STUDY, 8 TO 14 MICRON SPECTRAL REGION		5. TYPE OF REPORT & PERIOD COVERED Final Report 1 June 76 - 31 March 1977 6. PERFORMING ORG. REPORT NUMBER
7. AUTHOR(s) Ralph W. Fisher, Roger D. Helmick, George Licis, Alfred Rosenfeld		8. CONTRACT OR GRANT NUMBER(s) N00014-76-C-0699
9. PERFORMING ORGANIZATION NAME AND ADDRESS McDonnell Aircraft Company McDonnell Douglas Corporation P.O. Box 516, St. Louis, MO 63166		10. PROGRAM ELEMENT, PROJECT, TASK AREA & WORK UNIT NUMBERS
11. CONTROLLING OFFICE NAME AND ADDRESS Office of Naval Research 800 N. Quincy St. Arlington, VA 22217		12. REPORT DATE May 1977 13. NUMBER OF PAGES 77
14. MONITORING AGENCY NAME & ADDRESS (if different from Controlling Office)		15. SECURITY CLASS. (of this report) Unclassified 15a. DECLASSIFICATION/DOWNGRADING SCHEDULE

16. DISTRIBUTION STATEMENT (of this Report)

Reproduction in whole or part is permitted for any purpose of the United States Government.

DISTRIBUTION STATEMENT A
Approved for public release;
Distribution Unlimited

17. DISTRIBUTION STATEMENT (of the abstract entered in Block 20, if different from Report)

Approved for public release; distribution unlimited.

18. SUPPLEMENTARY NOTES

403 111

19. KEY WORDS (Continue on reverse side if necessary and identify by block number)

Infrared Lens Design
Night Viewing
Optical Systems

20. ABSTRACT (Continue on reverse side if necessary and identify by block number)

This study proves feasibility and establishes preliminary design for a non-linear lens capable of imaging in the 8-14μ spectral region. When coupled to existing linear infrared scanners this lens can fully support human vision in both field of view (160°) and resolution (1 cycle/milliradian). This capability is achieved through optical distortion which causes focal length to vary by a ratio of 50/1 from an axis (2 inches) to 80° field angles (.04 inch). The lens has an F number of two and a clear aperture of eight inches in diameter.

DD FORM 1 JAN 73 1473 EDITION OF 1 NOV 65 IS OBSOLETE

UNCLASSIFIED

SECURITY CLASSIFICATION OF THIS PAGE (When Data Entered)

TABLE OF CONTENTS

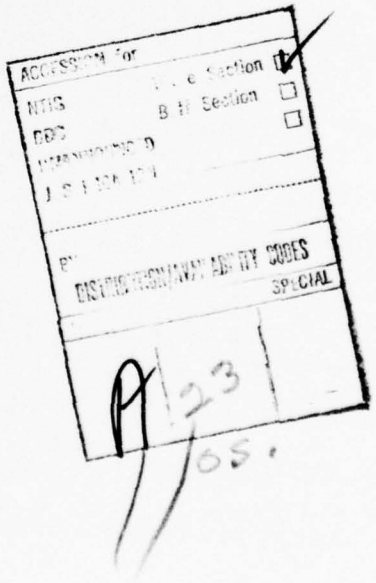

LIST OF ILLUSTRATIONS

LIST OF ILLUSTRATIONS (Continued)

Section 1

INTRODUCTION AND SUMMARY

This final report documents the results of Contract No. N00014-76-C-0699. The objective of this study was to determine the feasibility of constructing a nonlinear lens capable of operating in the 8 to 14 micron region of the infrared spectrum.

Under a previous ONR contract[1] MCAIR proved the feasibility of a unique nonlinear lens which had substantial bandwidth reduction capability for use in remote viewing systems. This lens takes advantage of the "variable acuity" characteristic of human vision to reduce the amount of information that must be transmitted in a wide field-of-view high resolution imaging system. A brief description of this concept is presented in Appendix A. A laboratory brassboard of this system was constructed under contract to the Office of Naval Research (ONR), (2) and is presently under final testing at MCAIR.[2]

The system developed for ONR operates in the visual wavelength spectrum and consequently is useable only during daylight hours. The goal of this effort was to determine the feasibility of achieving the same wide field-of-view, high resolution capability during night-time hours by operating the sensing lens in the 8 to 14 micron infrared wavelength spectrum. If successful, this sensor system could fully support human vision under clear night conditions; a capability impossible to achieve with conventional FLIR imaging systems.

A flow diagram of the overall effort is shown in Figure 1. It consists of two phases, an analysis phase and a design phase. In the analysis phase the optimum parameters and constraints are determined that establish requirements for the actual lens design effort which will be accomplished in the design phase.

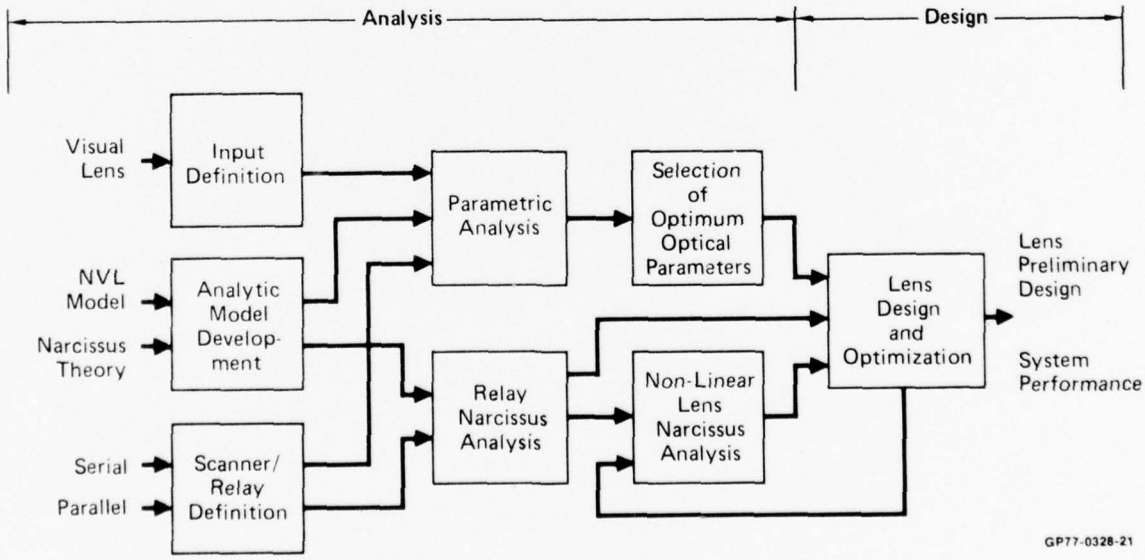

Figure 1. Work Flow Diagram

A computer controlled optimization analysis indicated that the lens should be designed as an F/2.0 with an optical quality represented by a point spread function in the focal plane which has a one sigma width (radius) of 16 microns. This lens produced the best performance within established size constraints. In addition, best performance was achieved when the lens was coupled to a serial type scanner.

A narcissus analysis shown in Figure 1 was also performed to establish any possible constraints on lens design due to internal optical surface reflections. The results of this effort indicated that the worst narcissus returns were eight times below the detector noise level (NEP). It is therefore concluded that narcissus is not a problem with the infrared nonlinear lens configuration selected.

The lens design phase indicated that realization of a practical configuration for the infrared nonlinear lens is feasible. The preliminary design has an 8 inch clear aperture and consists of only 4 elements. It is very similar in size to the visual lens [1]. The optical performance of this lens exceeds the F/2.0, 16 micron blur requirements because an F/2.0 lens with a maximum blur sigma of 12 microns was achieved. System performance predictions show that it is possible to achieve Minimum Resoluable Temperature (MRT) performance of better than 0.05° and spatial resolution as high as 0.95 cycles/mr (1.8 minutes of arc) which is adequate to support human dynamic resolution. All element surfaces have reasonable curvatures and no problems are anticipated in fabrication.

---

*Number in parenthesis refers to the corresponding item in the List of References.

Section 2

ANALYSIS

The analysis is divided into two parts; the parametric analysis which develops the Size/Performance data necessary for tradeoffs, optimization, and selection of design parameters; and the narcissus analysis which develops constraints for the optical design. These efforts are discussed separately in the following sections.

2.1 OPTIMIZATION ANALYSIS

The overall objectives of this effort are to establish the parameters for an infrared foveal lens design for the 8-14 micron spectral region. Since specific mission requirements and/or state-of-the-art in infrared variable acuity technology is not defined at this time, the approach selected was a computerized optimization. This allowed interactive variation of key parameters while size and performance were assessed. An optimum size/performance balance was achieved and a preliminary lens was designed for these optimum parameters. A flow diagram of this approach is shown in Figure 2. The design philosophy is as follows: Experience from our visual lens work showed that the lens size linear dimensions increase inversely with both optical quality (blur) and F/number. Conversely, performance as measured by Minimum Resolvable Temperature (MRT) improves directly with these two parameters. The approach shown on Figure 2 was developed to determine the best performance but with reasonable size.

Inputs for the study were -

(a) Parameters from our existing visual spectrum lens
(b) Current technology scanner and detector parameters
(c) System inputs

In general, these inputs fall within two categories, those that remain fixed throughout the study and those tradeoff parameters that will be tested over a range of values to determine the effect of each value on performance and size. The latter are F/number and blur. A state-of-the-art serial scanner and a parallel scanner were also evaluated separately in the analysis. The function of these inputs are described below along with rationale' for their selection.

LENS OPTICAL PARAMETERS

Starting at the upper left of Figure 2, the optical requirements of distortion, field-of-view and fabrication constraints are used to define focal length L(0) and image size requirements of the foveal lens. Basis for the selection of the value of these inputs is as follows: (1) The amount of distortion used was made equal to the existing lens. This function provides a good match to human visual acuity and is believed to be near the maximum distortion technically possible. In addition, any sensing system constructed with this function will be compatible with the display systems constructed on related contracts. (2) A field-of-view goal of 160° was utilized for the study. This value was selected because no significant reduction in either size or bandwidth is achieved for smaller 90° - 100° field-of-view. In

addition, this FOV does not impose any difficulty in design. Fabrication of our existing visual spectrum lens has shown that the rear element spherics are extremely difficult to produce if the diameter is less than 0.75 inch.

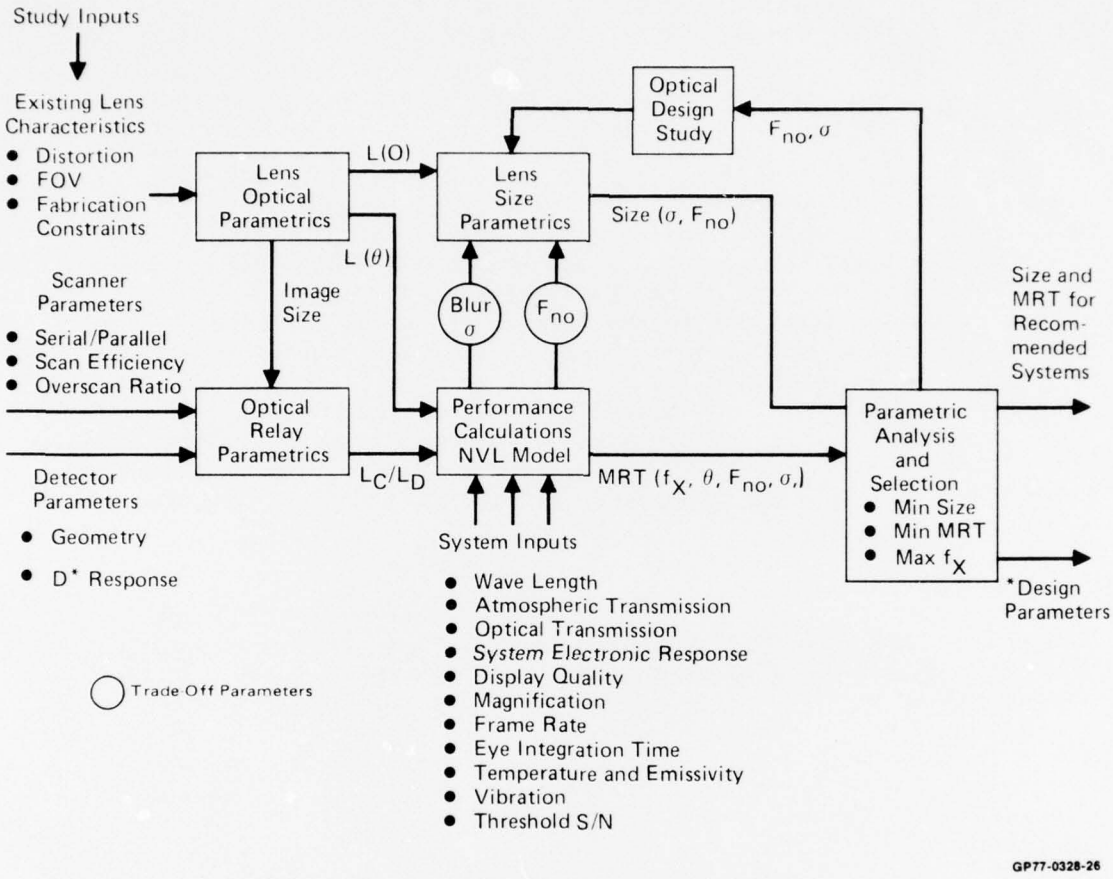

Figure 2. Optimization Analysis Technical Approach

The relationships established by these parameters are shown in Figure 3. These curves were used to select an on-axis focal length of 2 inches. This then established an image size of 0.72 inches for 160° coverage. A curve for a 100° FOV is also shown on Figure 3 to emphasize the point made above that little is gained through FOV reduction.

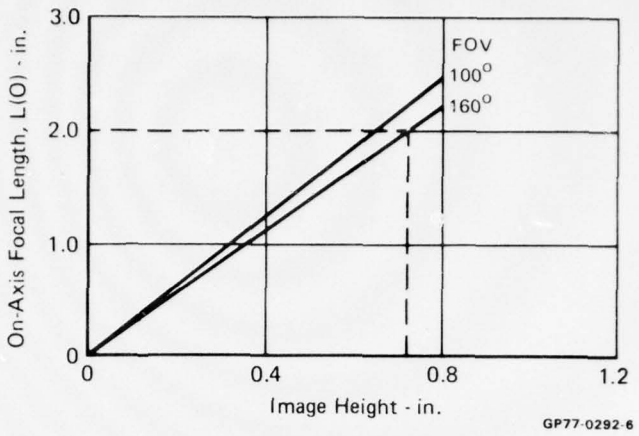

Figure 3. Focal Length/Image Size Parametrics

OPTICAL RELAY PARAMETERS

When the image size is known, it is possible to define the optical relay that is used to couple the image to the detector plane. The optical relay must be defined because it establishes how the nonlinear lens F/number appears to the detector which is required for sensitivity calculations, and to establish how the detector dimensions translate to the NLL focal plane which is required for spatial frequency calculations.

Review of available manufacturer's literature on the serial and parallel scanners, makes it apparent that the serial type places the most severe constraints on NLL design. This configuration is shown in Figure 4. The constraint is imposed by the high speed scan drum. This necessitates a stationary exit pupil at the scanner facet location. The optical equivalent of this type scanner is also shown in Figure 4. The relationships needed for analysis are computed as follows. The collimator focal length (L_C) must be sufficient to make the scan cover the image which has a half-height (H). Then the angular coverage (θ_s) is

$$\tan \frac{\theta_s}{2} = \frac{H}{L_C} \tag{1}$$

Then

$$L_C = \frac{H}{\tan \frac{\theta_s}{2}} \tag{2}$$

The detector focal length (L_D) is chosen to give the correct resolution element size at the detector (a_y) of an element in the image plane of size (Δh),

$$\frac{\Delta h}{L_C} = \frac{a_y}{L_D} \tag{3}$$

Solving for L_D

$$L_D = \frac{a_y L_C}{\Delta h} \tag{4}$$

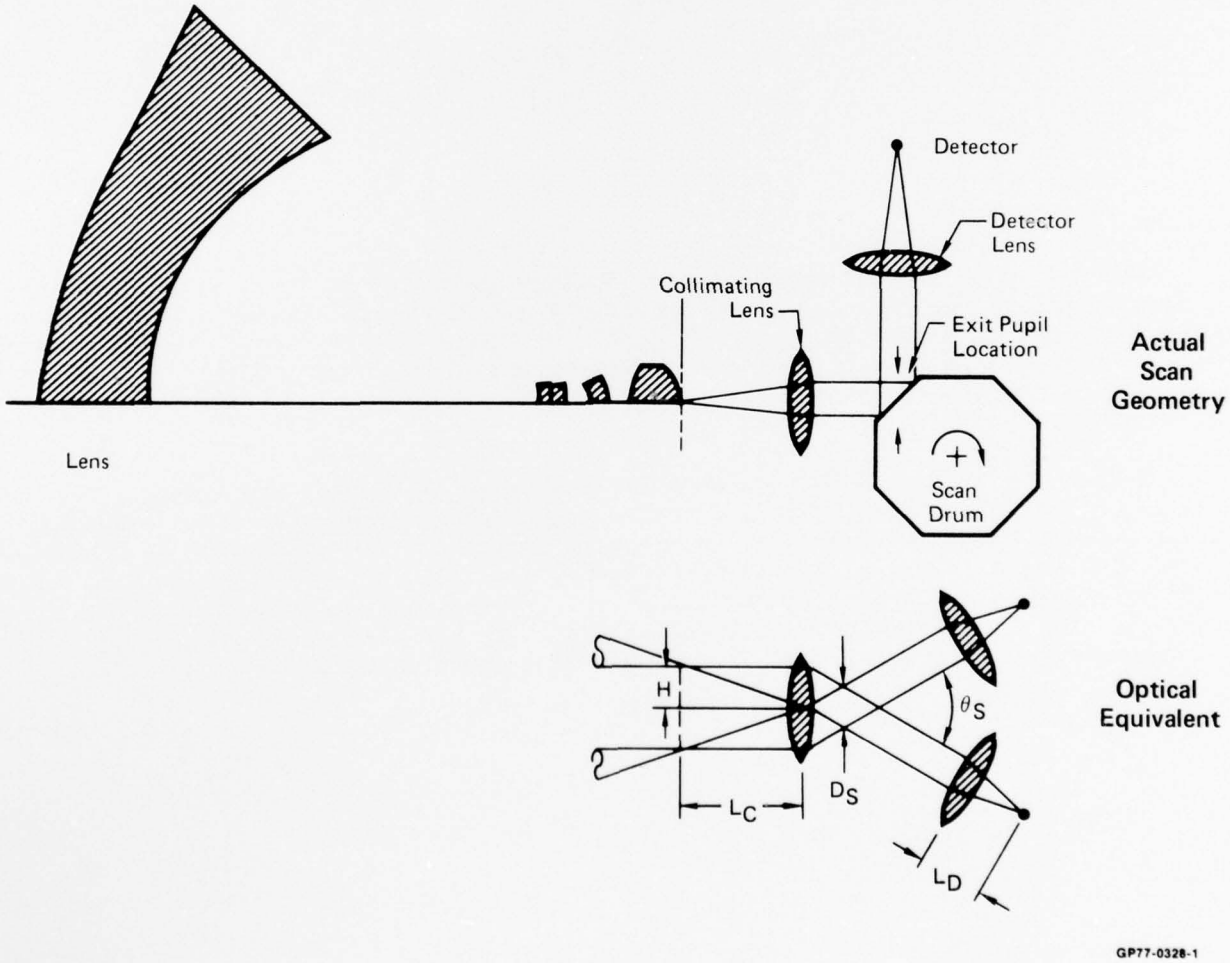

Figure 4. Optical Relay Parameters

The detector subtense (Δh) is determined by the number of scan lines (N) required across the image and the vertical overscan ratio (η_{ovsc}), i.e.

$$\Delta h = \frac{2H}{N} \eta_{ovsc} \tag{5}$$

Substituting Equation (5) into (4) results in

$$L_D = \frac{a_y N L_C}{2 H \eta_{ovsc}} \tag{6}$$

For the serial and parallel scanners under consideration the parameters are as shown in Figure 5. The effective F/number (F#) is related to lens F/number (F_{NO}) by

$$F\# = \frac{L_D}{L_C} F_{NO} \tag{7}$$

This is the effective F/number that is supplying optical energy to the detector. It will be used for performance calculations.

Type	a_x (in.)	a_y (in.)	N	η_{ovsc}	L_C (in.)	L_D (in.)
Serial	0.0013	0.0015	488	1.5	1.29	1.0
Parallel	0.002	0.002	360	1.0	2.46	2.67

GP77-0328-24

Figure 5. Scanner Parameters

Other parameters related to the scanner and detectors are scan efficiency, the detector geometry and detectivity and are listed in Figure 6. The detectivity values include improvements due to effective cold shielding. Manufacturer's actual data was used to estimate the improvement instead of the theoretical values. Detector equivalent electronic response BW was determined from manufacturer's literature. This parameter was found to be significant only in the case of the serial scanner.

	Serial	Parallel
Vertical Scan Efficiency	93%	N/A
Horizontal Scan Efficiency	82.7%	75%
Number Parallel Detectors	1	180
Number Serial Detectors	9	1
Detectivity - D*	5×10^{10}	5×10^{10}
Detector Equivalent Electronic Response BW	13 (10^6)	N/A

GP77-0328-25

Figure 6. Other Scanner Parameters

LENS SIZE PARAMETRICS

During initial phases of the study, the lens size parametrics, i.e., size as a function of F/number and optical blur of the existing visual spectrum lens was used. These parametrics are shown in Figure 7. As actual lens design progressed, these parametrics were updated. However, this was not found to be necessary. All optimized designs fit these data very accurately.

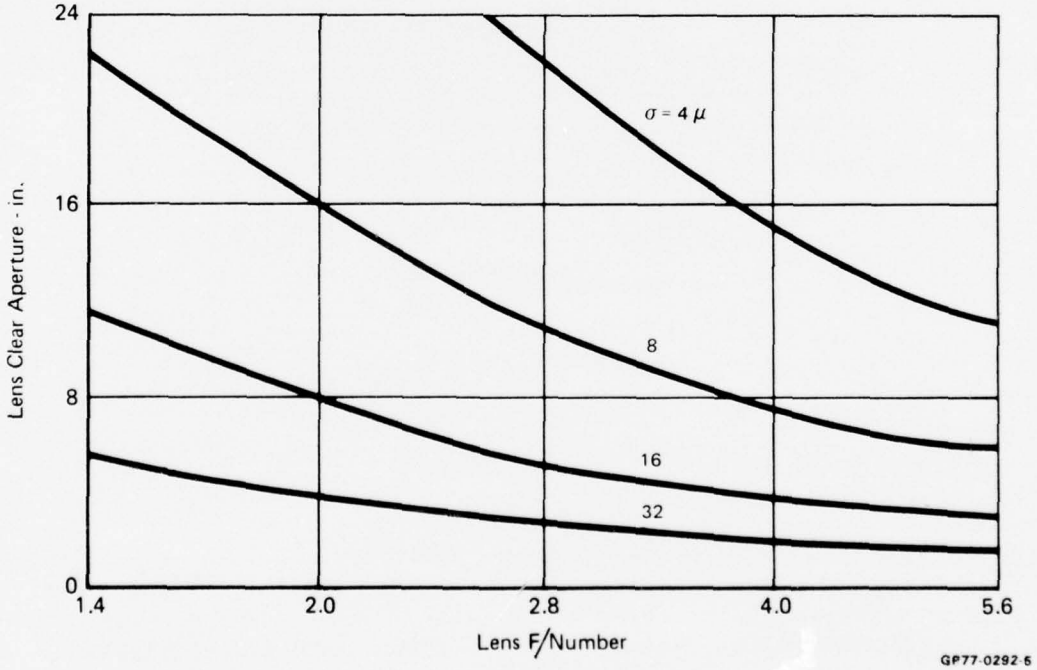

Figure 7. Size Parametrics for a 2-In. Focal Length Lens

PERFORMANCE CALCULATIONS

System performance in terms of MRT was computed using the Night Vision Laboratory (NVL) FLIR model which was suitably modified for the remote viewing system. This model and its modification is described in Appendix B. Other than our tradeoff parameters of F/number and blur and the detector and scanner parameters discussed above, this model required input of the parameters listed below:

(a) Wavelength Range - 8.5 to 13 microns. This range was selected for its good atmospheric transmission over reasonable path lengths.

(b) Atmospheric transmission - Original plans were to use 0.5 but were changed to 1.0 to reflect system performance rather than the extremely variable mission performance.

(c) Optical transmission - Based on state-of-the-art techniques a 0.5% reflectance for each of 10 elements (two surfaces each).

(d) (e) System electronic response - Since the NVL model includes no internal noise sources other than the detector, electrical response was made insignificant for all systems by assuming flat response out to the highest spatial frequency (f_x) of interest which was determined by

$f_x > \frac{1}{2I_{FOV}}$ where I_{FOV} is the instantaneous field of view. This assumption is entirely adequate for the NVL model because (1) response is limited by detector geometry and (2) noise bandwidth is limited by human observer factors such as eye integration time and the matched filter function (see Appendix B).

(f) Display blur - The characteristics of the direct view display were used for this parameter. This unit has a blur sigma in angular terms of 0.26 minutes arc. This is about 10 times better than the anticipated system resolution. When utilizing the NVL model it was most convenient to convert this to linear spatial blur at the same focal length as the foveal lens which is 3.9 microns.

(g) Display magnification - The remote viewing concept inherently has unity magnification.

(h) Frame rate - A TV compatible frame rate of 30 frames/second is utilized for all analyses with two fields per frame (2/1 interlace).

(i) Eye integration time - the NVL recommended value of 0.2 sec was used for this parameter.

(j) Temperature - The usual 300°K value was used for nominal scene temperature.

(k) Emissivity - An emissivity of 0.8 is utilized for both target and background.

(l) Threshold S/N - The NVL value of 2.25 was used for this parameter.

(m) Vibration sigma - The vibration sigma selected represents the residual sensor motion after stabilization. A value of 1μ was used and this does not cause any significant performance loss.

PARAMETRIC ANALYSIS AND SELECTION RATIONALE'

Using the parameters defined above, the analysis and selection proceeds as follows. For each scanner type the tradeoff parameters are iterated throughout their ranges. For each set of tradeoff parameters, MRT vs f_x and lens size are printed. Selection then proceeds as follows. First a specific value of f_x is chosen which is the spatial frequency at which the optimization will be made. Then the data is screened to determine the remaining tradeoff parameters (F/number and blur) that yield the smallest system for a range of MRT performance levels. This procedure is shown in Figure 8. The spatial frequency is then varied and the entire process is repeated. These data were used to locate the point where a reduction of MRT is not warranted by the corresponding increase in size. The knee points of the curves represent the best selection. Beyond these points excessive size results with little improvement in MRT. Finally the MRT curves for the selcted systems (one optimum for each design f_x) are plotted as shown on the lower right of Figure 8. A subjective choice is then made as to which is most acceptable from a mission performance and vehicle installation standpoint. The results of the analysis will now be presented.

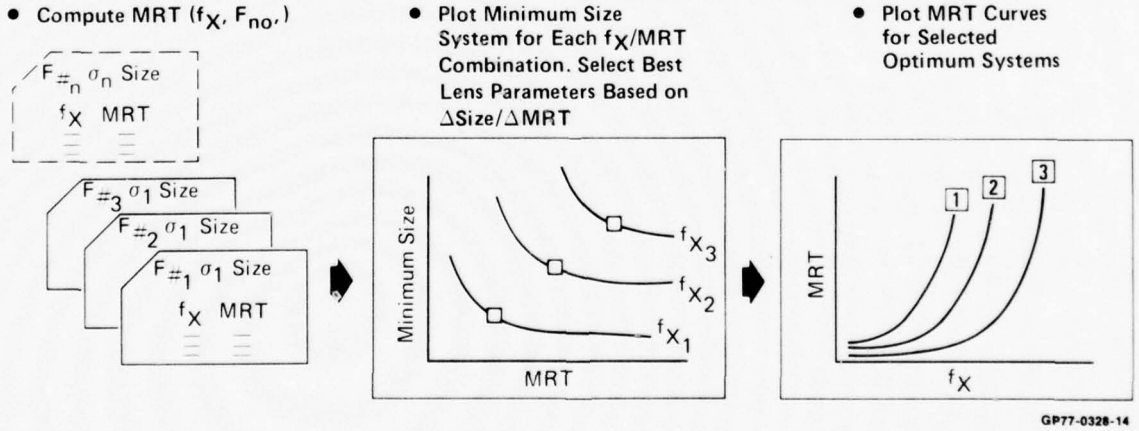

*This step not necessary for current scanners where N is specified.

Figure 8. Parametric Analysis and Selection

RESULTS

Size/Performance parametrics of the IR nonlinear lens are shown on Figure 9 for spatial frequencies of 0.3, 0.5, and 0.7 cycles/milliradian. The optimum systems for each of these frequencies are designated on the curves. Parameters of these "optimum" systems are listed in Figure 10. The first observation from these curves is the advantage of using the serial scanner. Performance is significantly better and the size is smaller regardless of spatial frequency. For this reason the serial scanner was selected for the lens design phase. The performance of the three systems coupled with a serial scanner is shown in Figure 11.

It should be noted that the next increase of spatial frequency to 1.0 cycles/mr results in a very large size lens, 60 inches or larger. This leads to selection of the 0.7 cycles/mr system with a serial scanner as the best choice. Its size is about the largest that can be accommodated in the manned vehicle application that is under consideration for the system. Also the spatial frequency (0.7 c/mr) is very compatible with human visual performance. To illustrate this human dynamic visual resolution is also shown on Figure 11. Note that only the 0.7 cycle/mr system has performance sufficient to support this requirement. Based on the observations, lens parameters of F/2.0 and 16 micron blur were chosen for the design phase of the study.

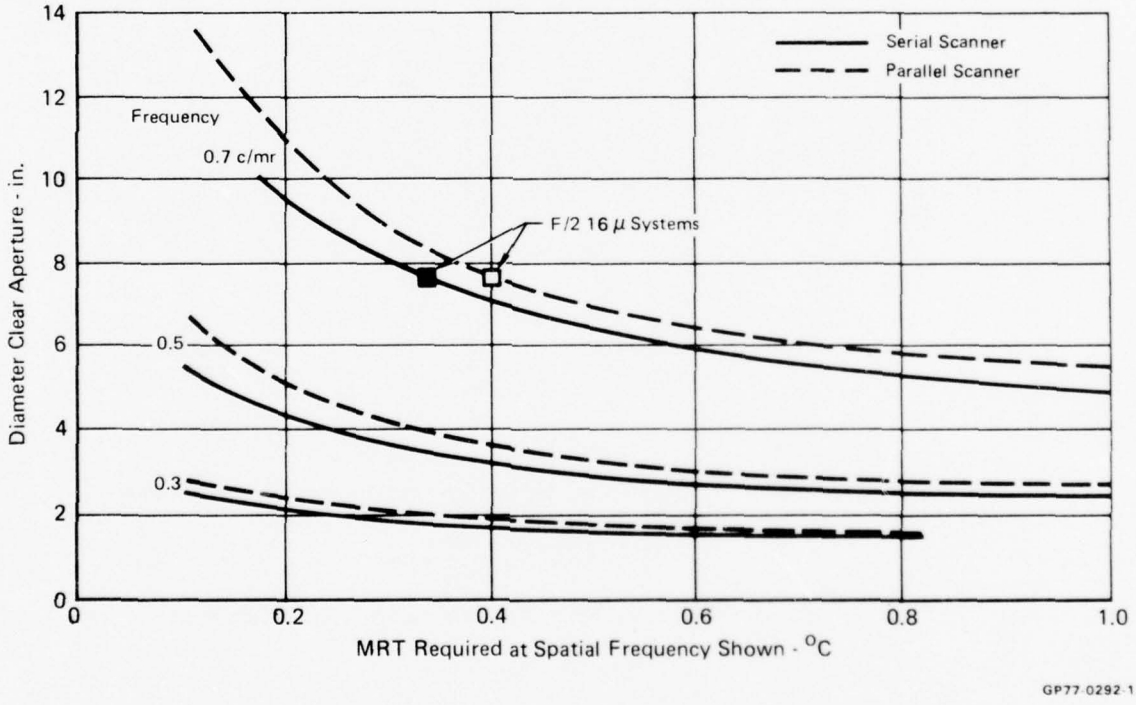

Figure 9. Scanner Size/Performance Parametrics
8-14 μ Spectral Region

	Serial				Parallel			
f_x	F_{NO}	Blur (μ)	MRT (^oC)	Size (in.)	F_{NO}	Blur (μ)	MRT (^oC)	Size (in.)
0.3	2.8	30	0.1	2.8	2.8	30	0.2	2.9
0.5	2.8	22	0.3	4.2	2	26	0.4	5.0
0.7	2.0	16	0.37	7.7	1.4	20	0.54	8.8

GP77-0328-22

Figure 10. Optimum Systems

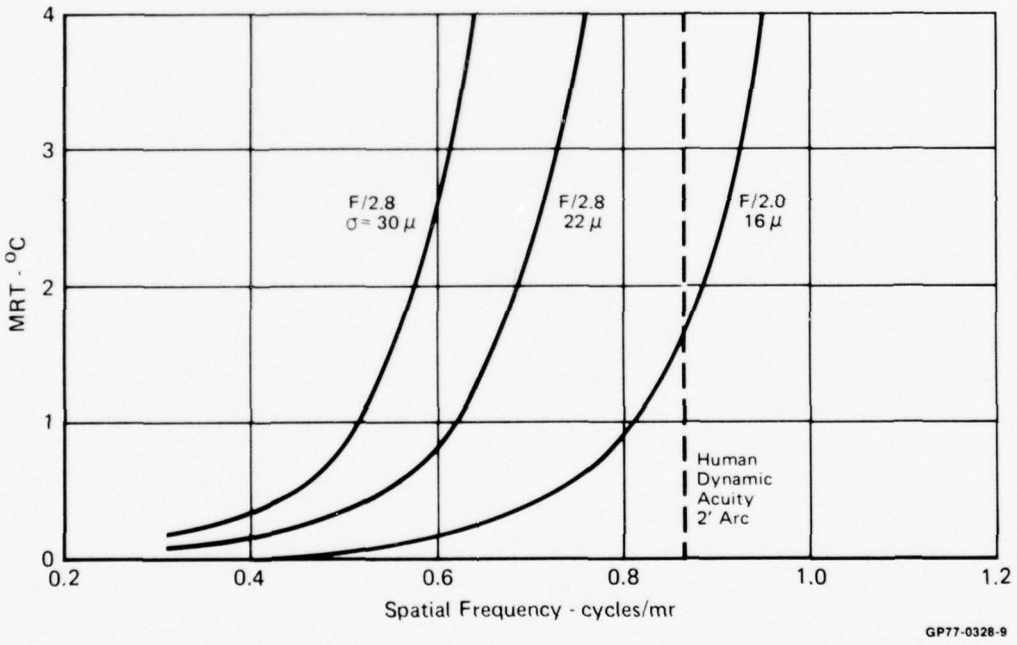

Figure 11. Serial Detector Performance as a Function of Resolution

8-14μ Spectral Region
488 Eff Scan Lines

2.2 NARCISSUS ANALYSIS

Before proceeding to the design phase a discussion of narcissus is in order. Two types of narcissus analysis were conducted during this effort. The first was conducted to devise the most efficient method of relaying the lens image to the detector focal plane. In the second effort, actual narcissus images were located and their effect on system operation was predicted. Details of these analyses are presented below. Basic narcissus theory is presented in Appendix C.

RELAY NARCISSUS

Concern with the possible requirement for a field lens at the nonlinear lens focal plane necessitated an early parametric analysis of the optical relay with respect to narcissus effects. Narcissus is caused by the cold detector "seeing" itself as a result of reflections from relay optical surfaces. This relay is shown in general form in Figure 12.

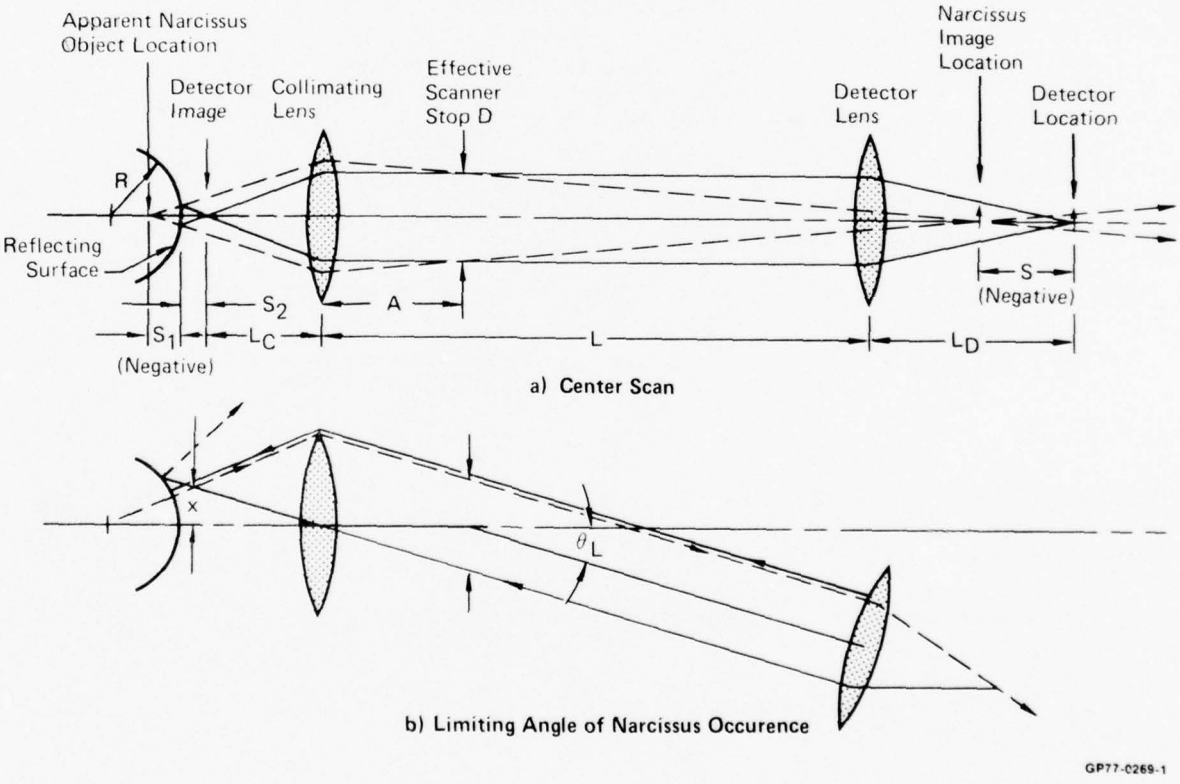

Figure 12. RVS Relay and Narcissus Geometry

The function of this relay is to reimage the lens image of the real world onto the detector. This would be an easy optical task if it were not for the scanning mechanism which essentially translates the real world image across the detector. The scanning mechanism requires that all ray bundles cross at a common plane shown as the Effective Scanner Stop of diameter D on Figure 12. A problem arises because the optical output of the nonlinear lens is not compatible with this requirement. The chief rays emerging from the image plane are not "well behaved" as they are in a conventional lens and therefore will not arrive at a common plane after collimation. This necessitates use of an aspheric field lens at the image plane. While field lenses create no special problem in visual systems, they can cause very serious "narcissus" problems in the infrared spectrum. The geometry of narcissus is also shown in Figure 12.

It is easy to see how optical surfaces near any image plane generate the worst possible narcissus effects because they reflect and return the image back through the system with maximum efficiency. The field lens is in an ideal location to create this proble. For this reason the Narcissus theory developed in Appendix C was applied to this relay. For this study, a reflecting surface was theorized with curvature (R) and separation (S_2) from the nominal image location.

Narcissus theory requires that the location, size and strength of the narcissus image be known. This requires definition of the distance (S) from the narcissus image to the image plane, magnification of the image (M), and reflectance (τ) of the reflecting surface, as shown in Figure 12. The first two can be determined from geometric optical theory. Using the definition of distances shown on Figure 12, the distance (S) and magnification (M) are:

$$S = \frac{L_D^2 \, (S_2 - S_1)}{L_C^2 + (S_2 - S_1)(L - L_C - L_D)} \tag{8}$$

where

$$S_2 = \frac{RS_1}{2S_1 + R} \tag{9}$$

and

$$M = - \frac{L_C^2 \, S_2}{S_1 \, [L_C^2 + (S_2 - S_1)(L - L_C - L_D)]} \tag{10}$$

The narcissus image power on an on-axis detector of area (A_d) is:

$$P_D = \frac{4 \, \tau \, A_d \, x \, y}{S^2} \quad \text{in watts} \tag{11}$$

where

τ = Surface reflectance determined from optical material and coating characteristics

$$x = \left(\frac{DS}{2L_D}\right. \text{ or } M\,\frac{a_{cax}}{2} \text{ whichever is smaller}$$

$$y = \left(\frac{DS}{2L_D}\right. \text{ or } M\,\frac{a_{cay}}{2} \text{ whichever is smaller}$$

$a_{cax,\ cay}$ = Effective cold assembly width, height

This is the worst case value which will occur at the center display scan position as shown in Figure 12. For other scan positions, narcissus returns are much more difficult to compute. However, the maximum scan angle beyond which the narcissus return vanishes is relatively easy to predict. This occurs at the angle (θ_L) shown in Figure 12 where the marginal ray from the detector strikes the curved reflecting surface normally. At this scan angle only this ray returns. At greater scan angles the reflection does not pass through the stop and thus no narcussus exists.

This maximum scan angle is

$$\theta_L = \arctan \frac{D}{2\left[\frac{L_c^2}{S_1 + R} + L_c - A\right]} \tag{12}$$

or image position

$$x = \frac{L_c\, D}{2\left[\frac{L_c^2}{S_1 + R} + L_c - A\right]} \tag{13}$$

If the image position (x) is divided by the format width, the portion of the display occupied by the narcissus image can be established.

The above theory was applied to both scanners postulated in this study. Characteristics of these scanners and their required relay components were computed to match the detector plane to the lens focal plane. The additional parameters that are required for narcissus calculations are also listed in Figure 13. See Appendix C for definition of these terms. The probable serial scanner includes a reflective detector surround to reduce narcissus. This narcissus reduction technique is also employed in the parallel scanner.

Scanner Type	Effective Cold Assembly Dimensions - cm		A_D - cm^2	NEP - watts	Lens Focal Length - in.		Separation (in.) (L)	A
	a_{cax}	a_{cay}			Collimating (L_C)	Detector (L_D)		
Worst Case Serial	0.3513	0.234	12.5×10^{-6}	8.05×10^{-11}	1.291	1	4	1
Probable Serial	0.116	0.0066	12.5×10^{-6}	8.05×10^{-11}	1.29	1	4	1
Parallel	0.0087	1.882	2.5×10^{-5}	2.57×10^{-11}	2.46	2.67	4	2

GP77-0328-4

Figure 13. Scanner Parameters

The equations developed in previous paragraphs were applied to the relay designed for each scanner type to determine how the strength and the size of the narcissus return varies with respect to the image location (S_1) as location of the field lens surface and its radii of curvature (R_1) are changed. Separation (S_1) was varied ± 2 cm and 4 radii were used, (±1 cm, ±∞). The results are presented in Figures 14 to 19. Figures 14 and 15 show narcissus for the worst case serial scanner with positive and negative field lens radii. Note on Figure 14 that with a flat field lens (infinite curvature, $R_1 = \infty$), separation must be maintained greater than approximately ±0.5 cm to make narcissus acceptable (below the NEP). If the field lens has positive radii, the negative separation must be increased. As shown in Figure 15 negative radii on the field lens reverse this situation.

The upper curves in Figure 14 show the raster ratio which were derived for an infinitesimal detector dimension. As such, it gives an indication of the spreading or expansion of the detector narcissus image with detector field lens separation, not actual narcissus image size.

The data shown was expected except for the negative curvature, negative separation case shown in Figure 15. Here, an inverted image occurs at the detector plane at about -1.8 cm separation.

Figures 16 and 17 show the narcissus reduction obtained by adding a reflective surround to the detector assembly. This reflective material reflects 300°K photons from the detector mechanical assembly into the relay optics, thereby making the detector cold assembly appear smaller. Theoretically, this technique can reduce the size of cold area to that of the detector material. As a practical value in this case, however, about seven times the total detector array area is assumed. Results using this scanner, show narcissus is insignificant for any configuration.

Figures 18 and 19 show narcissus for the parallel scanner. Here narcissus is acceptable except for separations of zero or one cm.

Since a serial scanner was selected and the modified detector surround is easily added if not already part of the scanner design, we conclude that relay narcissus is not a problem.

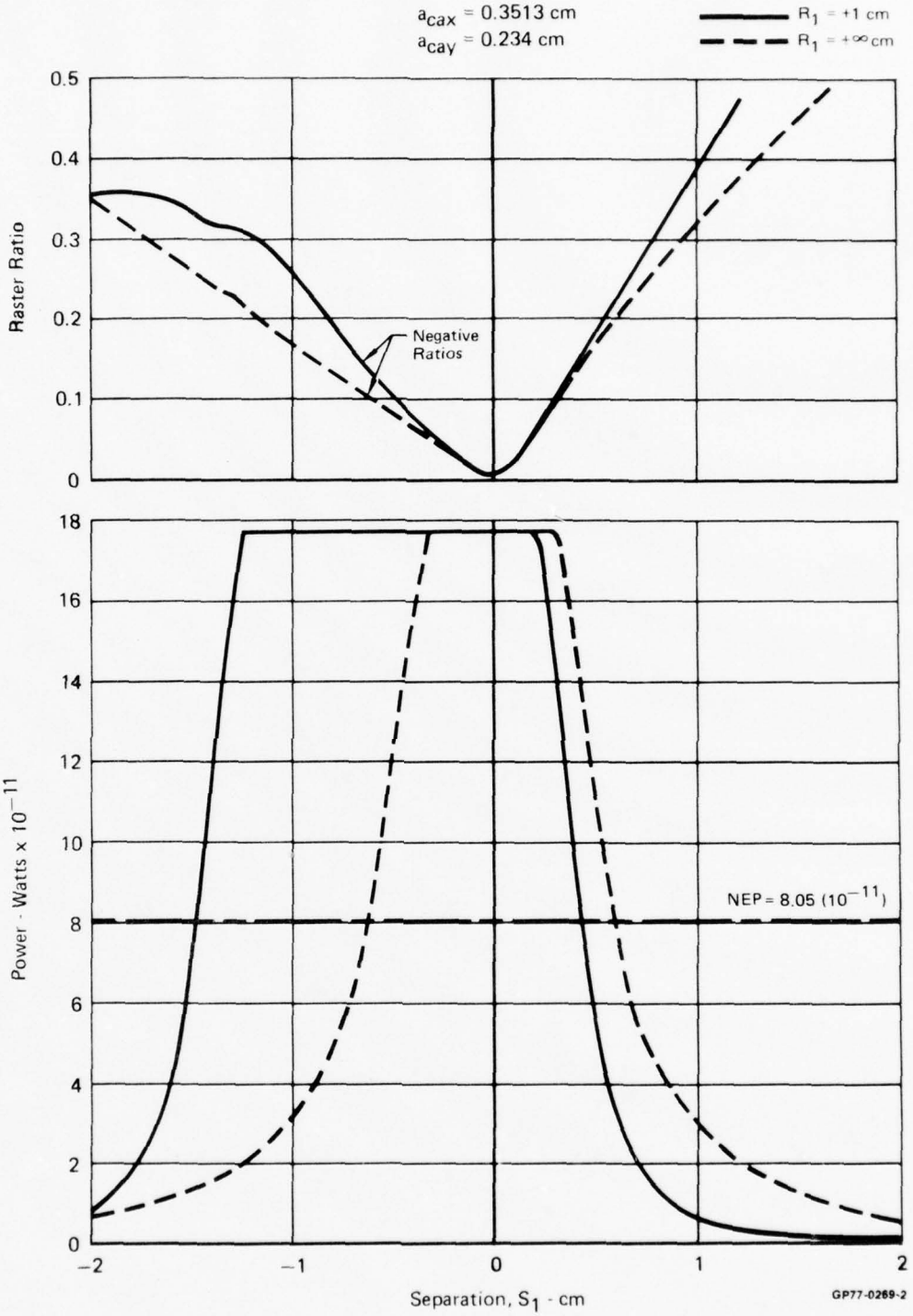

Figure 14. Serial Scan Assembly
Positive Case

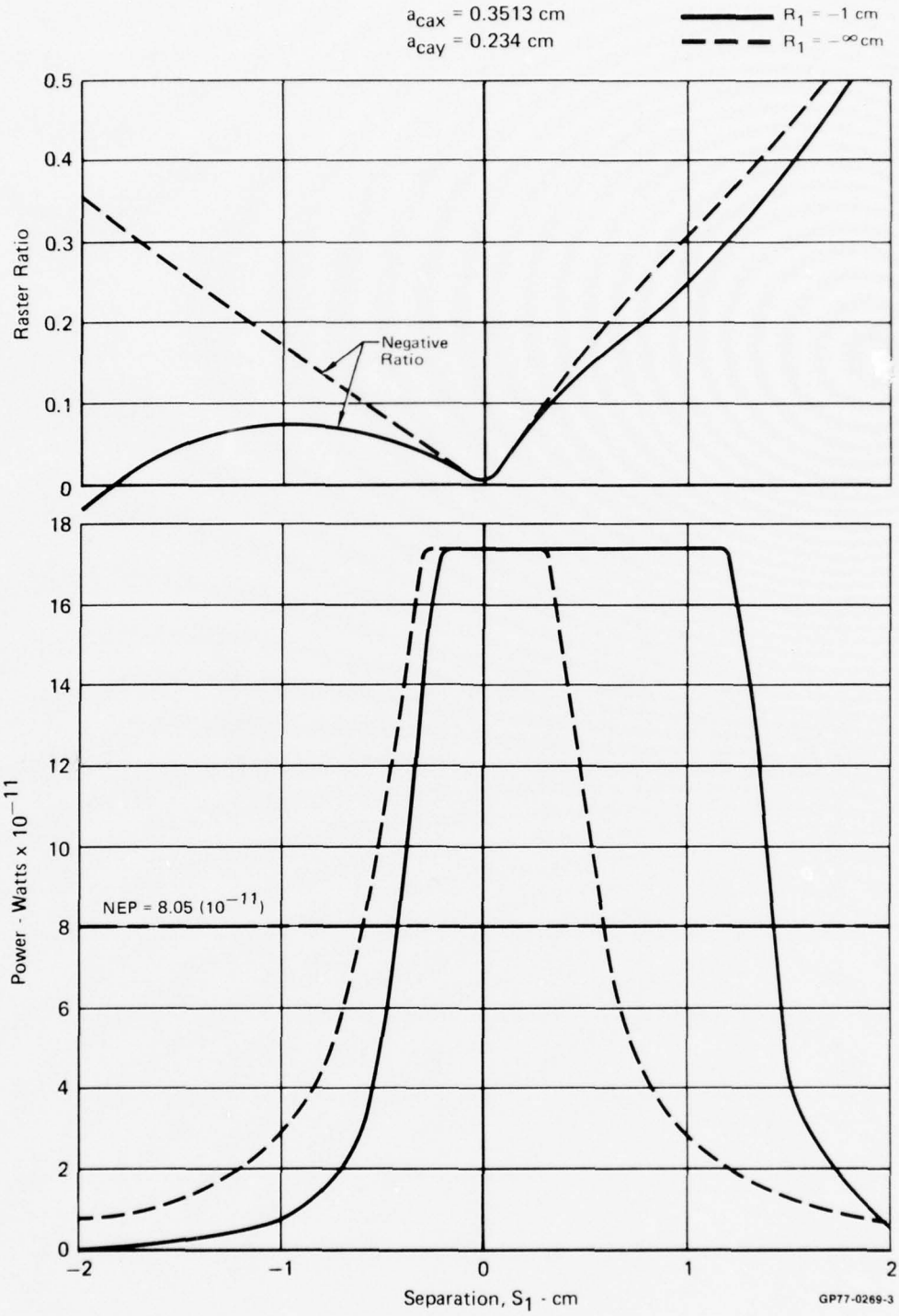

Figure 15. Serial Scan Assembly
Negative Case

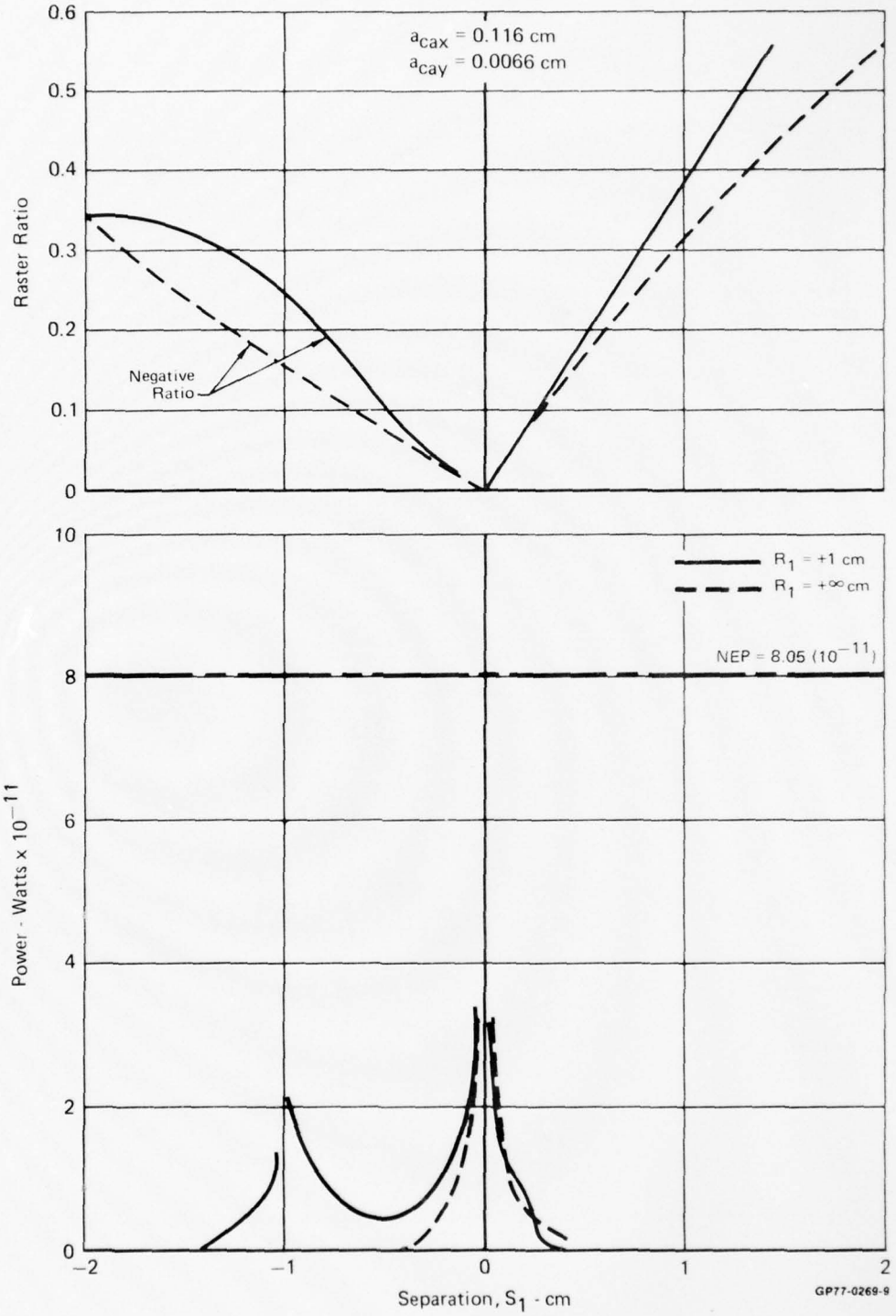

Figure 16. Serial Scan Assembly with Reflective Detector Surround Narcissus as a Function of Object Position (S_1) and Rear Surface Curvature (R)
Negative Case

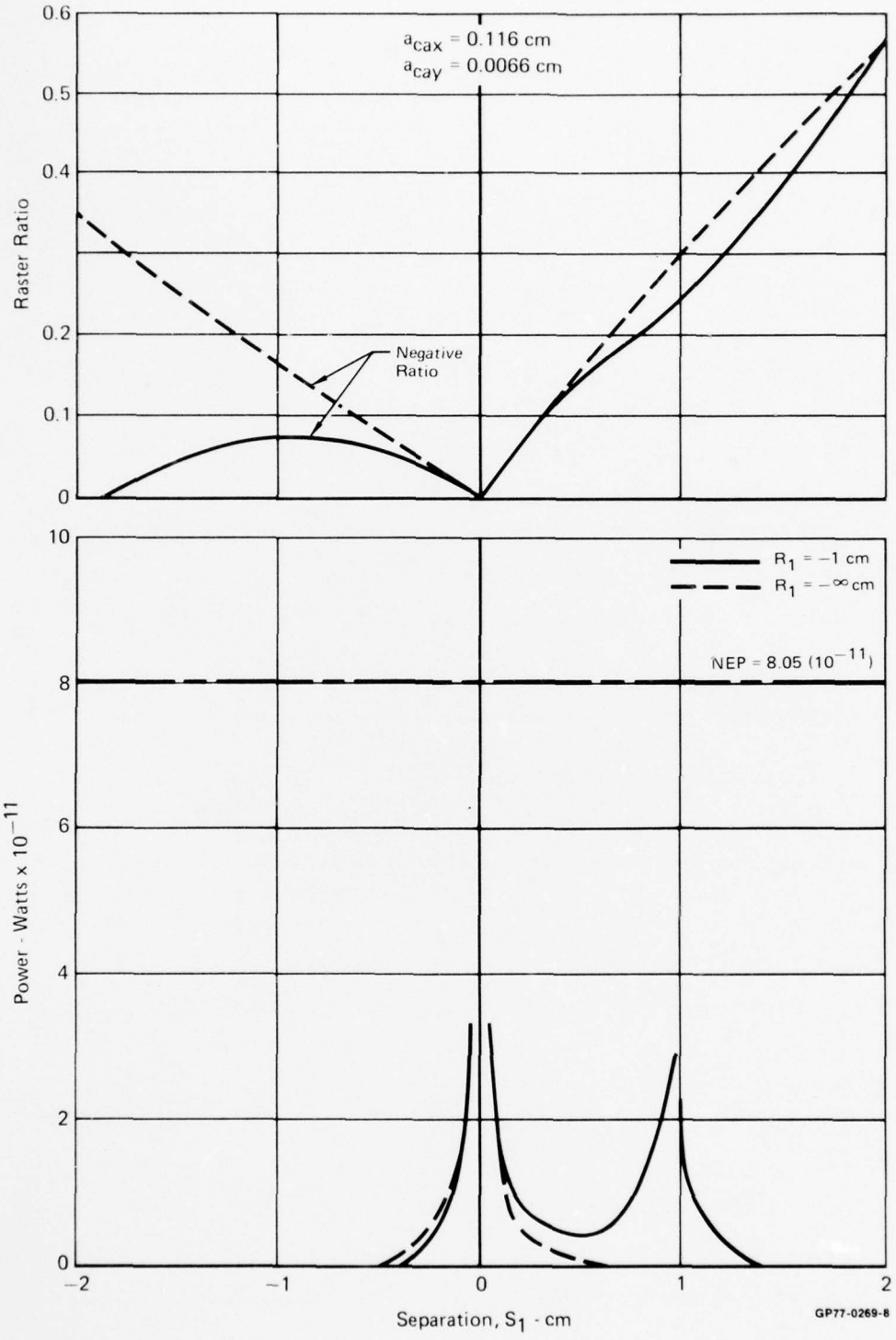

Figure 17. Serial Scan Assembly with Reflective Detector Surround Narcissus as a Function of Object Position (S_1) and Rear Surface Curvature (R) Negative Case

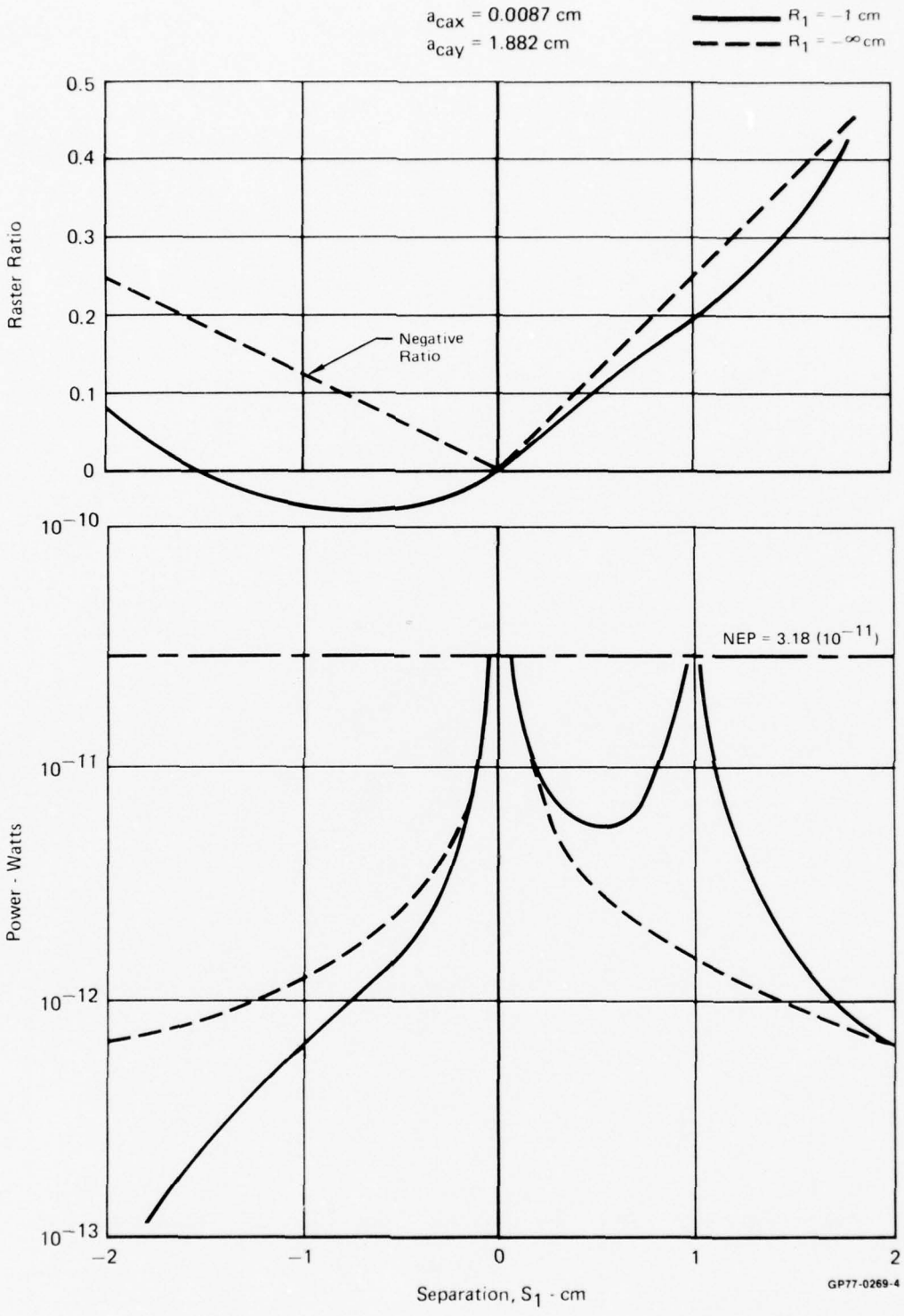

Figure 18. Parallel Scan Assembly with Reflective Detector Surround Narcissus
Negative Case

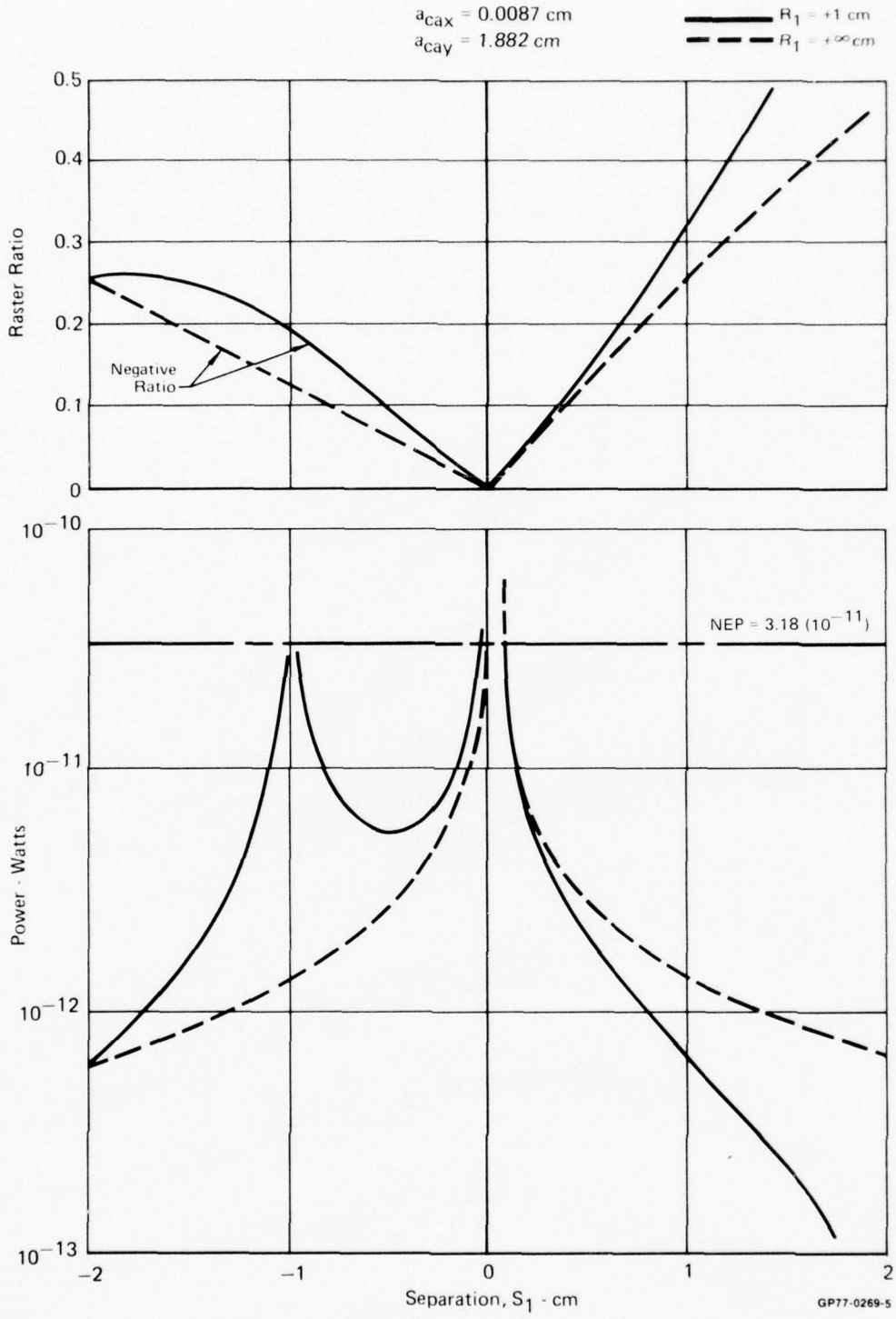

Figure 19. Parallel Scan Assembly with Reflective Detector Surround Narcissus Positive Case

NONLINEAR LENS NARCISSUS

Narcissus effects due to elements of the nonlinear lens were calculated by the procedures outline in Appendix C. In order to accomplish this task within a reasonable cost and time schedule an early lens design was utilized which is slightly different than the final design. In addition, all elements are considered spherical with radii equal to their on-axis curvatures. Neither of the above approximations are belived to introduce significant error. This will be verified during early analysis during the fabrication. Results of the narcissus analysis are presented in Figure 20 for each scanner type. They were obtained by scaling the detector forward to the nonlinear lens focal plane using the relay parameters developed earlier. These data show that acceptable narcissus (significantly below NEP) can be obtained for either serial or parallel scanners.

CONCLUSIONS

The analysis indicates that the F/2.0 lens with 16 micron optical blur for the 8-14 micron spectral region is optimum. This lens can be used most effectively with a serial scanner. Narcissus does not appear to be a problem if used with a properly designed serial scanner.

Surface	S_1 cm	Mag	Worst Case Serial (W)	Modified Serial (W)	Parallel (W)
1	3.889	−0.4408	1.503×10^{-11} (0.186)	1.4×10^{-14} (0.000174)	1.545×10^{-13} (0.00594)
2	0.3109	0.8996	2.135×10^{-10} (2.652)	9.126×10^{-12} (0.1134)	1.005×10^{-11} (0.3865)
3	0.652	0.8829	1.747×10^{-10} (2.17)	1.999×10^{-12} (0.0248)	4.702×10^{-12} (0.181)
4	0.8250	1.038	1.623×10^{-10} (2.016)	1.725×10^{-12} (0.02143)	4.368×10^{-12} (0.168)
5	0.8397	1.028	1.580×10^{-10} (1.96)	1.634×10^{-12} (0.0203)	4.251×10^{-12} (0.163)
6	6.751	1.743	7.801×10^{-12} (0.097)	7.26×10^{-14} (0.0009)	8.014×10^{-13} (0.031)
7	0.4983	0.4536	9.697×10^{-11} (1.205)	9.03×10^{-13} (0.01122)	3.161×10^{-12} (0.1216)
8	0.7752	0.1652	5.315×10^{-12} (0.06596)	4.95×10^{-14} (0.00061)	5.460×10^{-13} (0.021)
8 Detailed Ray Trace	0.7752	0.1652	3.879×10^{-13} (0.00482)	3.305×10^{-14} (0.00041)	3.153×10^{-14} (0.001213)
NEP			8.05×10^{-11}	8.05×10^{-11}	2.6×10^{-11}

Note:
Figure in parenthesis is Narcissus power divided by the NEP shown on bottom.

GP77-0328-3

Figure 20. Narcissus from Nonlinear Lens Surfaces

Section 3

LENS DESIGN AND OPTIMIZATION

The lens design phase proceeded along lines shown in Figure 21. The effort started with a materials survey to find the best material for construction of the infrared nonlinear lens. Germanium was selected for the severe aspherics. The remaining elements could be made of other materials based on dispersion requirements. The primary reason for the aspheric element selection was advice from the lens fabricator, Frank Cooke. This material can be worked as easily as glass and presents no fabrication problems. In addition, this material can be obtained with very good index homogeneity where all other materials are questionable in this area. Considering the thickness of the large aspheric elements, homogeneity is of upmost importance. Another reason for selecting germanium, was its low dispersion. The dispersion is nearly an order of magnitude smaller than that of any other applicable material. Low dispersion greatly simplifies optical design, especially in an unconventional design such as this one. Finally, germanium has good stable mechanical and thermal characteristics. The only disadvantage of this material is its high index of refraction which does not impose any restriction on design but does require sophisticated optical coatings to maintain high transmission. The required coating technology exists and does not outweigh advantages of employing the high index materials. While the design began with only the aspherics made of germanium, it was later shown that because of its low dispersion, the entire lens could be made of germanium.

The next step in lens design was to initialize the existing lens computer program with parameters of the IR lens and establish a first order design for a single wavelength. An index of 4.003 was used with an 8 inch clear aperture diameter and the original nonlinear lens distortion function. The initial design was established for an 11 micron wavelength and F/2.0. The target in the next design iteration, was a lens with an optical blur of no greater than 16 microns when imaging over the entire 8-15 micron spectral region. After an acceptable design was achieved, modifications were attempted to produce a well behaved optical output from the image plane, to facilitate optical relaying to the scanner and detector. In general, this consisted of establishing a fixed exit pupil for the F/2.0 ray cone output by using aspheric field lens surfaces. The design was iterated until a fixed pupil was achieved.

After a successful design was achieved, it was noted that there was a variation in exit pupil illumination with a change in field angle. This indicated that a non-uniform F/number existed at the image plane. When this problem was examined it was discovered that F/number was very difficult to define on the nonlinear lens because of the disparity that exists between radial and tangential focal length. A detailed radiometric analysis was required to determine how to define the lens F/number. This analysis is presented in Appendix D. The result showed that the best way to define F/number was to define entrance pupil geometry and compute an equivalent F/number by:

$$F/No = \frac{1}{2}\sqrt{\frac{f_r}{\frac{r(\theta)h(\theta)}{ab \sin \theta}}}$$

where θ = Object field angle
f_r = Focal length in the radial direction
$h(\theta)$ = Radial image height
a,b = major, minor radii of the entrance pupil ellipse.

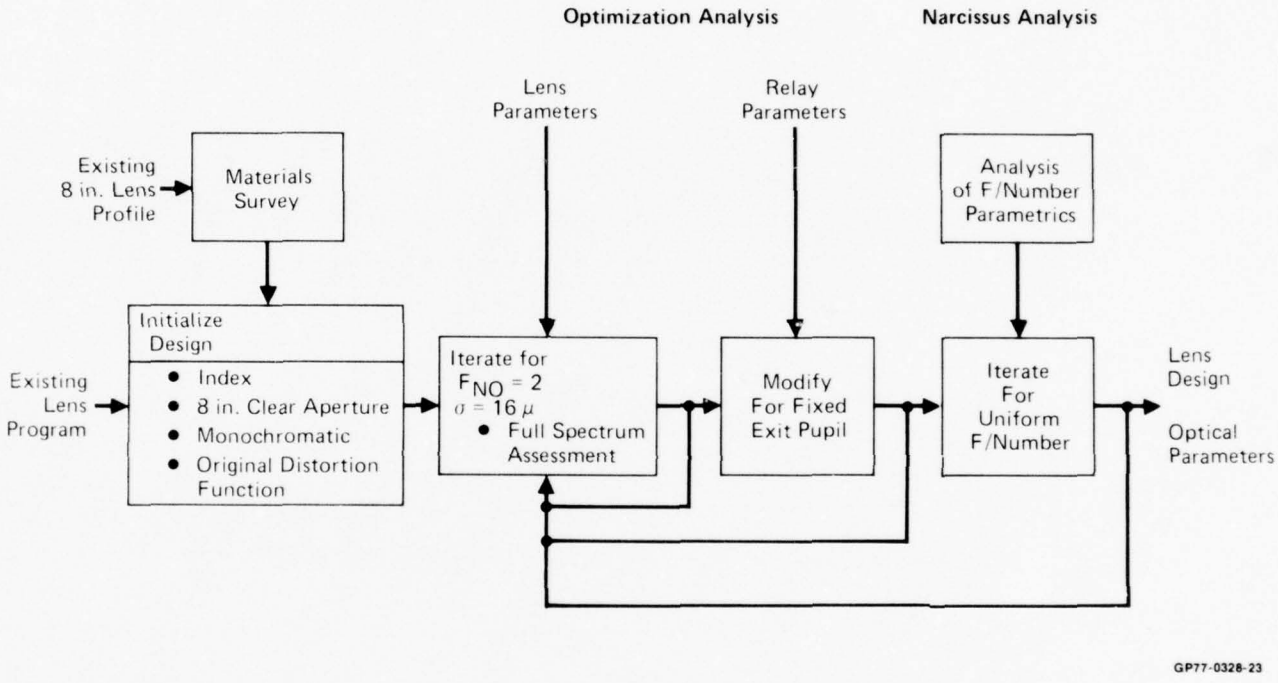

Figure 21. Lens Design and Optimization

Using this equation, the magnitude of the F/number problem was established. It was found to be excessive and led to reiteration of the entire design.

The best lens design achieved during this contracted effort is shown in Figure 22. Its blur and F/number performance are shown on Figure 23. The lens design computer data is included in Appendix E. Reiteration and further optimization of this design are continuing in an attempt to further improve F/number uniformity. We believe it will be acceptable for operating with the selected serial scanner if not by design then by designing for a smaller F/number and stopping down within the relay to achieve uniformity. As a last resort a radial filter or variable thickness element coating may be used to achieve final uniformity. However, we do not feel this will be necessary.

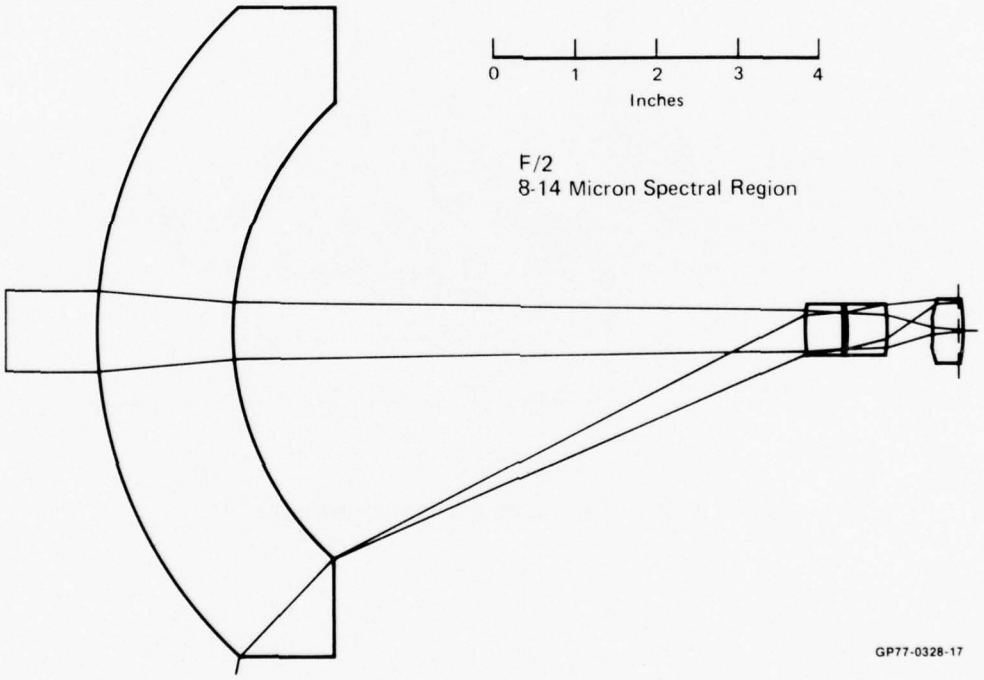

Figure 22. Infrared Nonlinear Lens

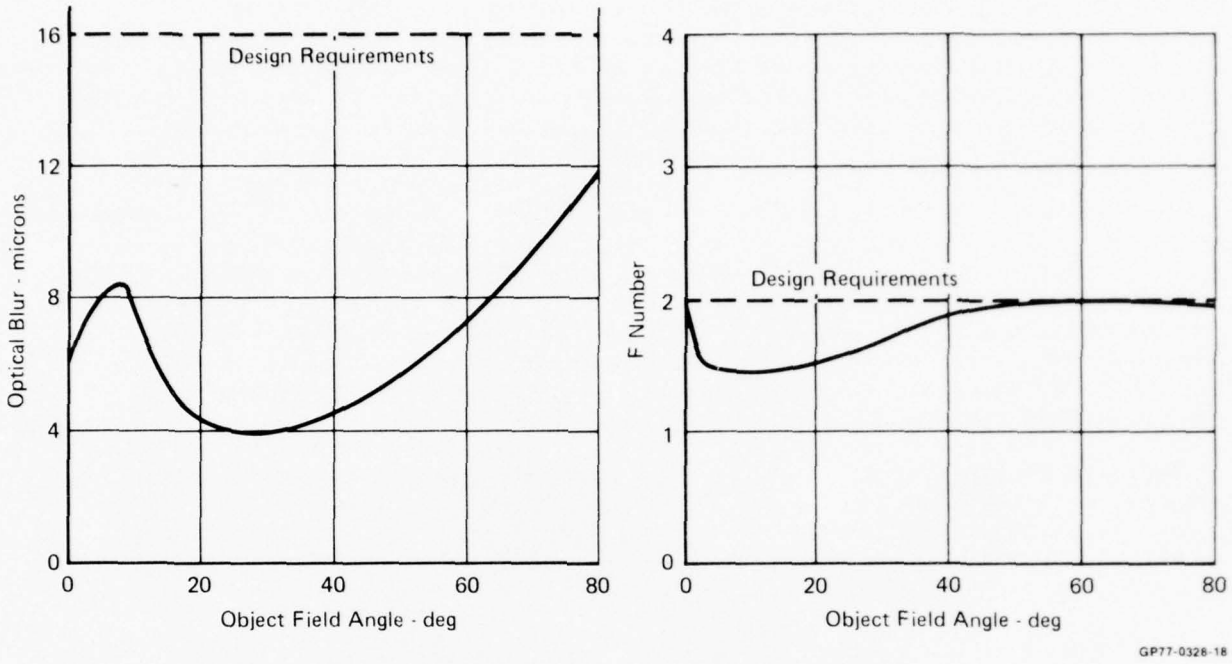

Figure 23. IR Nonlinear Lens Performance

Section 4

CONCLUSIONS

The analyses and design presented herein conclusively show that an infrared nonlinear lens is feasible and practical. The optimum lens for use with the selected current generation scanner is an F/2.0 lens with an 8 inch clear aperture. A remote viewing system using this lens would theoretically have the performance shown in Figure 24. The lens was designed for an optical blur of 16 microns. This is a worst case blur that the design program does not allow to be exceeded anywhere in the image plane. At many points on the image plane performance is considerably better (See Figure 23). On-axis, where detailed viewing is accomplished the blur is only 6 microns, also shown on Figure 24. The improvement is substantial but not as much as might be expected by examining only the ratio of the blur reduction. The reason for this is seen on Figure 25. Here the MTF's of each element of the system are shown. Blur is only one of the many degrading mechanisms. What has been achieved through the optimization process is the best balance between these MTF's. Reducing blur without changing other parameters leads to limited improvement in overall performance.

Other conclusions from this study concern narcissus and ease of fabrication. Basically, naricussus does not appear to be a problem if a properly designed scanner is utilized. Fabrication is expected to be free of unusual difficulty. All aspherics are relatively mild and the use of germanium for all elements permits fabrication by techniques similar to those used in our visual lens fabrications.

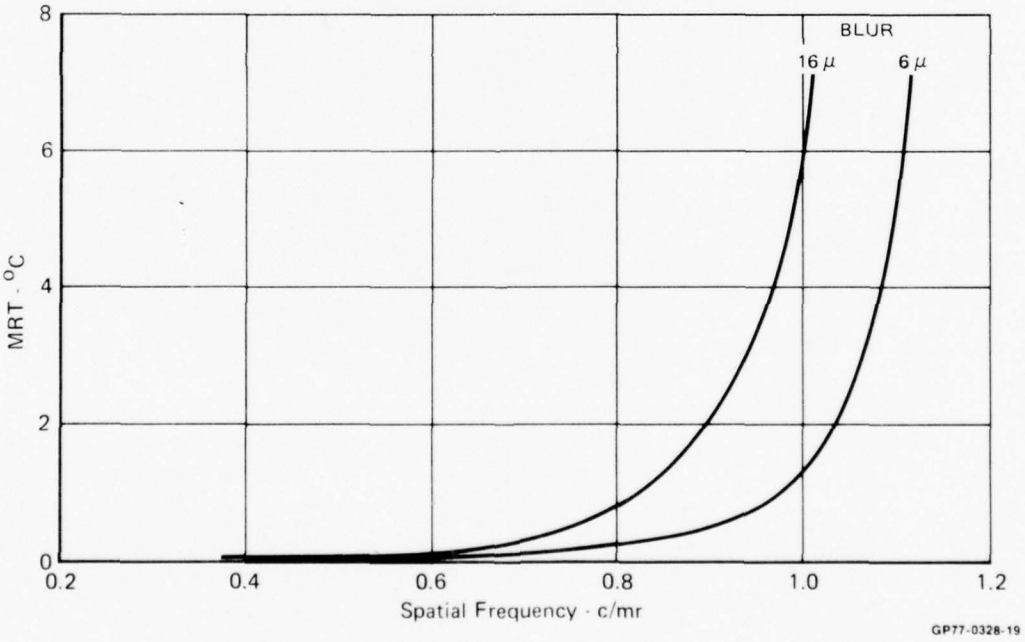

Figure 24. Serial Detector Performance as a Function of Resolution
8-14 μ Spectral Region
F/2 488 Effective Scan Lines

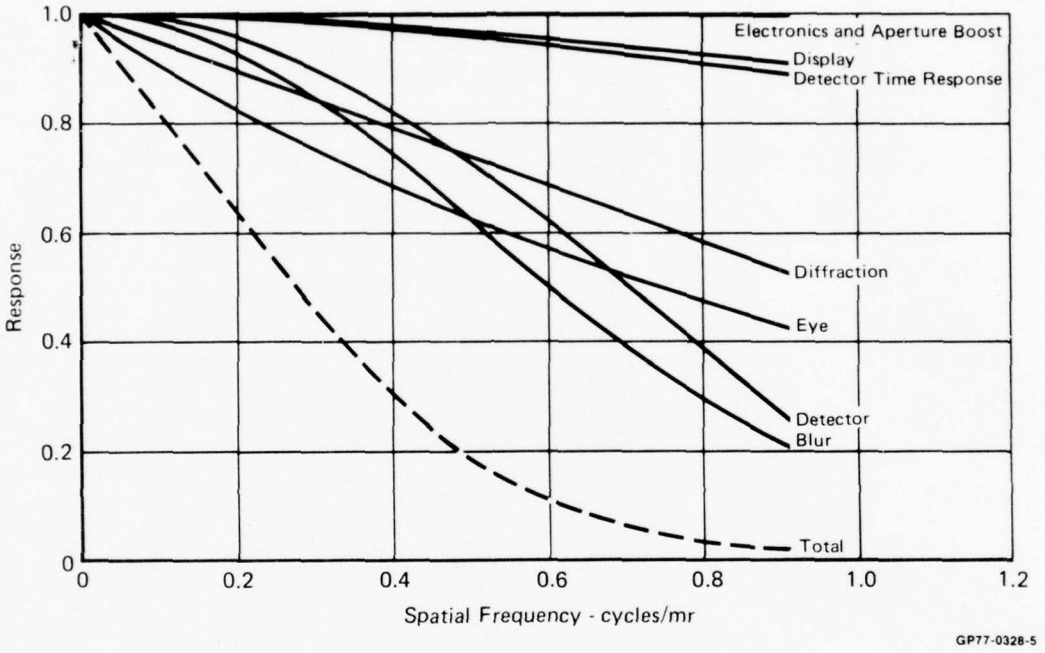

Figure 25. Serial Detector/Nonlinear System MTF's

F/2.0 Blur Circle 16μ 488 Line 8-14μ Spectral Region

Section 5

REFERENCES

1. Helmick, R. D., Fisher, R. W., Licis, G; McDonnell Aircraft Company, A Non Linear Lens for Bandwidth Reduction in Military TV Systems Applications; Published for Office of Naval Research, Department of the Navy, Arlington, VA, Under Contract Number N00014-73-C-0154, 12 November 1973.

2. "Remote Viewing System", Office of Naval Research, Arlington, VA, Contract No. N00014-75-C-0660

B-1 Ratches, James, et al, Night Vision Laboratory Static Performance Model For Thermal Viewing Systems, Army Electronics Cmd., Fort Monmouth, N. J., Report No. 7043, April 1975.

B-2 Lloyd, J. M., Thermal Imaging Systems, Plenum Press, New York 1975

Appendix A

BRIEF DESCRIPTION OF THE REMOTE VIEWING SYSTEM (RVS)

The RVS concept is based on the fact that the human visual capability can be represented by a resolution capability of about 130,000 elements, provided that these elements are sized non-linearly according to the acuity function as shown in Figure A-1. An image with this characteristic requires only about 2 MHz video bandwidth at 30 Hz frame rates. In comparison, standard techniques would require over 1,000 MHz bandwidth for this field-of-view (180°) and resolution. Even at smaller fields-of-view, the bandwidth saving is significant. A comparison of bandwidth requirements for varying fields-of-view for the conventional linear acuity function and for the RVS foveal concept is shown in Figure A-2. Approximately two orders of magnitude decrease in BW is achieved with the foveal system at FOV's greater than 20 degrees. In order to mechanize the concept described above, a method must be devised to generate an image which satisfies the optical requirements of the eye. The RVS concept contains a lens system that creates optical "distortion" by varying the spacing of the angular resolution elements to duplicate the acuity function shown in Figure A-1. This process is illustrated in Figure A-3. The lens transfer characteristic required and the technique for reconstructing the image at a remote location is also shown on this figure. System operation is as follows:

The image transmission system scans the photocathode of the vidicon or photodetectors of an imaging array, transmits this signal to the remote location, and recreates the image on a CRT or light valve tube. In the original RVS concept, the distorted image is expanded using a lens system with a transfer characteristic identical to the sensor lens and imaged on a spherical screen concentric with the nodal point of the lens.

Obviously, for the above image transmission system to perform adequately, the optical axes of both the sensor and projector must have the same alignment as the viewer's eye. The initial RVS system concept used the approach outlined in Figure A-4. The position of the projector is slaved to the camera by a high accuracy position servo, with the camera's angular position commanding the projector's position relative to fixed ground station reference coordinates. The viewer at the ground station thus has the same angular perspective as he would if he were located in the remote vehicle. The sensor and projector must also be aligned with the viewer's foveal axis. In the original concept a Honeywell oculometer was employed for this function. The oculometer measures the angle between the eye's foveal axis and the projector's optical axis. This error signal is transmitted to the remote vehicle and commands the camera to move until the angular error is reduced to zero. As the camera moves, the projector follows through the slaving loop. The control mode, presently under study, is somewhat different, however. The observer's head position instead of his eye position is utilized to point the remote camera. The operational difference resulting from this simplification is that when the viewer uses his peripheral vision, he must learn to rotate his head towards the area of interest rather than his eyes. A reticle may be required to show the observer the location of the highest acuity area of the display.

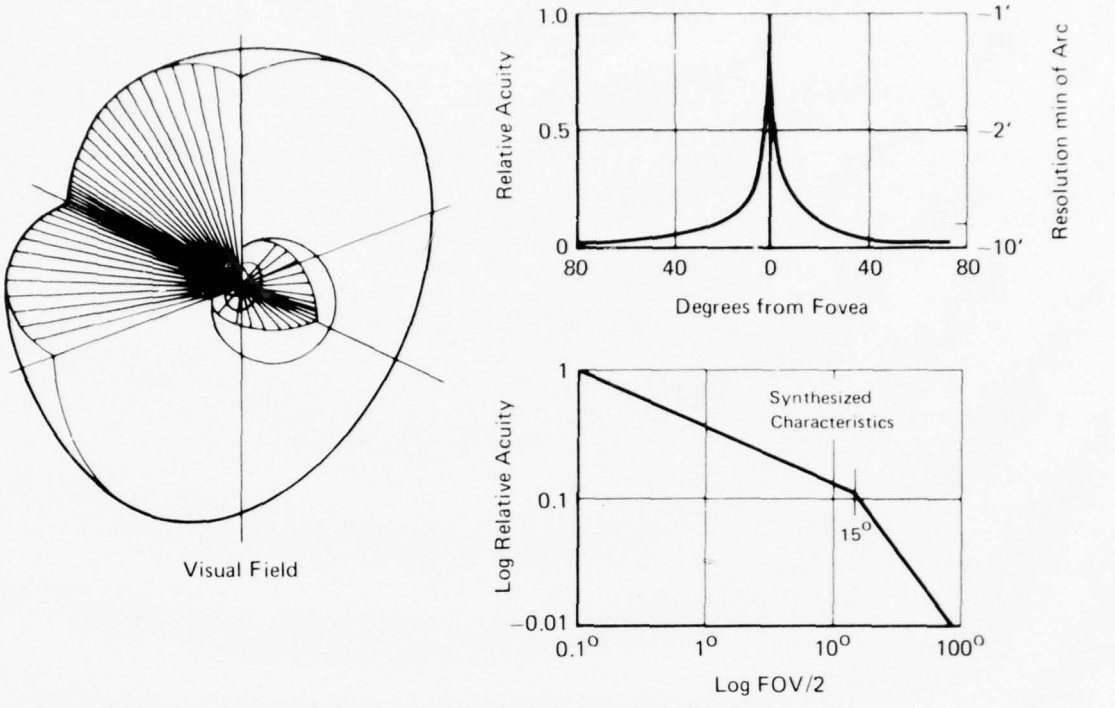

Figure A-1. Human Eye Characteristics

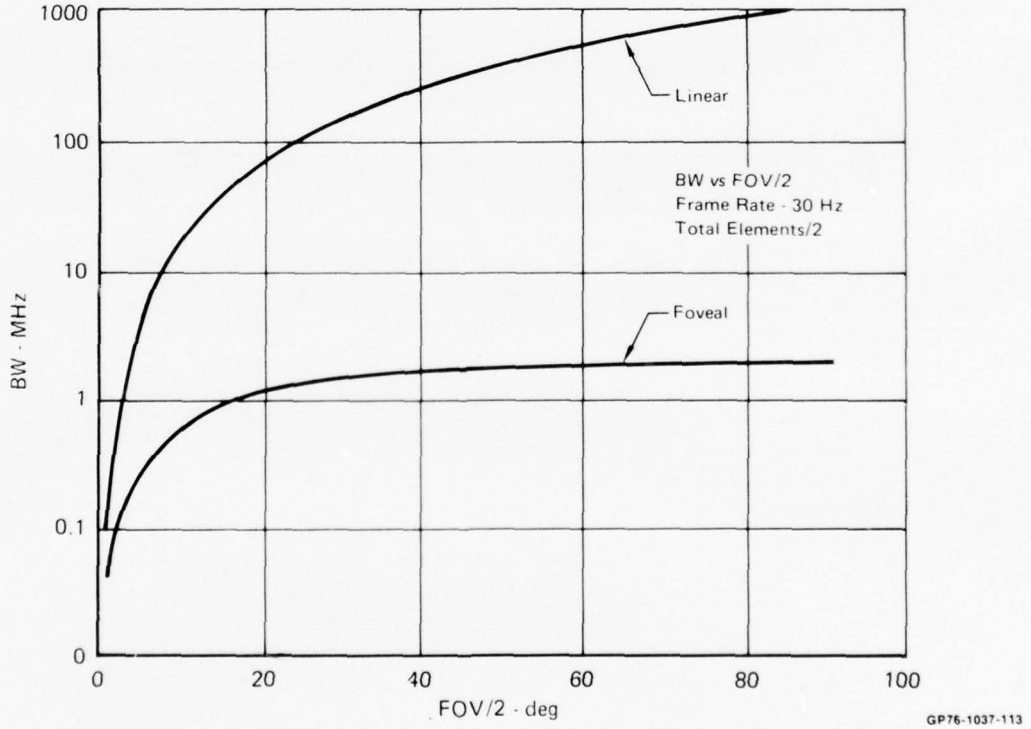

Figure A-2. Bandwidth Requirements

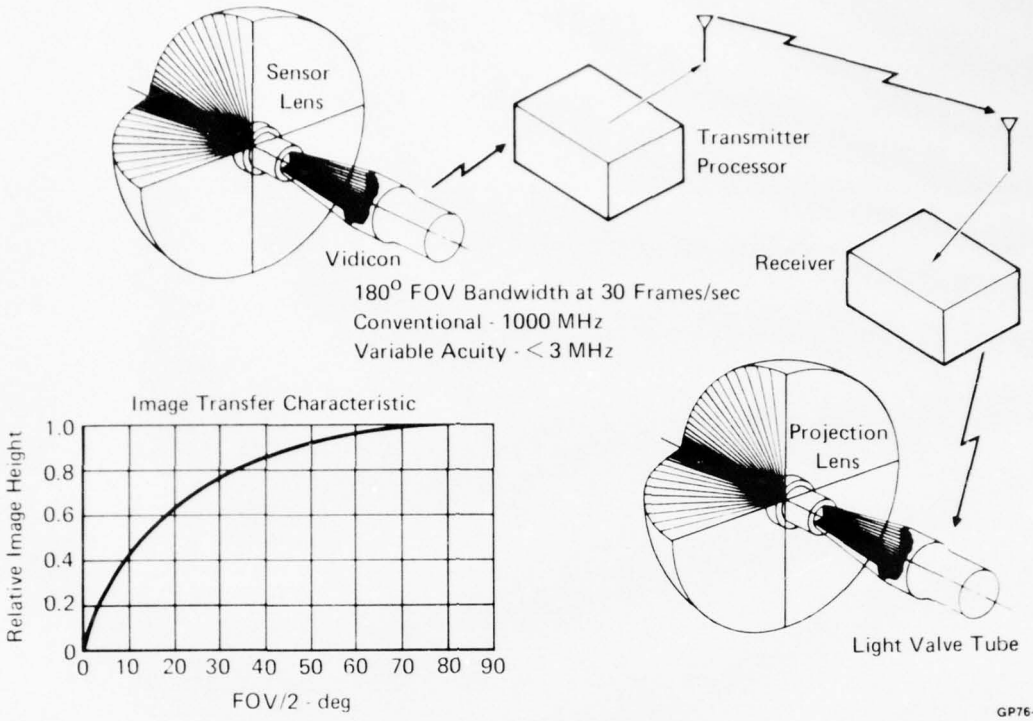

Figure A-3. Electro-Optical Schematic

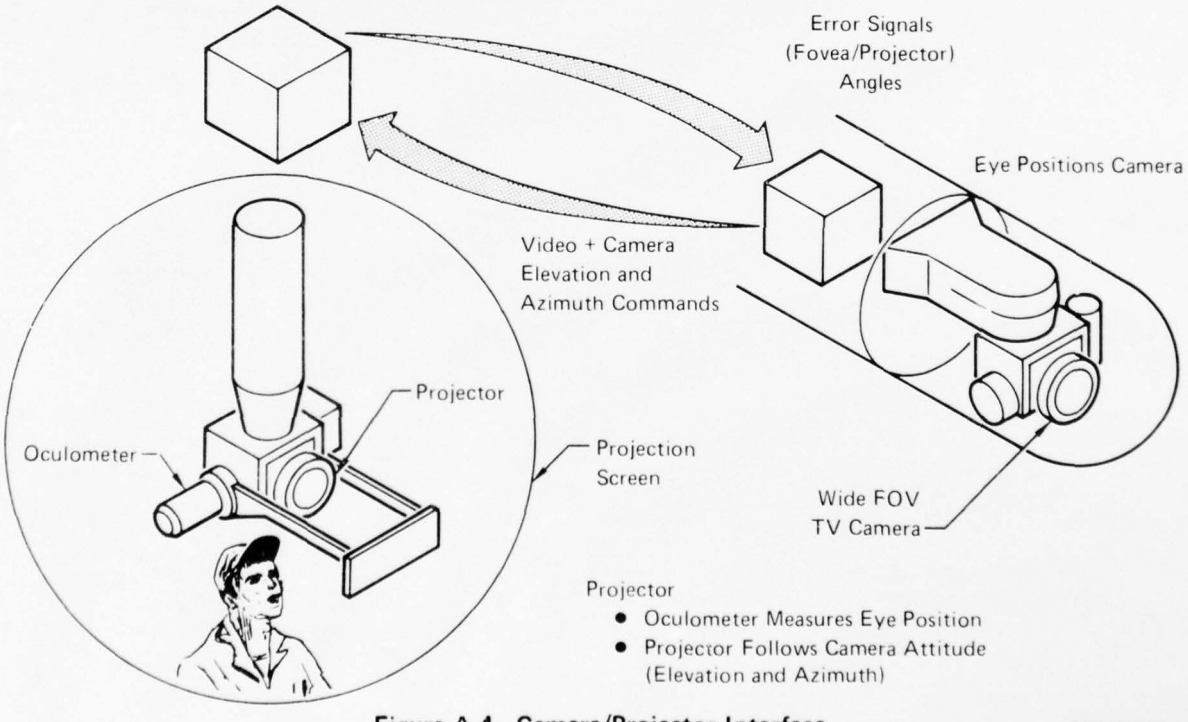

Figure A-4. Camera/Projector Interface

Appendix B

APPLICATION OF THE NIGHT VISION LABORATORY (NVL) THERMAL VIEWING SYSTEM STATIC PERFORMANCE MODEL TO THE RVS

It was suggested that the NVL Thermal Viewing System Static Performance Model [B-1] be used to evaluate the performance of the Remote Viewing System (RVS). However, repeated attempts to convert the RVS parameters directly to the NVL model have led to the following problem. The radial distortion function of the foveal lens does not lend itself to an MTF analysis as a function of object field angular spatial frequency as called for in the NVL model. All parameters can be converted successfully except for the scan velocity term because a linear raster scan on the lens image plane will create a variable angular velocity and variable direction scan in the object field. This is depicted in Figure B-1. Extreme complexity results when attempts are made to convert spatial into temporal frequency. This is illustrated by the rotation of the f_x bar pattern in the lens image plane shown in Figure B-1. Given enough time, an analysis could be made in a manner compatible with the NVL model. However, the analysis is much simpler if performed, not in object field angular frequency (cycles/milliradian) but in spatial frequency terms (lines/millimeter). For our purpose of optimizing the RVS lens, it is simpler to work in terms of spatial frequency on the foveal lens focal plane.

This simplicity arises because seven of the nine MTF's are independent of object field angle at this foveal lens focal plane location, and the scan velocity is undirectional and uniform at this location, thereby making easy conversions from spatial to temporal parameters. The only non-linear conversions necessary are simple geometrical ones which translate from focal plane to object field and display space. The advantages of working in the spatial frequency terms will become clear as the analysis is developed. In the following development, the NVL model approach will be used precisely but will be applied in the foveal lens focal plane as a function of linear spatial frequency (1/mm). Parameters will be covered in the same order as they are in the NVL Report [B-1], which describes the model in detail.

B.1 MTF's

1. Optical MTF The optical MTF's consist of a diffraction MTF and a Gaussian MTF.

(a) Diffraction In angular terms, the diffraction MTF is referenced as Equations (9) and (10) of the NVL report:

$$H_{opt}(f_x,\theta) = \frac{2}{\pi}\left[\cos^{-1} A - A(1 - A^2)^{1/2}\right] \qquad \text{(B-1)}$$

where

$$A = \lambda F_{\#} f_x / L(\theta) \qquad \text{(B-2)}$$

where $L(\theta)$ is the equivalent focal length which changes over a 50/1 range as object field angle θ changes. The angle θ is the absolute angle between the point of interest and the lens optical axis. At the foveal lens image plane

$$S_x = \frac{f_\mu}{L(\theta)} \qquad \text{(B-3)}$$

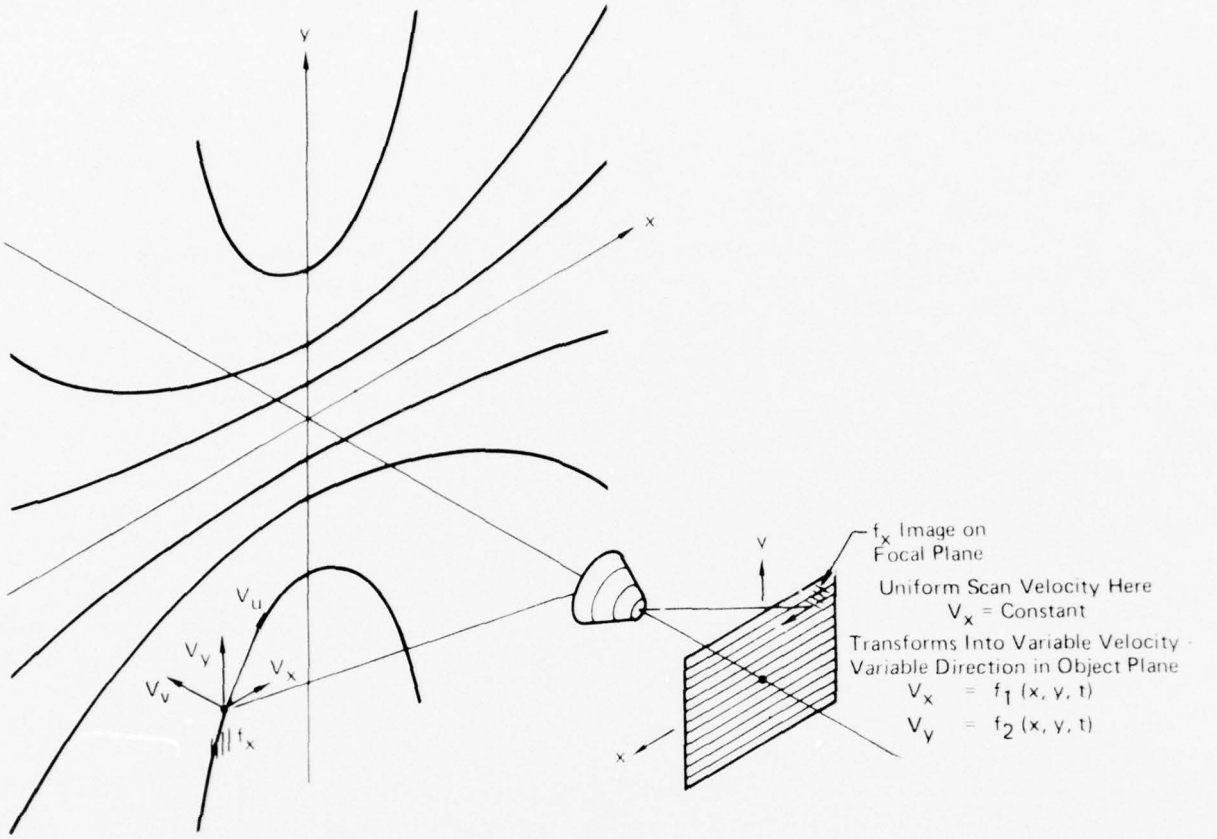

Figure B-1. Scan Distortion Introduced by FOVEAL Lens

where S_x is the image plane spatial frequency and f_μ is its object field angular equivalent measured along the scan line projection in the object field (μ direction on Figure B-1). Solving for f_μ in Equation (B-3) and substituting this for f_x in Equation (B-2).

$$A = \lambda F_{\#} S_x \tag{B-4}$$

Since the F/number of our lens is constant, the diffraction MTF is no longer a function of object field angle. Thus we may write $H_{opt}(S_x)$ which indicates that the MTF is a function of the independent variable S_x only. Note, however, that conversion to object field angular spatial frequency is very simple because focal length is constant over small angular increments and may be determined from

$$f_\mu = S_x L(\theta) \tag{B-5}$$

where μ is along the scan line projection in the object field

likewise

$$f_w = S_y L(\theta) \tag{B-6}$$

where w is normal to the scan direction in the object field

(b) Blur - A similar simplicity exists here. The MTF equation with the angular term b of Equation (11) of Reference(B-1)replaced with its equivalent is:

$$H_{blur}(f_x,\theta) = \exp\left[-\frac{2\pi^2\sigma^2}{L(\theta)^2} f_x^2\right] \tag{B-7}$$

The foveal lens inherently has a constant spatial blur over its entire focal plane, so that the sigma (σ) of Equation(B-7)is a constant. Substituting Equation(B-5)into (B-7) we see the blur MTF simplifies to

$$H_{blur}(S_x) = \exp\left[-2\pi^2\sigma^2 S_x^2\right] \tag{B-8}$$

Thus this MTF like the diffraction MTF, is no longer a function of object field angle because the focal length variable has been removed.

2. Detection MTF - The spatial filter MTF of the detector is defined as:

$$H_{Det}(f_x,\theta) = \frac{\mathrm{Sin}(\pi f_x \Delta x)}{\pi f_x \Delta x} \triangleq \mathrm{Sinc}(f_x \Delta x) \tag{B-9}$$

It is also complex in our system because the angular projection of the detector into the object field (Δx) in this equation varies with absolute object field angle (θ). Since the detector height is still uniform at the lens focal plane, shown in Figure(B-2)as Δh, Equation(B-9)can be restated as:

$$H_{Det}(S_x) = \frac{\mathrm{Sin}(\pi S_x \Delta h_x)}{\pi S_x \Delta h_x} \tag{B-10}$$

Again the MTF becomes independent of object field angle. Note from Figure(B-2)that the detector height (Δh_x) is a function of detector size(a), detector system focal length (L_D), and relay focal length (L_C), viz:

$$\Delta h_x \simeq a_x \frac{L_C}{L_D} \tag{B-11}$$

There are two ways to arrive at the required L_C and L_D based upon whether the scanner or detector characteristics are known. If the scanner is available, horizontal FOV (θ_s) and instantaneous FOV (α) are known. Then the detector focal length is

$$L_D = \frac{a_x}{\alpha_x} = \frac{a_y}{\alpha_y} \tag{B-12}$$

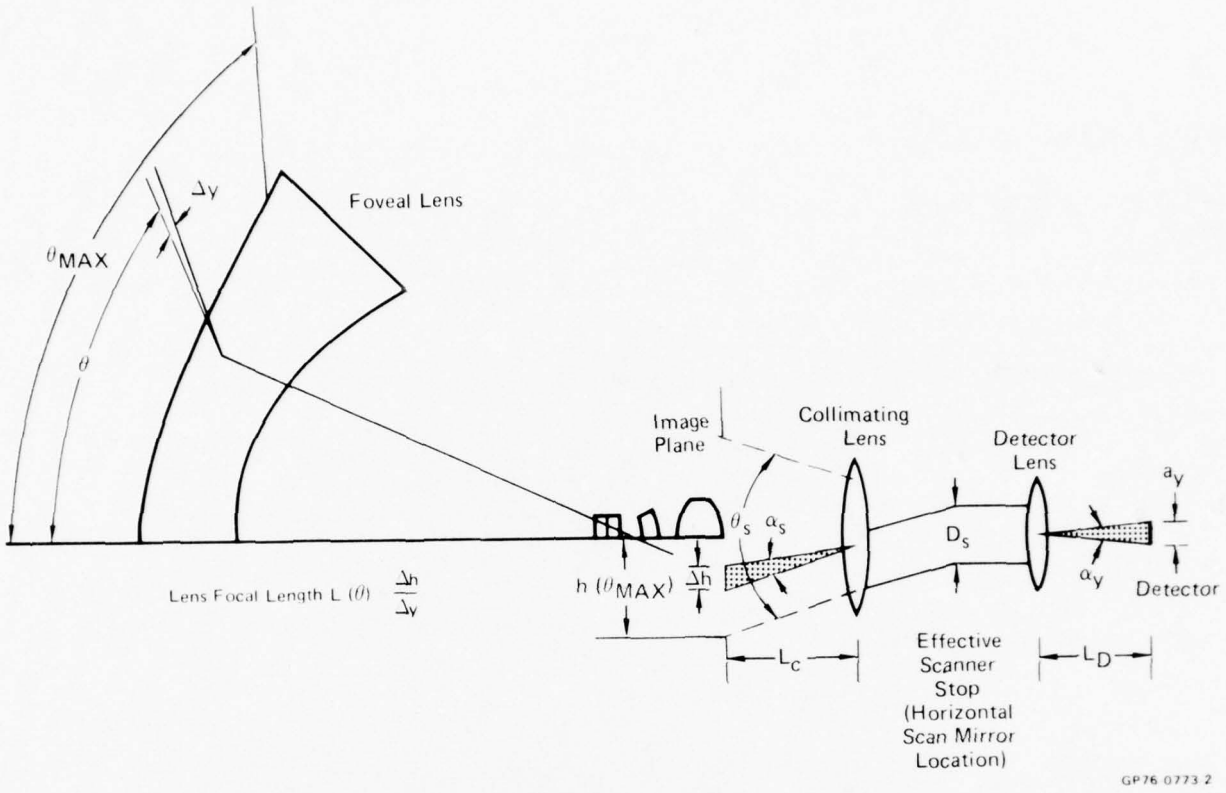

Figure B-2. Scanner Resolution Element Geometry

On the forward end of the scanner we must cover the foveal lens image plane height of $2h(\theta_{max})$ which subtends the angle θ_s. Thus,

$$\frac{h(\theta_{max})}{L_C} = \tan \frac{\theta_s}{2} \qquad \text{(B-13)}$$

Solving for L_C

$$L_C = \frac{h(\theta_{max})}{\tan \theta_s/2} \qquad \text{(B-14)}$$

If the detector characteristics are known, the focal lengths are a function of detector size (Δh) projected unto the image plane as shown in Figure (B-2). Detector size Δh can be computed directly from either the on-axis resolution required, the number of scan lines required across the vertical FOV, or bandwidth/response restrictions and frame rate requirements. The focal lengths, L_C and L_D, are then selected to make the detector dimension appear as the required Δh at the foveal lens focal plane. The scanner horizontal FOV given by scanner mechanics must cover the total image plane height ($2h(\theta_{max})$). In either case the detector

MTF becomes:

$$H_{Det}(S_x) = \text{Sinc}\ \frac{a_x L_C}{S_x L_D} \tag{B-15}$$

Again this MTF is independent of object field angle.

3. Detector Electronics MTF - It is in the MTF, the detector electrical response, that we get into real trouble trying to work in object field angular space. For a conventional linear optical system, a linear detector scan velocity converts into a scaled but linear angular scan in the object field. This is not true in our system as was shown in Figure B-1. A linear scan in the x direction on the image plane results in angular velocities in both θ_x and θ_y directions in the angular object field. Both of these angular components are nonlinear functions of both x and y position on the image plane. Thus, converting from spatial frequency to temporal frequency becomes very complex. All of this can be avoided by working in linear spatial plane terms. If the scanner has an angular scan velocity β, then the linear motion of the instantaneous FOV on the foveal lens image is

$$V_x = \beta L_C \tag{B-16}$$

The conversion to temporal frequency (f) is therefore

$$f = V_x S_x \tag{B-17}$$

This is a constant conversion and not a function of time. Therefore, all electronic MTF's of the NVL model are valid. These are

$$H'_{Det}(f)$$

$$H_{Elect}(f)$$

$$H_B(f)$$

4. Display - The RVS display is the inverse of the foveal lens, which results in a conventional linear raster generated on the CRT. The CRT has a constant spot size and the expansion optics has a constant blur at the object focal plane. Again this MTF, if derived in the linear spatial plane, will not be a function of object angle. If the optical blur and CRT spot size are combined and assumed to have a Gaussian MTF, a composite sigma (σ_d) results and the MTF is:

$$H_{Disp}(S_x) = \exp\left[-2\pi^2 (r\sigma_d)^2 S_x^{\,2}\right] \tag{B-18}$$

where r is the physical ratio of format sizes; viz

$$r = \frac{H_{\text{LENS IMAGE}}}{H_{\text{DISPLAY CRT}}} \tag{B-19}$$

By contrast, if this were accomplished in the object angular plane, the MTF would be much more complex, viz

$$H_{Disp}(f_{x,\theta,M}) = \exp\left[-\frac{2\pi^2(r\sigma_d)^2 f_x^2}{L(\theta)^2 M^2}\right] \quad \text{(B-20)}$$

where M is any system angular magnification from object field to the viewer. Again the simplicity is obvious.

5 & 6. Stabilization and Eyeball - The remaining two MTF's are the only two that are not simplified by working in linear spatial rather than angular terms. First, stabilization tends to be angular input to the system. Using the MTF from the NVL report:

$$H_{Los}(f_x) = \exp\ (-Pf_x^2) \quad \text{(B-21)}$$

Converting to the foveal lens image plane results in

$$H_{Los}(S_x, \theta) = \exp\left[-PS_x^2 L(\theta)^2\right] \quad \text{(B-22)}$$

Similarly, the eye views the display in angular terms. The NVL MTF is

$$H_{Eye}(f_x) = \exp\left[-\frac{\Gamma f_x}{M}\right] \quad \text{(B-23)}$$

Equation(B-23)must be converted to the foveal lens image plane

$$H_{Eye}(S_x, \theta) = \exp\left[-\frac{\Gamma S_x L(\theta)}{M}\right] \quad \text{(B-24)}$$

In conclusion, seven MTF's have been simplified at the expense of two that have been made slightly more complex by the conversion to linear spatial frequency.

B.2 NEΔT

NEΔT can be used as defined in the NVL document since it is independent of spatial frequency, therefore no changes are required. However, it is a function of F/number and a discussion is in order concerning which is the correct F/number to use in the calculation. It is not simply the foveal lens F/number or objective lens F/number as stated in the NVL document. For NEΔT calculations, the F/number must represent the actual ray cone supplying the detector.

In general our lens will be limited to a fixed image height $h(\theta_{max})$ that is based on fabrication considerations. The scanner must cover this total image in the most efficient manner. The optical geometry of the lens and scanner can be reduced to the basic arrangement shown in Figure(B-3). On this figure the ray cone that supplies the detector is ϕ_4. Note that a maximum ray cone (ϕ_3) that the detector can utilize exists. Obviously,

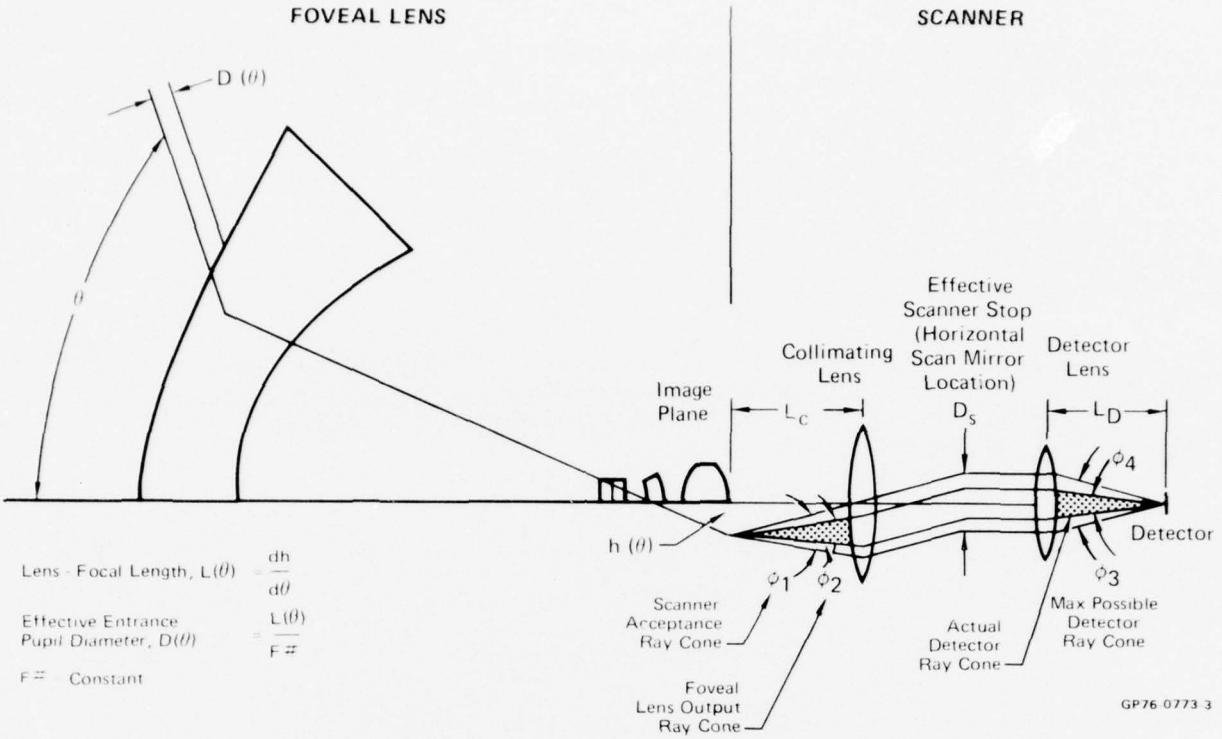

Figure B-3. General Lens/Scanner Geometry

the best design would have $\phi_3=\phi_4$. This is not always possible, however, because the lens may be required to operate with available scanners. Therefore, it will be necessary to define both of these ray cones and utilize the smallest for NEΔT and diffraction MTF calculations. Before processing, note that ray cones may also be defined by F/numbers as shown in Figure (B-4).

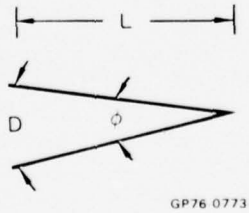

Figure B-4. Ray Cone Parameters

Since anywhere along the ray bundle

$$F_{\#} = L/D$$

$$\phi = 2 \tan^{-1}(D/2L) \tag{B-25}$$

and F/number may be defined by

$$F_{\#} = \frac{1}{2 \tan \phi/2} \tag{B-26}$$

Therefore, we can use F/number instead of ϕ to define ray cones. By the nature of collimation, the ray bundles between the collimating lens and the detector will be of constant cross section, i.e.,

$$\frac{L_C}{F_{\#2}} = \frac{L_D}{F_{\#4}}$$

And

$$\frac{L_C}{F_{\#1}} = \frac{L_D}{F_{\#3}}$$

Therefore

$$F_{\#4} = \frac{L_D}{L_C} F_{\#2} \tag{B-27}$$

And

$$F_{\#3} = \frac{L_D}{L_C} F_{\#1} \tag{B-28}$$

The larger of these two F/numbers must be used for both diffraction and NEΔT calculations. Now note that $F_{\#2}$ is the F/number of the foveal lens while $F_{\#1}$ is that generated by the scanner internal aperture stop (D_s) and we may write:

$$F_{\#1} = \frac{L_C}{D_S} \tag{B-29}$$

For any particular scanner, D_s will be known. From Equation (B-28) the smallest F/number which translates into the largest ray cone we can supply the detector with is:

$$F_{\#3} = \frac{L_D}{L_C} \frac{L_C}{D_s} = \frac{L_D}{D_s} \tag{B-30}$$

which is also obvious from inspection.

For our ONR work, a scanner has been specified while for the USAF effort only a detector geometry is available. The following derivations will try to accommodate both arrangements. If the scanner is specified, D_s and L_D will be known. If L_D is not given it can be calculated from the scanner instantaneous FOV (α) and detector size (a) in the same plane. Then

$$L_D = \frac{a_y}{\alpha_y} \tag{B-31}$$

Also, if the scanner is specified, its maximum scan angle (θ_s) shown in Figure (B-2) is known. Since the scanner must scan the entire image, θ_s must cover $2h(\theta_{max})$. Then

$$L_C = \frac{h(\theta_{max})}{\tan \frac{\theta_s}{2}} \tag{B-32}$$

It is now possible to compute $F_{\#4}$ from Equation (B-27).

$$F_{\#4} = \frac{a_y \tan \theta_s/2}{\alpha_y h(\theta_{max})} = F_{\#2} \tag{B-33}$$

where $F_{\#2}$ is the foveal lens F/number. Remember, for the diffraction MTF and NEΔT calculations, we use the larger of $F_{\#4}$ or $F_{\#3}$.

If a scanner is not defined, one must be theorized. This can easily be accomplished by procedures outlined in Lloyd [B-2]. Generally, scanning hardware (mirror, drum, etc.) are selected to accomplish a given scan angle θ_s (number of facets). Collimation lens focal length (L_C) can then be computed by Equation (B-32). From the required scan lines across the maximum image height $h(\theta_{max})$, the apparent detector size (Δh) at the image can be calculated. The angular instantaneous FOV of the scanner can be calculated as follows, using the on-axis geometry of Figure (B-2):

$$\alpha_y = \frac{\Delta h}{L_C} \tag{B-34}$$

L_D can then be calculated by

$$L_D = \frac{a_y}{\alpha_y} \tag{B-35}$$

D_s can then be defined by matching the lens F/number

$$D_s = \frac{L_C}{F_\#} \tag{B-36}$$

B.3 MRT Calculations

The following MRT equation modifications are required so that the computation may be performed in linear spatial frequency terms. First, in the NVL MRT equation, Δy must be replaced by the apparent detector size at the foveal lens image plane, i.e., it must be the Δh defined on Figure (B-2). As previously demonstrated in Equation (B-11),

$$\Delta h_y = a_y \frac{L_C}{L_D} \tag{B-37}$$

Also, in the MRT equation, it is best to compute the Q integral in terms of temporal frequency. This eliminates the velocity term in the MRT equation and makes the Q integral easier to compute. The Q integral is therefore

$$Q(f,\theta) = \int_o^\infty \frac{S(f)}{S(f_o)} H_N^2(f) H_w\left(\frac{f}{V_x}\right)^2 H_{Eye}\left(\frac{f}{V_x}\right) df \tag{B-38}$$

Of these terms, only H_w, the transfer function for a rectangular bar of width w, has not been defined. This transfer function is in linear rather than angular dimensions, i.e.,

$$H_w\left(\frac{f_x}{V_x}\right) = \text{Sinc}\left(W \frac{f_x}{V_x}\right) = \text{Sinc}\left(WS_x\right) \tag{B-39}$$

where

$$W \triangleq \frac{1}{2S_x} \tag{B-40}$$

The MRT equation written to show the dependency of two variables is

$$MRT(S_x,\theta) = \frac{SNR\pi^2 NE\Delta T}{4\sqrt{14}\ MTF_{TOTAL}(S_x,\theta)} \left[\frac{\Delta h_y\ S_x Q(f,\theta)}{\Delta f_N F_R\ t_e\ \eta_{OVSC}}\right]^{1/2} \tag{B-41}$$

This equation results in an MRT very weakly dependent on θ. To obtain the MRT for any field angle θ we convert the spatial frequency term S_x into an angular frequency term by using Equation (B-5) containing the focal length function:

$$f_\mu = S_x L(\theta) \tag{B-5}$$

Note this will be the angular spatial frequency in the scan direction (target bars normal to the scan direction). It could be related to f_x and f_y but this does not appear to be required at this point.

Appendix C

THEORY OF NARCISSUS ANALYSES

The problem of the IR detector "seeing" cold focal plane surfaces which are reflected by the system optics in addition to the warm target is labeled the "Narcissus Problem". The source of the narcissus problem is illustrated in Figure C-1. In Figure C-1 the detector assembly is shown at the center scan position. All areas of the rear clear aperture of the optics are flooded with photons emitted from the 300°K structure surrounding the detector assembly. Most of these photons are absorbed by the lens structure or pass out into the object field. A small number however, are reflected back to the image plane by the various lens elements and therefore some of these returning photons fall on the detector to alter its electrical output. Alternatively, the emitted photon flux field from the warm structure may be thought of as being disrupted by the cold detector assembly which for all practical purposes has no emission. Therefore a cold "hole" is introduced into the flux field. The narcissus problem is generated when this hole is made to translate across the optical image as illustrated by the dashed lines in Figure C-1. This occurs during the mechanical scanning. This translating region of non-emission will cause a fluctuation in the reflected photon distribution at the detector plane. If this spatial fluctuation is smaller than the total scan, an unwanted signal will be generated during the scan. The generation and prediction of the narcissus image are described below.

The best way to compute significance of the "narcissus" energy is to assume that the detector cold assembly is emitting at 300°K and trace the reflections that return to the detector plane. The spatial distribution of reflected portion of this energy in the detector plane is the photon energy that will be absent in the actual situation, hence, a "cold" output will be obtained from the detector. This process is shown in Figure C-2.

At the "start scan" position shown in Figure C-2(a), three points of emission on the detector cold assembly are shown. In the most severe situation (negative magnification) the reflected energy will appear on the opposite end of the scan. For example, if the optics are theorized to form an image somewhat in front of the focal plane by reflection, the three ray bundles will converge forward of the focal plane and expand towards the focal plane. This energy forms a "blur" area in the focal plane as shown in Figure C-2(a). Remember this area represents a region of "less photons" than the surrounding area. Since the detector does not lie within this area, its output is not influenced by it.

In Figure C-2(b) the detector cold assembly is shown at 1/4 scan. Note that here the "narcissus" image has moved towards the detector but still has not influenced its output. In Figure C-2(c) the detector is shown at center scan. Here it lies directly within the "narcissus" area and will, therefore, have less output or will have a cold output created by the lower photon input. As the detector completes the scan, it moves outside of the "narcissus" area as shown in Figure C-2(d) and is no longer affected by narcissus. The total result then is a "cold" image resembling the narcissus blur area at the center of the FLIR display. This is illustrated in Figure C-3.

To compute the true effect of narcissus, a ray trace of all points within the detector cold assembly should be conducted. Sufficient ray tracing must be conducted to map the power density in the detector plane. Much of this laborious procedure can be avoided by a series of simplications. For example, if the portion

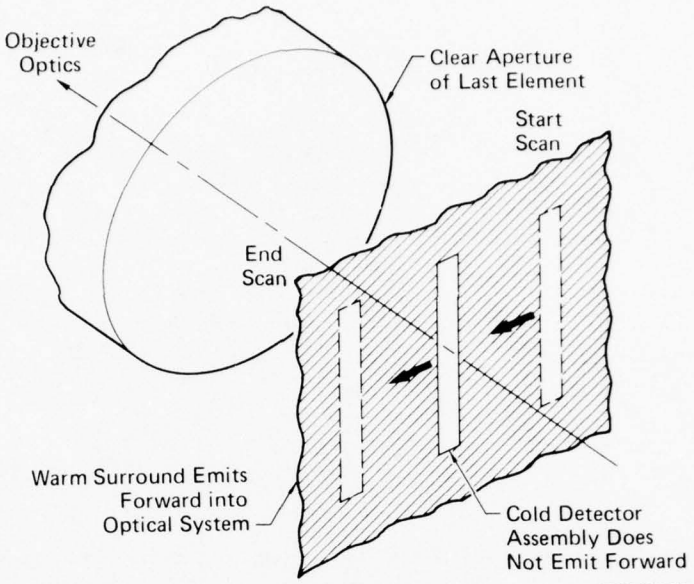

Figure C-1. Source of Narcissus Energy

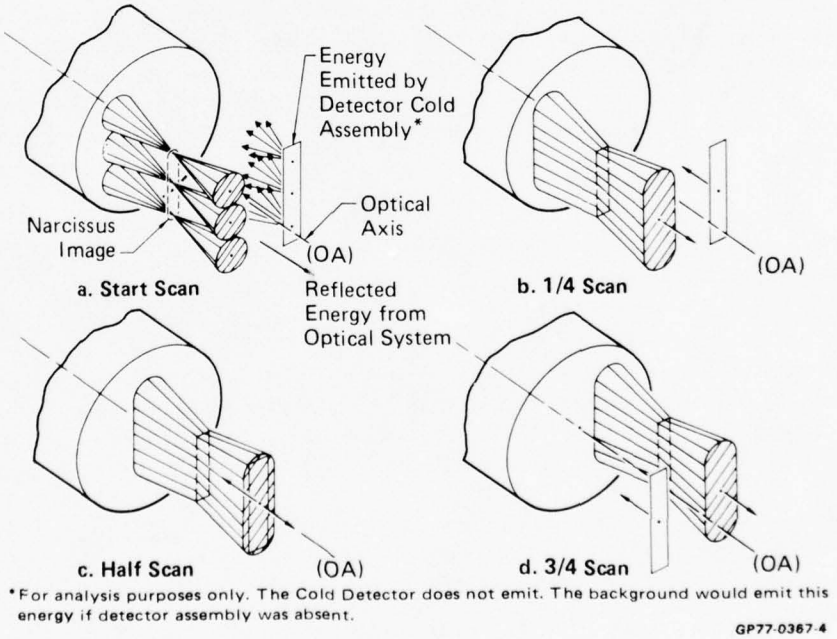

Figure C-2. Narcissus Image Generation

GP77-0367-5

Figure C-3. Narcissus Display of Figure C-2

of the narcissus image that contributes to illumination of the on-axis detector can be established, simple optical and radiometric theory can be utilized to define the maximum strength of the narcissus effect. A similar procedure can be used to estimate the size of the narcissus image. This is developed in the following paragraphs.

On Figure C-4(a), emission of the on-axis point of the cold assembly is illustrated. If narcissus analysis is being performed on a surface forward of the scan mechanism, the only energy that will be reflected back to the detector is confined within the F/number cone of detector. This cone is defined by the basic optical design. From elementary geometric optics, the energy returning from the forward surface will be confined to this cone but altered by the optical magnification. With reference to Figure C-4 it is easily seen that the blur circle radius is:

$$R = S \tan \frac{\theta i}{2} = \frac{S}{2\ M\ FNo} \qquad \text{(C-1)}$$

where S = Distance narcissus image is in front of detector plane
M = Magnification

The above are shown in Figure C-4(a) and (b) and is the narcissus power contribution for a single point on the cold emitting assembly. Obviously, the detector will be affected by the integrated results of the emission of all points on the cold assembly that can pass through the optical system and be reflected back to the detector. Three of these are shown in Figure C-4(c). It is easily seen that all of these points contribute to output of the detector located near the optical axis. The difficult task is to estimate just how much of narcissus image is capable of illuminating the detectors. This is a function of direction of the chief rays forming the narcissus image.

In Figure C-5 the image cone of the on-axis detector is shown. For a correctly designed optical system, it will be impossible for any returning ray to reach the on-axis detector unless it falls within this cone. Therefore, rays forming the

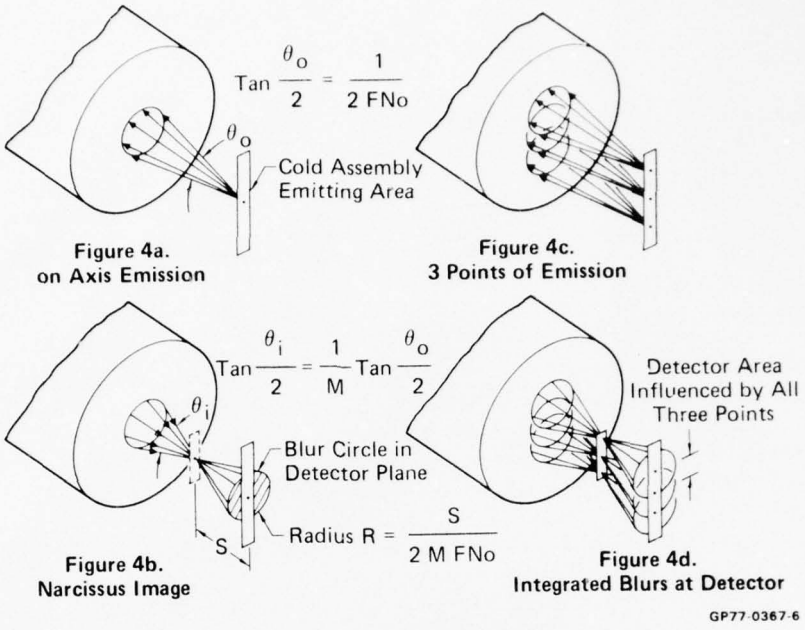

Figure C-4. Narcissus Blur Circle Radius

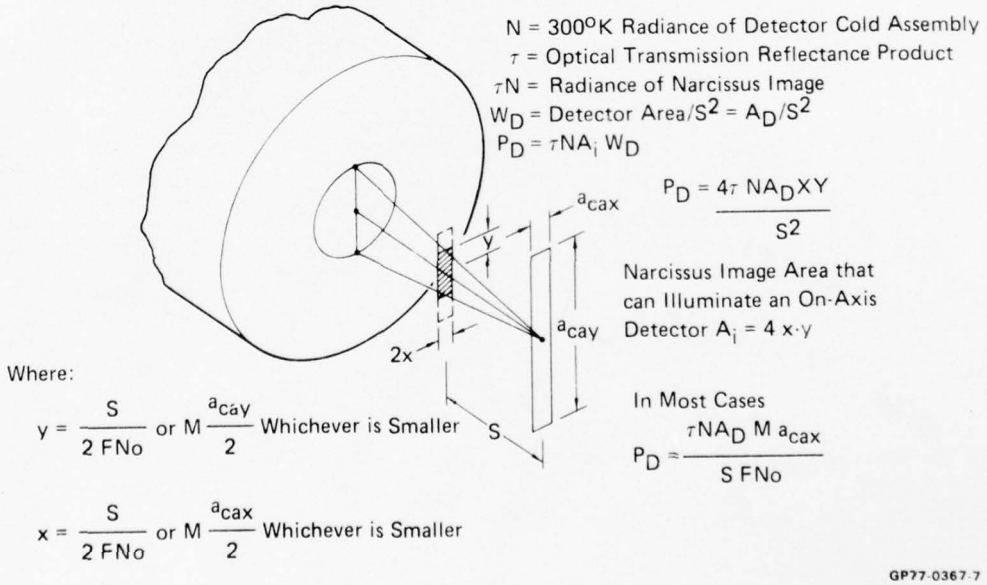

Figure C-5. On Axis Narcissus Power Calculation

narcissus image cannot illuminate this detector if they occur farther from the optical axis than the distance y on Figure C-5. The narcissus area (A_i) on Figure C-5 is therefore

$$A_i = 4 \times y \tag{C-2}$$

Now employing another simple optical theory, that the image radiance (N_i) is numerically equal to the object brightness (N) times an attenuation factor T, which is the product of all transmissions and reflectances throughout the narcissus path. The derivation of the on-axis power equaiton is shown on Figure C-5. For a linear array, the last equation almost always applies, i.e.:

$$P_D = \frac{T\ N\ A_D\ M\ a_{cax}}{S^2} \tag{C-3}$$

Unfortunately on-axis power is not sufficient to fully assess the significance of narcissus. The spatial structure on the display must be known, because in many cases the narcissus power may be many times the detector NEP but its influence may cover all detectors equally during scan. Therefore it will not be seen. This is especially possible if positive magnification exists.

Starting with the more simple case of negative magnification, the case depicted on Figure C-2, estimation of narcissus image size is very easy. For $S > a_{cax}$, the blur image width (w) in the detector plane is

$$w = 2R = \frac{S}{M\ FNo} \tag{C-4}$$

The velocity of this blur during scan is

$$V_{blur} = MV. \tag{C-5}$$

Since the detector moves in the opposite direction with velocity V, the relative velocity between the two is

$$V_r = V(1 - M) \tag{C-6}$$

The time required to scan the narcissus image is

$$t_{blur} = \frac{2R}{V_r} = \frac{2R}{V(1-M)} \tag{C-7}$$

The time required to scan the total format is

$$t_s = \frac{X}{V} \tag{C-8}$$

where X is format width

The ratio of the display width covered by the narcissus image is

$$r = \frac{t_{blur}}{t_s} = \frac{2R}{(1-M)x} \tag{C-9}$$

For positive magnification, the theory is much more complex. First it is necessary to know the nature of the basic image to proceed with this calculation. For a telecentric image (all chief rays parallel to the optical axis). The theory

can be developed as follows. Figure C-6 must be used for this derivation. This figure is a view in the x plane. Therefore the detector and Narcissus image are vertical lines normal to the paper that move from the bottom of the page (start scan) to the top (end scan). In this case (positive magnification), the narcissus image goes in the same direction as the detector, and may continue to illuminate all detectors throughout the scan, unless vignetting occurs within the optical system. Again, by assuming a telecentric optical image, an assessment can be made of this effect on the displayed image. In this case the optics will limit narcissus rays to the format diagonal dimension on the detector plane because the optics were designed to do this. This means that no ray can rise higher than the height (W) in the narcissus image plane, again remembering that moving vertical pencils are being considered. In this case, the narcissus energy will be completely vignetted when the detector array is at a height $(\frac{W}{M})$ from the optical axis. It seems logical therefore, to assume the image disappears at this point. The derivation shows that for this assumption the ratio of narcissus occupied display format height is:

$$r\ (S) = \frac{1.41}{M} + \frac{S}{M\ a_{cay}\ FNo} \qquad (C\text{-}10)$$

A similar analysis for negative values of S yields

$$r\ (-S) = \frac{1.41}{M} - \frac{S}{M\ a_{cay}\ FNo}$$

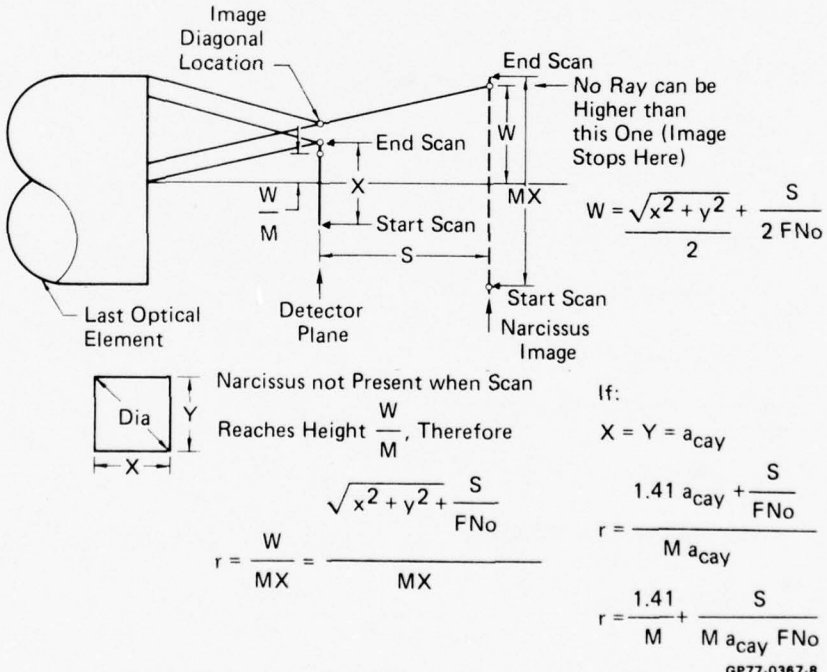

Figure C-6. Narcissus Size for Positive Magnification

Appendix D

NON LINEAR LENS F/NUMBER DETERMINATION

The derivation of the F/number of the nonlinear lens is defined in this Appendix. Germaine terms are defined on Figure D-1. Photons are radiated from the earth (or target) at a slant distance (S) and radial distance (R) from the nonlinear lens. The variables S and R are much greater than the clear aperture diameter (DCA). This photon flux is specified by a radiance (N) in watts/CM^2-Steradian. For an infinitesimal area in the object field (A_t), the power (P_a) entering the lens pupil of area (A) is:

$$P_a = NA_t W \tag{D-1}$$

where ω = Solid angle subtended by the entrance pupil (D-2)

$$\omega = \frac{A}{S^2}$$

Then

$$P_a = \frac{NA_t A}{S^2} \tag{D-3}$$

This entire flux must appear on the lens image plane within the image (A_i) of object area (A_t).

$$A_i = dt\ dr$$

The power density of the focal plane is therefore

$$W = \frac{P_a}{A_i} = \frac{NA_t A}{S^2\ dt\ dr} \tag{D-4}$$

Now A_t can be related to the image plane through lens focal length. By definition the radial focal length (f_r) is

$$f_r(\theta) = \frac{dr}{d\theta} \tag{D-5}$$

and the tangential focal length (f_t) is

$$f_t(\theta) = \frac{dt}{d\theta_t} \tag{D-6}$$

where θ_r and θ_t are the radial and tangential angular subtense of A_t. Therefore,

$$dr = f_r(\theta)d(\theta_r) \tag{D-7}$$

$$dt = f_t(\theta)d(\theta_t) \tag{D-8}$$

$$\text{Now } A_t = Sd\theta_r \cdot Sd\theta_t = S^2 d\theta_r d\theta_t \tag{D-9}$$

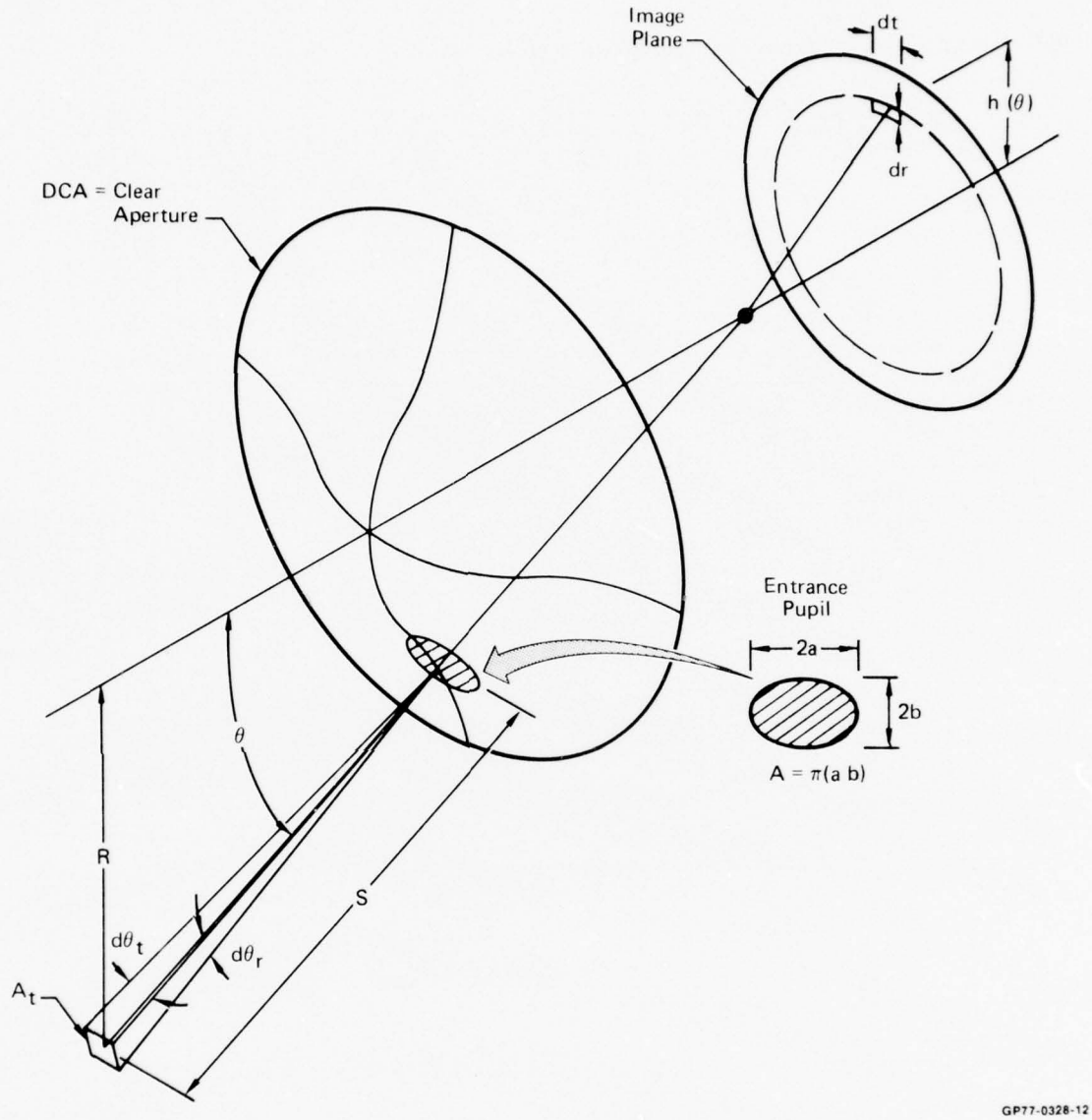

Figure D-1. Nonlinear Lens F/Number Determination from Entrance Pupil Size

Substituting this into Equation (D-4) we have

$$W = \frac{N\ A\ d\theta_r d\theta_t}{dt\ dr} \tag{D-10}$$

Now substituting Equation (D-8) and (D-9) into (D-10)

$$W = \frac{N\ A}{f_r(\theta) f_t(\theta)} \tag{D-11}$$

The focal length $f_r(\theta)$ is available from the original image height function used in lens design in the form of $h(\theta)$ vs θ, thus

$$f_r(\theta) = \frac{dh(\theta)}{d\theta} \tag{D-12}$$

The tangential focal length is not so obvious. It must be calculated by circular symmetry considerations. The same number of area elements must exist around the object field circumference $2\pi R$ as exist around the image plane circumference $2\pi\ h(\theta)$. In the object field the number of elements is:

$$N_{eo} = \frac{2\pi R}{d\theta_t S} = \frac{2\pi\ \mathrm{Sin}\ \theta}{d\theta_t} \tag{D-13}$$

In the image plane the number of elements is

$$N_{ei} = \frac{2\pi h(\theta)}{dt} \tag{D-14}$$

Then Equation (D-13) and (D-14) may be set equal to each other

$$\frac{\mathrm{Sin}\theta}{d\theta_t} = \frac{h(\theta)}{dt} \tag{D-15}$$

Or by definition of the focal length

$$f_t(\theta) = \frac{dt}{d\theta_t} = \frac{h(\theta)}{\mathrm{Sin}\theta} \tag{D-16}$$

Substituting into Equation (D-11)

$$W = \frac{N\ A\ \mathrm{Sin}\theta}{f_r(\theta)\ h(\theta)} \tag{D-17}$$

This expression can be evaluated over the image plane as a function of θ to determine uniformity of focal plane illumination (W). If the pupil is elliptical the area A is:

$$A = \pi ab \tag{D-18}$$

Equation (D-17) then becomes

$$W = \frac{N\pi ab\ \mathrm{Sin}\ \theta}{f_r(\theta)h(\theta)} \tag{D-19}$$

To put this in relative terms, we can refer to the equivalent F/number of the nonlinear lens, i.e., the circular aperture F/number for a conventional lens that yields the same focal plane illumination as Equation (D-19).

If A was circular with diameter (D) and focal length constant (f) the flux through A would be

$$P_a = NA_t \frac{A}{S^2} \tag{D-20}$$

where

$$A = \frac{\pi D^2}{4}$$

then

$$P = \frac{N\pi D^2 A_t}{4S^2} \tag{D-21}$$

If the lens is conventional, all this power falls on an image area

$$A_i = A_t \frac{f^2}{S^2}$$

Therefore,

$$W = \frac{P}{A_i} = \frac{N\pi D^2}{4f^2} = \frac{N\pi}{4(F_{NOE})^2}$$

Equating this to Equation (D-19) and solving for F_{NOE}

$$F_{NOE} = \frac{1}{2}\sqrt{\frac{f_r(\theta)h(\theta)}{ab\sin\theta}} \tag{D-22}$$

This equation gives the nonlinear lens F/number in conventional terms. It is used to assess F/number uniformity of the nonlinear lens designs.

Appendix E

LENS PRELIMINARY DESIGN COMPUTER DATA

This Appendix contains the seventeenth computer run out of 50 runs for the design of the nonlinear lens shown schematically in Figure 22.

SEE UPDATE 10/ 1/71
RN*170 8-14 MICRON OBJ. F/2

NST	NWT	MT	NPASS	MS	M	NHELD	NLOOP	NFT	NINC	NN4	M1	M2	M3	M4	M5	M6	M7	MOR		
12	2	0	2	0	1	11	2	5	-1	-0	-0	-0	9	-0	0	-0	-0	5	1	4
-0	-0	-0	-0	-0	-0	-0	-0	-0	-0	-0	-0	-0	-0	-0	-0	-0	-0	-0	-0	-0

NNE,RAD,SASC,NNA
NSE,X,4RN,HM,NSA

1	20	.053000000	-.000000000	.001000000	.001000000	.001000000	.000050000	-0	1
1	6	-9.553745220	1.000000000	0.000000000	0.000000000	45.000500000	0.000000000	1	1
2	3	.444774730	.180065460	.334488480	.615513090	.742651930	.759591110	0	2
2	10	.940862200	4.003000000	1000.000500000	0.000000000	1000.000500000	.000000310	0	2
3	3	0.000000000	.000957600	.749657450	1.384440000	1.688340000	1.896940000	0	3
3	7	0.000000000	4.003000000	1000.000500000	0.000000000	1000.000500000	.055224310	0	3
4	3	.594258770	.145707690	.344430100	.609683310	.808493470	1.017744450	0	4
4	10	3.491766650	1.000000000	0.000000000	0.000000000	45.000500000	1.517952670	0	4
5	3	.930589650	.245000000	.582000000	1.000000000	1.227000000	1.329000000	0	5
5	1	.240514790	4.003000000	1000.000500000	0.000000000	1000.000500000	1.000000000	0	5
6	3	0.000000000	-0.000000000	-0.000000000	-0.000000000	-0.000000000	-0.000000000	-0	6
6	1	.001986630	4.003000000	1000.000500000	0.000000000	1000.000500000	0.000000000	0	6
7	3	.017601640	0.000000000	9.268166010	400.258519000	-0.000000000	-0.000000000	0	7
7	1	.005424360	1.000000000	0.000000000	0.000000000	45.000500000	-0.000000000	0	7
8	3	-.330461510	-.091642460	-.185664180	-.284290230	-.392144470	0.000000000	0	8
8	1	.509488630	4.003000000	1000.000500000	0.000000000	1000.000500000	-0.000000000	0	8
9	3	-.798015820	-0.000000000	-0.000000000	-0.000000000	-0.000000000	-0.000000000	-0	9
9	1	.278760380	1.000000000	0.000000000	0.000000000	45.000500000	-0.000000000	0	9
10	3	-1.999897380	-.028144570	.032156350	.127717260	.202484510	.133087330	0	10
10	10	.180045460	4.003000000	1000.000500000	0.000000000	1000.000500000	-0.000000000	0	10
11	3	-.544563020	.041250000	.082500000	.123750000	.165000000	.200000000	0	11
11	1	-.001580820	1.000000000	0.000000000	0.000000000	45.000500000	-0.000000000	0	11
12	3	-.998507480	-0.000000000	-0.000000000	-0.000000000	-0.000000000	-0.000000000	-0	12
12	2	-.002333050	1.000000000	0.000000000	0.000000000	45.000500000	-0.000000000	2	12

```
DELO,2,3,4,M
 -0       .000000001    100.000000000     -0.000000000      1.000000000       .000100000
                CRIT           CNORM            DENOM             CONF            CONFM
 -0       .005000000       .000000000     -0.000000000     50.800000000     -0.000000000

APM,AFM,SSF
  0       .250000000       .984800000      1.000000000

W
     1.0000000     1.0000000     1.0000000     1.0000000     1.0000000     1.0000000     1.0000000     1.0000000     1.0000000
     1.0000000     1.0000000     0.0000000      .0287000     -.1622000      .3097000     -.5057000     1.8131000     -.7830000
     5.6117000     -.9395000    47.2100000     -.8926000     0.0000000     0.0000000     0.0000000     0.0000000     0.0000000
     0.0000000     0.0000000     0.0000000     0.0000000     0.0000000     0.0000000     0.0000000

U
     0.0000000     0.0000000     0.0000000     0.0000000     0.0000000     0.0000000     0.0000000     0.0000000     0.0000000
     0.0000000     0.0000000     0.0000000     0.0000000     0.0000000     0.0000000     0.0000000     0.0000000     0.0000000
     0.0000000     0.0000000     0.0000000     0.0000000     0.0000000     0.0000000     0.0000000     0.0000000     0.0000000
     0.0000000     0.0000000     0.0000000     0.0000000     0.0000000     0.0000000     0.0000000     0.0000000     0.0000000
     0.0000000

D
     0.0000000     0.0000000     0.0000000     0.0000000     0.0000000     0.0000000     0.0000000     0.0000000     0.0000000
     0.0000000     0.0000000     0.0000000     0.0000000     0.0000000     0.0000000     0.0000000     0.0000000     0.0000000
     0.0000000     0.0000000     0.0000000     0.0000000     0.0000000     0.0000000     0.0000000     0.0000000     0.0000000
     0.0000000     0.0000000     0.0000000     0.0000000     0.0000000     0.0000000     0.0000000     0.0000000     0.0000000
     0.0000000

W
    -1.0000000    -1.0000000    -1.0000000    -1.0000000    -0.0000000    -0.0000000    -0.0000000    -1.0000000    -1.0000000
    -0.0000000    -0.0000000

BOUND1
    -0.0000000    -0.0000000     .0500000    -0.0000000    -0.0000000     .0100000     .0100000     .0100000     .0100000
     .0100000      .2000000

BOUND2
    -0.0000000     2.0000000     1.0000000     1.0000000     1.0000000     .3000000     .6000000     1.0000000     .2000000
     1.0000000     .5300000

W
    -1.0000000    -1.0000000    -1.0000000    -1.0000000    -0.0000000    -0.0000000    -0.0000000    -1.0000000    -1.0000000
    -0.0000000    -0.0000000    -0.0000000    -0.0000000    -0.0000000    -0.0000000    -0.0000000    -1.0000000    -1.0000000
    -0.0000000

BOUND1
    -0.0000000    -0.0000000     .0500000    -0.0000000    -0.0000000     .0100000     .0100000     .0100000     .0100000
     .0100000      .2000000    -.0090600     -.0636600     -.2444200     -.6883100    -5.4988000    0.0000000    0.0000000
    -0.0000000

BOUND2
    -0.0000000     2.0000000     1.0000000     1.0000000     1.0000000     .3000000     .6000000     1.0000000     .2000000
     1.0000000     .5300000     -.0061800     -.0308300     -.2402600     -.6832400    -5.4884000    0.0000000    0.0000000
     8.5000000
```

```
A
  -0.0000   .9000   .6000-0.0000
  -0.0000-0.0000-0.0000-0.0000
   .9000  0.0000 -.9000-0.0000
  -0.0000-0.0000-0.0000   .9000
   .9000  0.0000 -.9000-0.0000
  -0.0000-0.0000-0.0000   .9000
   .9000  0.0000 -.9000-0.0000
  -0.0000-0.0000-0.0000   .7000
   .9000  0.0000 -.9000-0.0000
  -0.0000-0.0000-0.0000   .6000
  DW2
    1.0000000     .7000000     .7000000     .7000000     .7000000     .5000000     .7000000     .7000000     .7000000
     .7000000     .7000000     .5000000    -0.0000000    -0.0000000    -0.0000000    -0.0000000    -0.0000000    -0.0000000
    -0.0000000   -0.0000000   -0.0000000   -0.0000000   -0.0000000   -0.0000000   -0.0000000


F
    0.0000000     .0442700     .1325000     .3473000     .6527000    1.0000000
MAX. NUMBER VARIABLES= 40NF=149
  DW1
     .0410333     .0000000    -0.0000000   -0.0000000   -0.0000000   -0.0000000   -0.0000000   -0.0000000   -0.0000000
    0.0000000
  DW
     .0166667     .0001389     .0008333     .0001243   16.0000000     .5000000     .0166667     .0000000     .0000000
     .0000000
     .0333333     .0005556     .0033333     .0004972     .0029833     .5000000     .0333333    0.0000000    0.0000000
    0.0000000
     .0333333     .0005556     .0033333     .0004972     .0029833     .5000000     .0333333    0.0000000    0.0000000
    0.0000000
     .0333333     .0005556     .0033333     .0004972     .0029833     .5000000     .0333333    0.0000000    0.0000000
    0.0000000
     .0333333     .0005556     .0033333     .0004972     .0029833     .5000000     .0333333     .0000000     .0000000
     .0000000
     .0333333     .0005556     .0033333     .0004972     .0029833     .5000000     .0333333     .0000000     .0000000
     .0000000

   NS   CV    X  ASC    N    V
    1    0   10    0    0    0
    2    1   11   20    0    0
    3    2   12    0    0    0
    4    3   13   25    0    0
    5    4   14    0    0    0
    6    5   15    0    0    0
    7    6   16    0    0    0
    8    7   17    0    0    0
    9    0    0    0    0    0
   10    8   18   30    0    0
   11    9   19    0    0    0
   12    0    0    0    0    0

      X01* 1       X02* 2       X03* 3       X04* 4       X05  5       X06  6       X07  7       X08* 8       X09* 9
      X10 10       X11 11     THIRD 12     THIRD 13     THIRD 14     THIRD 15     THIRD 16     AXGP*17     X02&X02*18

  Y02/HQ1 19
B VIOL. ATTEMPTED        6
B VIOL. ATTEMPTED        7
B VIOL. ATTEMPTED       11
B VIOL. ATTEMPTED       12
B VIOL. ATTEMPTED       14
B VIOL. ATTEMPTED       15
```

	AT	CV	HK	H	HHK	KLC	D	N	
1	0.0000000	.0030000	.0001243	1.0000000	0.0000000	0.0000000	-9.5537451	1.0000000 0.0000000	1
2	-1.3356585	.4447747	.4447747	1.0000000	.4447747	-9.5537451	.8408622	4.0030000 1000.0000000	2
3	-1.3356585	0.0000000	-1.3356585	.7194342	-.9609185	-9.2617684	0.0000000	4.0030000 1000.0000000	3
4	-.0517856	.5942588	.3757445	.7194342	.2703235	-9.2617684	3.4917666	1.0000000 0.0000000	4
5	-1.5569667	.9305947	.4494402	.5386110	.2420734	-.2906454	.2405148	4.0030000 1000.0000000	5
6	-1.5569667	0.0000000	-1.5569667	.4450627	-.6929474	.0000000	.0019866	4.0030000 1000.0000000	6
7	-1.5334825	.0176016	-1.5158823	.4442900	-.6778866	.0025098	.0054244	1.0000000 0.0000000	7
8	-.3153004	-.9304615	-1.9391376	.4359719	-.8454095	.0305140	.5094886	4.0030000 1000.0000000	8
9	-1.2639114	-.7980158	-1.5797991	.3958415	-.6253501	.7680261	.2787604	1.0000000 0.0000000	9
10	-1.0025831	-1.9993974	-1.3504331	.0435131	-.0537833	16.9521717	.1800455	4.0030000 1000.0000000	10
11	-1.0000000	-.5445630	-.9991391	-.0015808	.0015795	-636.9250607	-.0015808	1.0000000 0.0000000	11

	B	F	C	P	E				
2	.0082447	-.0602309	.4500119	.1668322	-4.4332483	0.0000000	0.0000000	0.0000000	0.0000000 2
3	0.0000000	0.0000000	0.0000000	0.0000000	0.0000000	0.0000000	0.0000000	0.0000000	0.0000000 3
4	-.0016032	.0089179	-.0496058	-.2229027	1.5158276	0.0000000	0.0000000	0.0000000	0.0000000 4
5	.0024086	.0095788	.0371691	.3490583	1.4986909	0.0000000	0.0000000	0.0000000	0.0000000 5
6	0.0000000	0.0000000	0.0000000	0.0000000	0.0000000	0.0000000	0.0000000	0.0000000	0.0000000 6
7	.7426838	-1.0938040	1.6109240	-.0066023	-2.3628002	0.0000000	0.0000000	0.0000000	0.0000000 7
8	-1.2403403	1.4294758	-1.6477098	-.3490102	2.3009098	0.0000000	0.0000000	0.0000000	0.0000000 8
9	.6146068	-.5107864	.4245035	.2993307	-.6015629	0.0000000	0.0000000	0.0000000	0.0000000 9
10	-.0477007	.0028368	-.0001687	-.7501499	.0446212	0.0000000	0.0000000	0.0000000	0.0000000 10
11	-.0007397	.0028064	-.0106474	.2042622	-.7345787	0.0000000	0.0000000	0.0000000	0.0000000 11
11	.0771200	-.2108057	.8044767	-.3091808	-2.7721406				
1	.0775030	-.2091390	.7968232	-.3092579	-2.7431194				

COLOR LONG,LAT,SEC,PRIM,*1000 .000417 -.002622 -.610608 1.005699

TOTAL LENGTH= 5.5472682

```
FOCUS
 -.0023331 -.0070227 -.0221192 -.2410104 -.6873022-5.4975424 0.0000000
 0.0000000 0.0000000 0.0000000 0.0000000 0.0000000 0.0000000 0.0000000

DOLD=  2.058539E-09
  2  .87712 2.01154 -.03626
  3 0.00000 0.00000  .63492
  4  .63492 1.40358 2.86687
  5  .01203  .16031  .22644
  6 0.00000  .12326  .00212
  7  .00013  .12293 -.00183
  8 -.00712  .12348  .50445
  9 -.01216  .17413  .30575
 10  .01483  .19422  .15695
 11 -.00827  .17404  .00669

DOLD=  1.645689E-09  3.597970E-06
 -61 -130  -97 -151   24  156   24    8
  36 -312   90  231 -178  139  -21 -115   -0  -23   40 -118
 142 -102  -89
  45 -329   57  146  -99  172   -7  -73    7 -160   -5 -150
  46  -44 -128
   5    7   19  106  -21  -55   -6  -58   -4  122   -6  -95
  20 -178 -158
  -4    7   58  169   28  -37    7  -32  -35 -103 -108 -109
  11 -119  -89
 -46  153   10   12  -48 -125    2  -57  -55   34 -259  -88
 150 -105   44
 109 -119  -64   10  -41
  43  -47  107   15 -106   96  -44
  20  -37   94    3  -73   68  -42
-156  -71   96  -26   88   35  -28
-249 -113   92  -43  136   12   21
-204 -124   67  -55  111  -83   24
   0    0    0    0    0    0    0
 0.00000 0.00000 0.00000 0.00000 0.00000 -.00000 -.00000 0.00000 0.00000
 0.00000 -.00002  .00000 0.00000  .00000 -.00000 0.00000 0.00000 0.00000
 0.00000



 1 20   333.3333 0.
 1  6    -9.5537  1.0000000  0.0000000   .0270648

 2  3     2.2483 1.8007E-01 3.3949E-01 6.1551E-01 7.4265E-01 7.5959E-01
 2 10      .8409  4.0030000*00.0000000   .4433649

 3  3     0.0000 4.0446E-01
 3  7    0.0000  4.0030000*00.0000000   .4433649

 4  3     1.6828 1.4571E-01 3.4443E-01 6.0965E-01 8.0849E-01 1.0177E+00
 4 10    3.4918  1.0000000  0.0000000   .0270648

 5  3     1.0746 2.4500E-01
 5  1      .2405  4.0030000*00.0000000   .4433649

 6  3     0.0000 0.
 6  1      .0020  4.0030000*00.0000000   .4433649

 7  3    55.8129 0.
 7  1      .0054  1.0000000  0.0000000   .0270648

 8  3    -1.0747-9.1642E-02
 8  1      .5095  4.0030000*00.0000000   .4433649

 9  3    -1.2531 0.
 9  1      .2788  1.0000000  0.0000000   .0270648

10  3     -.5000-2.8145E-02 3.2156E-02 1.2772E-01 2.0248E-01 1.3309E-01
10 10      .1400  4.0030000*00.0000000   .4433649

11  3    -1.8363 4.1250E-02
11  1     -.0016  1.0000000  0.0000000   .0270648

12  3    -1.0015 0.
12  2     -.0023  1.0000000  0.0000000   .0270648

13  0     0.0000 0.
13  0     -.0000  0.0000000   .0014618  0.0000000

EFL,PP1,PP2       1.00000       6.21469      -1.00158
```

```
SURFACE  4 ONE SPACE EQUALS     .00641335
```

```
 HEIGHT      DEPTH       SLOPE
0.00000     0.00000     0.00000
 .02506      .00019      .01490
 .05013      .00075      .02979
 .07519      .00168      .04469
 .10026      .00299      .05960
 .12532      .00467      .07450
 .15038      .00672      .08941
 .17545      .00915      .10432
 .20051      .01195      .11923
 .22558      .01513      .13415
 .25064      .01868      .14906
 .27570      .02260      .16397
 .30077      .02689      .17885
 .32583      .03156      .19371
 .35090      .03661      .20855
 .37596      .04202      .22337
 .40102      .04780      .23817
 .42609      .05396      .25295
 .45115      .06048      .26771
 .47622      .06738      .28245
 .50128      .07464      .29717
 .52634      .08227      .31187
 .55141      .09027      .32654
 .57647      .09864      .34120
 .60154      .10738      .35589
 .62660      .11648      .37072
 .65166      .12596      .38571
 .67673      .13582      .40085
 .70179      .14606      .41614
 .72686      .15668      .43158
 .75192      .16769      .44717
 .77698      .17910      .46292
 .80205      .19090      .47881
 .82711      .20310      .49486
 .85218      .21571      .51106
 .87724      .22872      .52741
 .90230      .24215      .54391
 .92737      .25599      .56057
 .95243      .27025      .57737
 .97750      .28493      .59433
1.00256      .30004      .61144
1.02762      .31559      .62925
1.05269      .33159      .64811
1.07775      .34809      .66802
1.10282      .36509      .68900
1.12788      .38263      .71103
1.15294      .40074      .73411
1.17801      .41944      .75825
1.20307      .43876      .78345
1.22814      .45872      .80972
1.25320      .47941      .84307
1.27826      .50109      .88855
1.30333      .52405      .94616
1.32839      .54862     1.01590
1.35346      .57508     1.09778
1.37852      .60375     1.19178
1.40358      .63492     1.29792
```

HEIGHT	DEPTH	SLOPE
0.00000	0.00000	0.00000
.00347	-.00001	-.00655
.00694	-.00004	-.01234
.01040	-.00010	-.01735
.01387	-.00016	-.02160
.01734	-.00025	-.02507
.02081	-.00034	-.02778
.02428	-.00044	-.02973
.02775	-.00054	-.03090
.03121	-.00065	-.03130
.03468	-.00076	-.03094
.03815	-.00086	-.02981
.04162	-.00096	-.02791
.04509	-.00106	-.02524
.04855	-.00114	-.02243
.05202	-.00121	-.01847
.05549	-.00127	-.01503
.05896	-.00132	-.01061
.06243	-.00134	-.00570
.06590	-.00135	-.00032
.06936	-.00135	.00555
.07283	-.00132	.01191
.07630	-.00126	.01874
.07977	-.00119	.02606
.08324	-.00108	.03384
.08670	-.00095	.04179
.09017	-.00079	.04976
.09364	-.00061	.05774
.09711	-.00039	.06573
.10058	-.00015	.07375
.10405	.00012	.08178
.10751	.00042	.08983
.11098	.00074	.09789
.11445	.00110	.10597
.11792	.00148	.11407
.12139	.00189	.12218
.12486	.00233	.13029
.12832	.00279	.13841
.13179	.00328	.14654
.13526	.00380	.15300
.13873	.00435	.15994
.14220	.00491	.16658
.14566	.00550	.17291
.14913	.00611	.17892
.15260	.00674	.18463
.15607	.00739	.19002
.15954	.00806	.19511
.16301	.00874	.19988
.16647	.00944	.20417
.16994	.01016	.20653
.17341	.01087	.20666
.17688	.01159	.20454
.18035	.01229	.20017
.18381	.01297	.19357
.18728	.01363	.18472
.19075	.01425	.17363
.19422	.01483	.16030

UPDATED VT PUNCHED

1.0000	1.0000	1.0000	1.0000	1.0000	1.0000	1.0000	1.0000	1.0000
1.0000	1.0000	0.0000	.0287	-.1822	.3077	-.5057	1.5131	-.7830
5.6117	-.9395	47.2160	-.3926	0.0000	0.0000	0.0000	0.0000	0.0000
0.0000	0.0000	0.0000	0.0000	0.0000	0.0000	0.0000		

.01362795	.24750000	0.00000000	.99661113	-.08225724	0.00000000
.01103821	.22275000	0.00000000	.99725151	-.07409065	0.00000000
.00872121	.19800000	0.00000000	.99782570	-.06590509	0.00000000
.00667691	.17325000	0.00000000	.99833381	-.05770271	0.00000000
.00490530	.14850000	0.00000000	.99877483	-.04948570	0.00000000
.00340632	.12375000	0.00000000	.99914850	-.04125624	0.00000000
.00217996	.09900000	0.00000000	.99945481	-.03301654	0.00000000
.00122618	.07425000	0.00000000	.99969321	-.02476882	0.00000000
.00054495	.04950000	0.00000000	.99986381	-.01651533	0.00000000
.00013623	.02475000	0.00000000	.99996570	-.00825830	0.00000000
.00000000	-.00000000	0.00000000	1.00000000	.00000000	0.00000000
.00013623	-.02475000	0.00000000	.99996570	.00825830	0.00000000
.00054495	-.04950000	0.00000000	.99986381	.01651533	0.00000000
.00122618	-.07425000	0.00000000	.99969321	.02476882	0.00000000
.00217996	-.09900000	0.00000000	.99945481	.03301654	0.00000000
.00340632	-.12375000	0.00000000	.99914850	.04125624	0.00000000
.00490530	-.14850000	0.00000000	.99877483	.04948570	0.00000000
.00667691	-.17325000	0.00000000	.99833381	.05770271	0.00000000
.00872121	-.19800000	0.00000000	.99782570	.06590509	0.00000000
.01103821	-.22275000	0.00000000	.99725151	.07409065	0.00000000
.01362795	-.24750000	0.00000000	.99661113	.08225724	0.00000000
.00013623	-.00000000	.02475000	.99996570	.00000000	-.00825830
.00054495	-.00000000	.04950000	.99986381	.00000000	-.01651533
.00122618	-.00000000	.07425000	.99969321	.00000000	-.02476882
.00217996	-.00000000	.09900000	.99945481	.00000000	-.03301654
.00340632	-.00000000	.12375000	.99914850	.00000000	-.04125624
.00490530	-.00000000	.14850000	.99877483	.00000000	-.04948570
.00667691	-.00000000	.17325000	.99833381	.00000000	-.05770271
.00872121	-.00000000	.19800000	.99782570	.00000000	-.06590509
.01103821	-.00000000	.22275000	.99725151	.00000000	-.07409065
.01362796	-.00000000	.24750000	.99661113	.00000000	-.08225724
.01335535	.17325000	.17325000	.99667846	-.05758492	-.05758492
.01158341	.14850000	.17325000	.99711656	-.04938548	-.05761640
.01008414	.12375000	.17325000	.99743786	-.04117352	-.05764293
.00885750	.09900000	.17325000	.99772207	-.03295117	-.05766455
.00790348	.07425000	.17325000	.99802874	-.02472056	-.05768130
.00790348	-.07425000	.17325000	.99802874	.02472056	-.05768130
.00885750	-.09900000	.17325000	.99772207	.03295117	-.05766455
.01008414	-.12375000	.17325000	.99743786	.04117352	-.05764293
.01158341	-.14850000	.17325000	.99711656	.04938548	-.05761640
.01335535	-.17325000	.17325000	.99667846	.05758492	-.05758492

SAG FANY
SAG FANZ
MP FAN Y
Y,Z MICRONS, PL MICRONSX1GO.
SINE(ANGLE)= 0.00000

.00724896	-.18051810	0.00000000	.99747874	.07096597	0.00000000
.00900342	-.20117749	0.00000000	.99696907	.07779390	0.00000000
.01094707	-.22182862	0.00000000	.99641365	.08461586	0.00000000
.01307972	-.24247151	0.00000000	.99581282	.09141364	0.00000000
.01540115	-.26310616	0.00000000	.99516699	.09819705	0.00000000
.01791116	-.28373258	0.00000000	.99447636	.10495889	0.00000000
.02060954	-.30435078	0.00000000	.99374197	.11170001	0.00000000
.02349609	-.32496077	0.00000000	.99296368	.11841927	0.00000000
.02657059	-.34556255	0.00000000	.99214218	.12511554	0.00000000
.02983285	-.36615615	0.00000000	.99127796	.13178773	0.00000000
.03328265	-.38674155	0.00000000	.99037155	.13843476	0.00000000
.03691979	-.40731879	0.00000000	.98942350	.14505561	0.00000000
.04074409	-.42788785	0.00000000	.98843415	.15165070	0.00000000
.04475539	-.44844876	0.00000000	.98740390	.15821990	0.00000000
.04895357	-.46900151	0.00000000	.98633332	.16476220	0.00000000
.05333848	-.48954611	0.00000000	.98522298	.17127661	0.00000000
.05790999	-.51008257	0.00000000	.98407348	.17776215	0.00000000
.06266796	-.53061089	0.00000000	.98288543	.18421791	0.00000000
.06761226	-.55113108	0.00000000	.98165944	.19064296	0.00000000
.07274274	-.57164315	0.00000000	.98039617	.19703643	0.00000000
.07805928	-.59214710	0.00000000	.97909626	.20339745	0.00000000
.03340107	-.38673639	.02315211	.99034302	.13842835	-.00763506
.03375634	-.38672088	.04630422	.99025744	.13840913	-.01526843
.03434847	-.38669504	.06945633	.99011486	.13837709	-.02289843
.03517746	-.38665887	.09260844	.98991541	.13833226	-.03052336
.03624331	-.38661236	.11576055	.98965921	.13827464	-.03814153
.03754604	-.38655551	.13891266	.98934644	.13820436	-.04575132
.03908566	-.38648832	.16206477	.98897728	.13812170	-.05335115
.04086220	-.38641079	.18521688	.98855196	.13802678	-.06093948
.04287568	-.38632293	.20836899	.98807078	.13791977	-.06851479
.04512613	-.38622472	.23152110	.98753403	.13780078	-.07607557
.01889706	-.24221755	.16206477	.99438356	.09118661	-.05372471
.02121643	-.26285239	.16206477	.99374196	.09795558	-.05368064
.02372438	-.28347890	.16206477	.99305604	.10470510	-.05363342
.02642071	-.30409719	.16206477	.99232622	.11143400	-.05358307
.02930521	-.32470726	.16206477	.99155295	.11814115	-.05352961
.03055269	-.44819577	.16206477	.98602680	.15788031	-.05315037
.05474911	-.46874860	.16206477	.98496233	.16441366	-.05307877
.05913233	-.48929328	.16206477	.98382831	.17091902	-.05300479
.06370220	-.50982981	.16206477	.98271534	.17739545	-.05292842
.06845859	-.53035820	.16206477	.98153401	.18384206	-.05284967

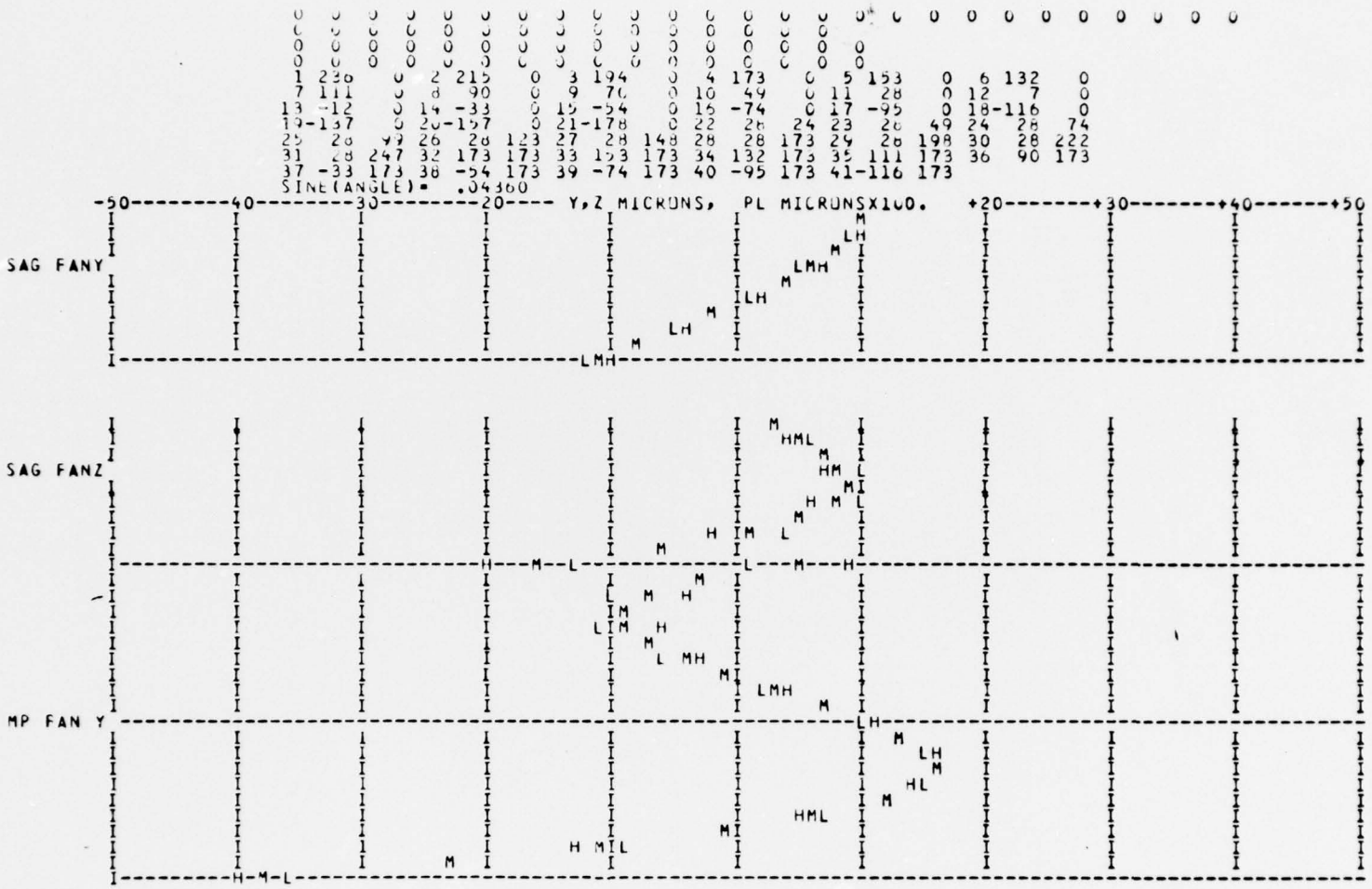

.14484004	-.80628136	0.00000000	.95763344	.28808832	0.00000000
.14907249	-.81795715	0.00000000	.95659194	.29143073	0.00000000
.15336314	-.82962528	0.00000000	.95557271	.29475548	0.00000000
.15771184	-.84128576	0.00000000	.95456633	.29806257	0.00000000
.16211844	-.85293863	0.00000000	.95351297	.30135197	0.00000000
.16658280	-.86459389	0.00000000	.95247280	.30462365	0.00000000
.17110479	-.87622157	0.00000000	.95142597	.30787762	0.00000000
.17568425	-.88785169	0.00000000	.95037265	.31111386	0.00000000
.18032105	-.89947426	0.00000000	.94931300	.31433236	0.00000000
.18501504	-.91108930	0.00000000	.94824718	.31753312	0.00000000
.18976609	-.92269683	0.00000000	.94717536	.32071613	0.00000000
.19457405	-.93429688	0.00000000	.94609769	.32388141	0.00000000
.19943878	-.94588945	0.00000000	.94501432	.32702894	0.00000000
.20436015	-.95747456	0.00000000	.94392542	.33015875	0.00000000
.20933802	-.96905224	0.00000000	.94283114	.33327083	0.00000000
.21437224	-.98062251	0.00000000	.94173162	.33636521	0.00000000
.21946268	-.99218537	0.00000000	.94062703	.33944189	0.00000000
.22460921	-1.00374086	0.00000000	.93951750	.34250090	0.00000000
.22981169	-1.01528898	0.00000000	.93840319	.34554225	0.00000000
.23506998	-1.02682975	0.00000000	.93728425	.34856597	0.00000000
.24038394	-1.03836320	0.00000000	.93616082	.35157208	0.00000000
.18984357	-.92268664	.01912934	.94715981	.32070644	-.00597314
.19007600	-.92265605	.03825867	.94711316	.32067735	-.01194548
.19046338	-.92260506	.05738801	.94703544	.32062888	-.01791620
.19100571	-.92253368	.07651734	.94692669	.32056103	-.02388448
.19170300	-.92244191	.09564668	.94678695	.32047382	-.02984953
.19255525	-.92232975	.11477601	.94661631	.32036725	-.03581053
.19356245	-.92219719	.13390535	.94641483	.32024134	-.04176667
.19472460	-.92204424	.15303468	.94618262	.32009612	-.04771716
.19604172	-.92187089	.17216402	.94591979	.31993161	-.05366117
.19751379	-.92167715	.19129335	.94562646	.31974784	-.05959792
.16152526	-.84078383	.13390535	.95375355	.29761172	-.04220690
.16592974	-.85243702	.13390535	.95272479	.30089732	-.04214603
.17039167	-.86408260	.13390535	.95168921	.30416534	-.04208445
.17491119	-.87572061	.13390535	.95064698	.30741577	-.04202219
.17948817	-.88735105	.13390535	.94959827	.31064859	-.04195925
.20814881	-.95697593	.13390535	.94317874	.32967543	-.04156884
.21312408	-.96855396	.13390535	.94208907	.33278488	-.04150182
.21815509	-.98012456	.13390535	.94099417	.33587673	-.04143429
.22324352	-.99168777	.13390535	.93989418	.33895097	-.04136627
.22838741	-1.00324360	.13390535	.93878926	.34200763	-.04129776

```
 0   0   0   0   0   0   0   0   0   0   0   0   0   0   0   0   0   0   0   0   0   0   0   0   0   0
 0   0   0   0   0   0   0   0   0   0   0   0   0   0   0
 0   0   0   0   0   0   0   0   0   0   0   0   0   0   0   0
 0   0   0   0   0   0   0   0   0   0   0   0   0   0   0   0
 1 432   0   2 419   0   3 407   0   4 395   0   5 383   0   6 370   0
 7 358   0   8 346   0   9 334   0  10 321   0  11 309   0  12 297   0
13 285   0  14 273   0  15 260   0  16 248   0  17 236   0  18 224   0
19 211   0  20 199   0  21 187   0  22 309  24  23 309  49  24 309  74
25 309  99  26 309 123  27 309 148  28 309 173  29 309 198  30 309 222
31 309 247  32 395 173  33 383 173  34 370 173  35 358 173  36 346 173
37 273 173  38 260 173  39 248 173  40 236 173  41 224 173
SINE(ANGLE)=   .13049
```

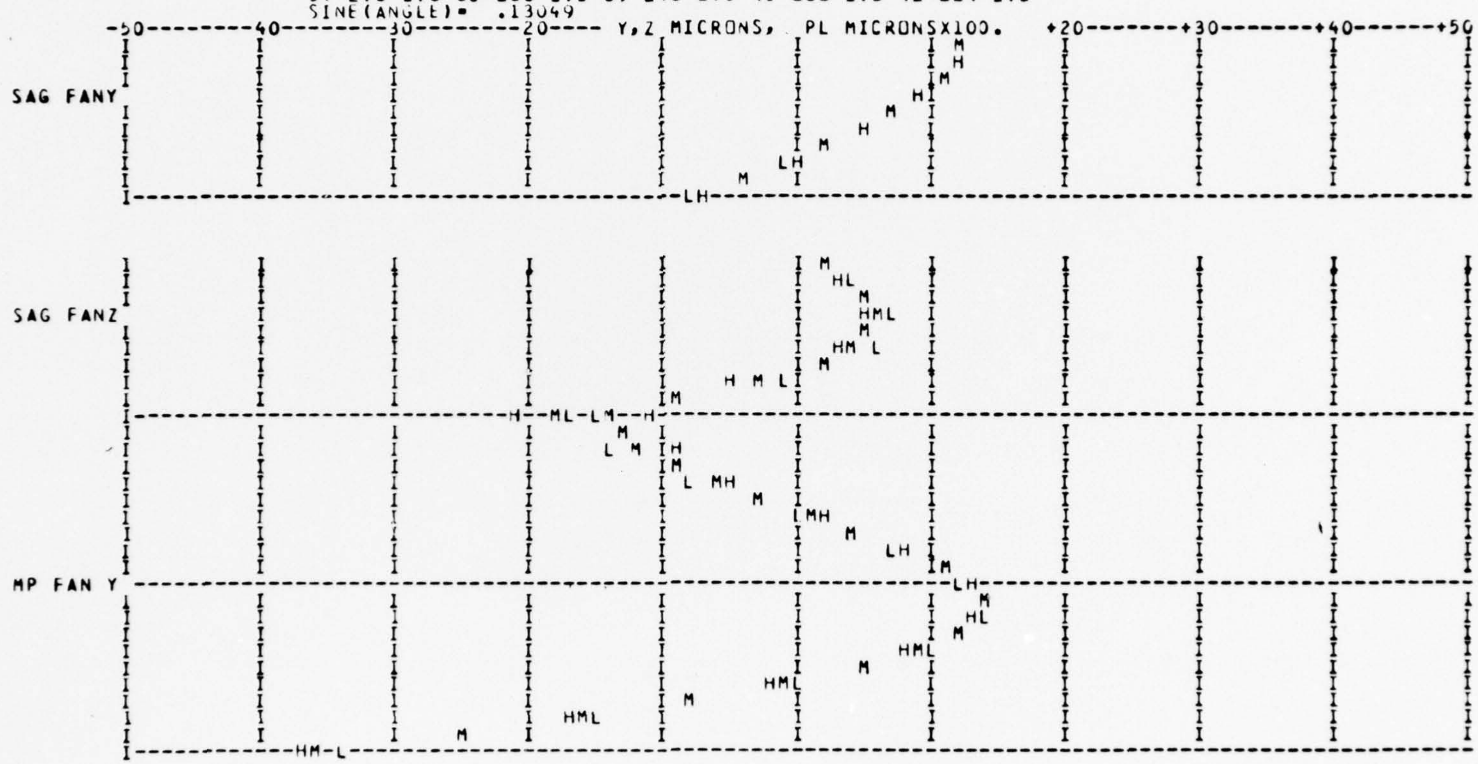

.46318605	-1.44185760	0.00000000	.87033741	.49245588	0.00000000
.46597903	-1.44621274	0.00000000	.86984381	.49332722	0.00000000
.46877861	-1.45056548	0.00000000	.86935101	.49419513	0.00000000
.47158476	-1.45491582	0.00000000	.86885899	.49505965	0.00000000
.47439746	-1.45926378	0.00000000	.86836777	.49592078	0.00000000
.47721670	-1.46360936	0.00000000	.86787735	.49677853	0.00000000
.48004245	-1.46795257	0.00000000	.86738772	.49763294	0.00000000
.48287471	-1.47229341	0.00000000	.86689890	.49848400	0.00000000
.48571345	-1.47663189	0.00000000	.86641088	.49933173	0.00000000
.48855865	-1.48096803	0.00000000	.86592367	.50017616	0.00000000
.49141029	-1.48530181	0.00000000	.86543727	.50101729	0.00000000
.49426836	-1.48963326	0.00000000	.86495169	.50185514	0.00000000
.49713283	-1.49396237	0.00000000	.86446691	.50268972	0.00000000
.50000370	-1.49828916	0.00000000	.86398296	.50352105	0.00000000
.50288094	-1.50261363	0.00000000	.86349982	.50434915	0.00000000
.50576453	-1.50693579	0.00000000	.86301750	.50517402	0.00000000
.50865445	-1.51125564	0.00000000	.86253601	.50599568	0.00000000
.51155070	-1.51557320	0.00000000	.86205534	.50681415	0.00000000
.51445324	-1.51988845	0.00000000	.86157550	.50762944	0.00000000
.51736207	-1.52420143	0.00000000	.86109649	.50844157	0.00000000
.52027716	-1.52851212	0.00000000	.86061831	.50925054	0.00000000
.49143771	-1.48529183	.01238127	.86543364	.50101160	-.00346416
.49151999	-1.48526188	.02476255	.86542273	.50099451	-.00692818
.49165712	-1.48521197	.03714382	.86540455	.50096605	-.01039191
.49184910	-1.48514210	.04952510	.86537910	.50092619	-.01385520
.49209593	-1.48505226	.06190637	.86534639	.50087495	-.01731791
.49239762	-1.48494245	.07428765	.86530642	.50081233	-.02077989
.49275416	-1.48481268	.08666892	.86525921	.50073833	-.02424101
.49316555	-1.48466295	.09905020	.86520476	.50065295	-.02770111
.49363180	-1.48449324	.11143147	.86514308	.50055620	-.03116005
.49415291	-1.48430358	.12381275	.86507418	.50044808	-.03461768
.47293487	-1.45442442	.08666892	.86867513	.49478128	-.02439291
.47574666	-1.45877270	.08666892	.86818475	.49564231	-.02437096
.47856503	-1.46311861	.08666892	.86769516	.49649996	-.02434937
.48138990	-1.46746214	.08666892	.86720637	.49735427	-.02432776
.48422125	-1.47180330	.08666892	.86671838	.49820525	-.02430611
.50134488	-1.49780101	.08666892	.86380732	.50324195	-.02417567
.50422122	-1.50212581	.08666892	.86332498	.50407001	-.02415384
.50710391	-1.50644830	.08666892	.86284346	.50489485	-.02413199
.50999293	-1.51076848	.08666892	.86236276	.50571649	-.02411012
.51288827	-1.51508636	.08666892	.86188288	.50653495	-.02408823

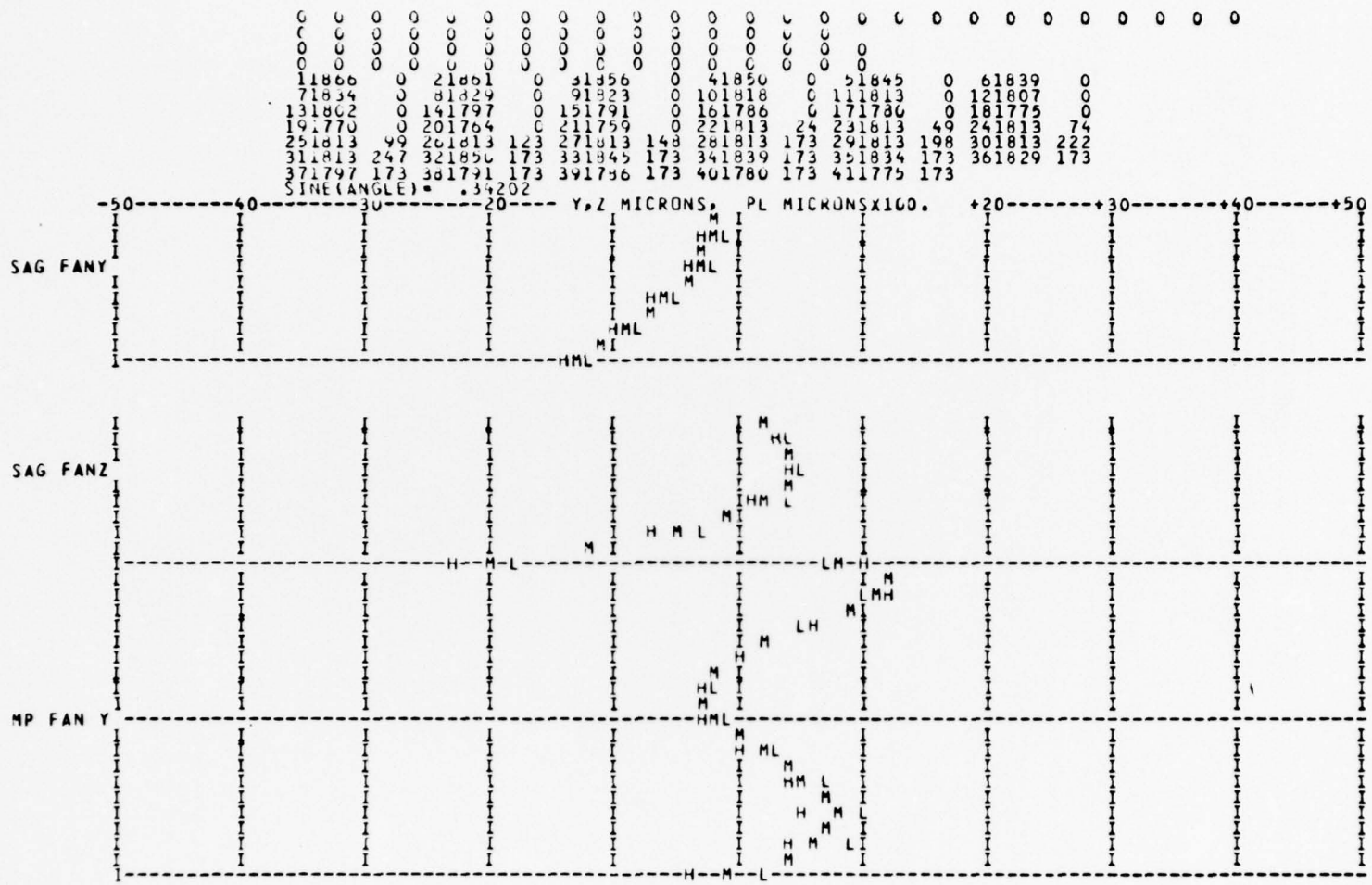
SAG FANY
SAG FANZ
MP FAN Y
Y,Z MICRONS, PL MICRONSX100.
-50
-40
-30
-20
+20
+30
+40
+50
SINE(ANGLE)= .34202

.71234023	-1.79200930	0.00000000	.78666666	.61737797	0.00000000
.71303955	-1.79292030	0.00000000	.78664679	.61740329	0.00000000
.71373891	-1.79383157	0.00000000	.78662708	.61742764	0.00000000
.71443830	-1.79474281	0.00000000	.78660733	.61745102	0.00000000
.71513773	-1.79565402	0.00000000	.78659173	.61747344	0.00000000
.71583719	-1.79656521	0.00000000	.78657439	.61749489	0.00000000
.71653669	-1.79747637	0.00000000	.78655681	.61751537	0.00000000
.71723621	-1.79838750	0.00000000	.78654349	.61753489	0.00000000
.71793576	-1.79929861	0.00000000	.78652893	.61755344	0.00000000
.71863534	-1.80020970	0.00000000	.78651512	.61757102	0.00000000
.71933494	-1.80112076	0.00000000	.78650207	.61758764	0.00000000
.72003457	-1.80203181	0.00000000	.78648977	.61760330	0.00000000
.72073422	-1.80294283	0.00000000	.78647824	.61761799	0.00000000
.72143389	-1.80385384	0.00000000	.78646746	.61763172	0.00000000
.72213358	-1.80476483	0.00000000	.78645744	.61764448	0.00000000
.72283329	-1.80567581	0.00000000	.78644817	.61765628	0.00000000
.72353302	-1.80658677	0.00000000	.78643966	.61766711	0.00000000
.72423276	-1.80749772	0.00000000	.78643191	.61767698	0.00000000
.72493252	-1.80840866	0.00000000	.78642491	.61768589	0.00000000
.72563229	-1.80931959	0.00000000	.78641867	.61769384	0.00000000
.72633207	-1.81023050	0.00000000	.78641319	.61770082	0.00000000
.71934350	-1.80111358	.00812553	.78650250	.61758365	-.00206175
.71936918	-1.80109203	.01625106	.78650382	.61757165	-.00412344
.71941198	-1.80105612	.02437660	.78650601	.61755165	-.00618501
.71947189	-1.80100585	.03250213	.78650908	.61752366	-.00824641
.71954893	-1.80094121	.04062766	.78651303	.61748765	-.01030757
.71964308	-1.80086221	.04875319	.78651788	.61744364	-.01236843
.71975434	-1.80076885	.05687873	.78652362	.61739161	-.01442894
.71988273	-1.80066113	.06500426	.78653027	.61733155	-.01648904
.72002822	-1.80053905	.07312979	.78653784	.61726346	-.01854866
.72019083	-1.80040261	.08125532	.78654633	.61718733	-.02060775
.71485907	-1.79438975	.05687873	.78662787	.61725768	-.01447599
.71555831	-1.79530112	.05687873	.78661070	.61727971	-.01446934
.71625758	-1.79621247	.05687873	.78659430	.61730077	-.01446267
.71695688	-1.79712379	.05687873	.78657865	.61732087	-.01445597
.71765620	-1.79803509	.05687873	.78656376	.61734000	-.01444925
.72185270	-1.80350243	.05687873	.78649030	.61743454	-.01440842
.72255219	-1.80441359	.05687873	.78648070	.61744692	-.01440154
.72325170	-1.80532474	.05687873	.78647186	.61745835	-.01439463
.72395122	-1.80623587	.05687873	.78646378	.61746880	-.01438770
.72465076	-1.80714699	.05687873	.78645645	.61747830	-.01438074

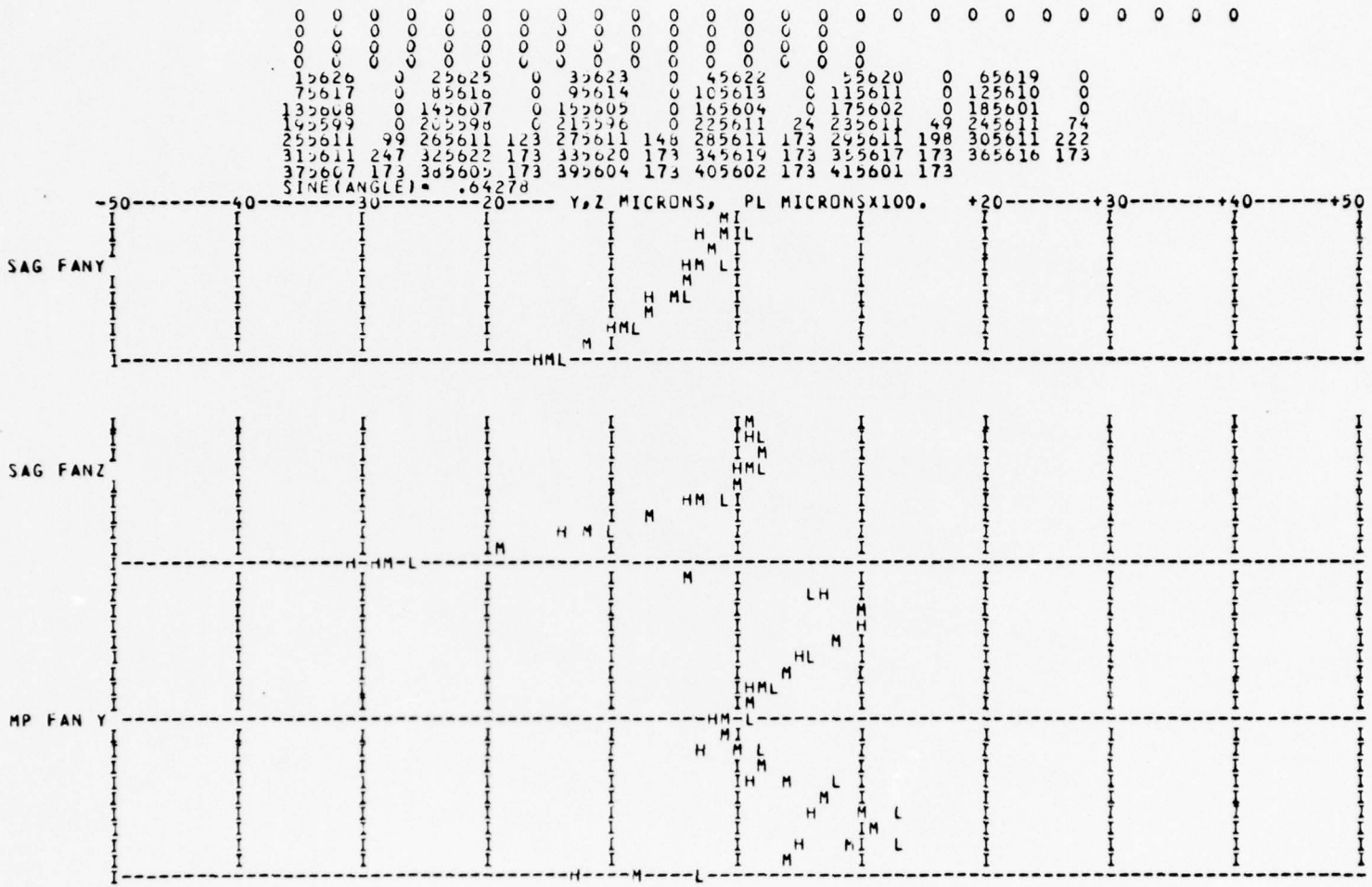

.86957484	-2.00094039	0.00000000	.69919280	.71493316	0.00000000
.86995072	-2.00146519	0.00000000	.69931052	.71481802	0.00000000
.87032656	-2.00199216	0.00000000	.69942862	.71470246	0.00000000
.87070238	-2.00251832	0.00000000	.69954713	.71458646	0.00000000
.87107817	-2.00304466	0.00000000	.69966603	.71447005	0.00000000
.87145392	-2.00357118	0.00000000	.69978533	.71435320	0.00000000
.87182964	-2.00409788	0.00000000	.69990502	.71423593	0.00000000
.87220533	-2.00462476	0.00000000	.70002512	.71411822	0.00000000
.87258098	-2.00515183	0.00000000	.70014561	.71400009	0.00000000
.87295660	-2.00567908	0.00000000	.70026650	.71388152	0.00000000
.87333219	-2.00620652	0.00000000	.70038780	.71376252	0.00000000
.87370775	-2.00673415	0.00000000	.70050949	.71364308	0.00000000
.87408328	-2.00726196	0.00000000	.70063159	.71352321	0.00000000
.87445877	-2.00778995	0.00000000	.70075409	.71340291	0.00000000
.87483423	-2.00831814	0.00000000	.70087699	.71328216	0.00000000
.87520965	-2.00884651	0.00000000	.70100030	.71316097	0.00000000
.87558504	-2.00937508	0.00000000	.70112402	.71303935	0.00000000
.87596040	-2.00990383	0.00000000	.70124813	.71291728	0.00000000
.87633572	-2.01043278	0.00000000	.70137266	.71279478	0.00000000
.87671101	-2.01096192	0.00000000	.70149759	.71267182	0.00000000
.87708627	-2.01149125	0.00000000	.70162293	.71254843	0.00000000
.87333339	-2.00619974	.00582498	.70038858	.71376045	-.00135809
.87333698	-2.00617941	.01164995	.70039095	.71375426	-.00271618
.87334295	-2.00614552	.01747493	.70039489	.71374393	-.00407424
.87335132	-2.00609808	.02329991	.70040041	.71372947	-.00543228
.87336208	-2.00603708	.02912488	.70040750	.71371089	-.00679029
.87337523	-2.00596253	.03494986	.70041617	.71368816	-.00814826
.87339077	-2.00587441	.04077484	.70042642	.71366131	-.00950617
.87340870	-2.00577274	.04659982	.70043824	.71363033	-.01086403
.87342903	-2.00565750	.05242479	.70045164	.71359521	-.01222181
.87345174	-2.00552871	.05824977	.70046663	.71355596	-.01357952
.87076110	-2.00218540	.04077484	.69933543	.71448527	-.00954047
.87113686	-2.00271185	.04077484	.69970438	.71436885	-.00953559
.87151259	-2.00323849	.04077484	.69982372	.71425200	-.00953070
.87188829	-2.00376530	.04077484	.69994346	.71413473	-.00952581
.87226396	-2.00429230	.04077484	.70006360	.71401702	-.00952091
.87451728	-2.00745819	.04077484	.70079285	.71330169	-.00949137
.87489272	-2.00798650	.04077484	.70091580	.71318094	-.00948642
.87526812	-2.00851499	.04077484	.70103915	.71305975	-.00948146
.87564349	-2.00904367	.04077484	.70116291	.71293813	-.00947650
.87601883	-2.00957254	.04077484	.70128707	.71281606	-.00947153

			YT,ZT MICRONS		PL*10,SCALE= 5.0866+01MM							
2	.2475	.5921	1.0304	1.5265	1.8102	2.0112	0.0000	0.0000	0.0000	0.0000	0.0000	0.0000
3	0.0000	0.0000	0.0000	0.0000	0.0000	0.0000	0.0000	0.0000	0.0000	0.0000	0.0000	0.0000
4	.1785	.4227	.7502	1.1170	1.3004	1.4036	0.0000	0.0000	0.0000	0.0000	0.0000	0.0000
5	.1363	.1432	.1578	.1582	.1595	.1611	0.0000	0.0000	0.0000	0.0000	0.0000	0.0000
6	.1134	.1152	.1221	.1153	.1125	.1193	0.0000	0.0000	0.0000	0.0000	0.0000	0.0000
7	.1132	.1150	.1218	.1149	.1121	.1193	0.0000	0.0000	0.0000	0.0000	0.0000	0.0000
8	.1135	.1155	.1232	.1160	.1130	.1152	0.0000	0.0000	0.0000	0.0000	0.0000	0.0000
9	.1058	.1084	.1216	.1497	.1661	.1762	0.0000	0.0000	0.0000	0.0000	0.0000	0.0000
10	.0105	.0417	.0893	.1458	.1784	.1943	0.0000	0.0000	0.0000	0.0000	0.0000	0.0000
11	.0017	.0383	.0802	.1233	.1556	.1778	0.0000	0.0000	0.0000	0.0000	0.0000	0.0000

*** LENS TOLERANCE DATA ***

SCALE 1.00MM/INCHES

	RMS PL ERROR MICRON/INCH 10-3		PERT .0011N FOR DISPL AND TIR					
	DISPL	TIR	DISPL	TIR	DISPL	TIR	DISPL	TIR
2	20.000000	.00000	I0.000000	.00000	I0.000000	.00000	I0.000000	.00000 I
0	00.00000	*.00000	I					
4	40.000000	.00000	I0.000000	.00000	I0.000000	.00000	I0.000000	.00000 I
0	00.00000	*.00000	I					
5	50.000000	.00000	I0.000000	.00000	I0.000000	.00000	I0.000000	.00000 I
0	00.00000	.00000	I					
6	60.000000	.00000	I0.000000	.00000	I0.000000	.00000	I0.000000	.00000 I
0	00.00000	*.00000	I					
7	70.000000	.00000	I0.000000	.00000	I0.000000	.00000	I0.000000	.00000 I
0	00.00000	*.00000	I					
8	80.000000	.00000	I0.000000	.00000	I0.000000	.00000	I0.000000	.00000 I
0	00.00000	-.00000	I					
9	90.000000	.00000	I0.000000	.00000	I0.000000	.00000	I0.000000	.00000 I
0	00.00000	*.00000	I					
10	100.000000	.00000	I0.000000	.00000	I0.000000	.00000	I0.000000	.00000 I
0	00.00000	-.00000	I					
11	110.000000	.00000	I0.000000	.00000	I0.000000	.00000	I0.000000	.00000 I
0	00.00000	-.00000	I					
2	40.000000	.00000	I0.000000	.00000	I0.000000	.00000	I0.000000	.00000 I
0	00.00000	-.00000	I					
5	70.000000	.00000	I0.000000	.00000	I0.000000	.00000	I0.000000	.00000 I
0	00.00000	-.00000	I					
8	90.000000	.00000	I0.000000	.00000	I0.000000	.00000	I0.000000	.00000 I
0	00.00000	*.30167	I					
10	110.000000	.00000	I0.000000	.00000	I0.000000	.00000	I0.000000	.00000 I
0	00.00000	.00000	I					

SEE UPDATE 10/ 1/71
TT 30 30 4 1 -1

NST	NWT	MT	NPASS MS	M	NHELD	NLOOP	NFT	NINC	NN4	M1	M2	M3	M4	M5	M6	M7	MOR		
34	29	24	33	28	23	32	27	22	31	26	21	30	25	20	9	16	19	18	7	6

TO MANY RAYS PER FIELD ANGLE FOR THIS VALUE OF NFT

DISTRIBUTION LIST

Chief of Naval Research
800 N. Quincy Street
Arlington, VA 22217
ATTN: Codes 221 10
455 1
421 1

Defense Documentation Center
Cameron Station
Alexandria, VA 23314 12

Director
Naval Research Laboratory
Washington, DC 20390
ATTN: Tech Info Division 1
Library, Code 2039 1

Office of Naval Research Branch Office
New York Area Office
715 Broadway (5th Floor)
New York, NY 10003 1

Director
Office of Naval Research Branch Office
1030 East Green Street
Pasadena, CA 91106 1

Office of Naval Research Branch Office
495 Summer Street
Boston, MA 02210 1

Director
Office of Naval Research Branch Office
536 Clark Street
Chicago, IL 60605 1

Director of Defense Research and Engineering
Washington, DC 20350
ATTN: ODDR&E/E&PS 1
ODDR&E/E&LS 1

Office of the Chief of Naval Operations
Department of the Navy
Washington, DC 20350
ATTN: OP 987 1
OP 986 1
OP 982 1
OP 596 1
OP 506 1

Headquarters
Department of the Navy
Naval Material Command
Washington, DC 20360
ATTN: MAT 08T231 1

Commandant, U.S. Marine Corps
Headquarters, U.S. Marine Corps
Washington, DC 20380
ATTN: RD-1 1

Commander
Naval Air Systems Co-mand
Washington, DC 20360
ATTN: AIR 5103F 1
5105 1
340D 1
340F 1
360E 1
PMA 247 1

Commander
Naval Sea Systems Command
Washington, DC 20360
ATTN: NSEA 0341 1
NSEA 653C 1

Commander
Naval Electronic Systems Command
Washington, DC 20360
ATTN: ELEX 320 1
330 1

Commanding Officer
U.S. Naval Air Development Center
Warminster, PA 18974
ATTN: Code 402 1
304 1
54P3 1
30P8 1

Naval Oceans Systems Center
271 Catalina Boulevard
San Diego, CA 92152
ATTN: Code 8235 1

Commander
Naval Weapons Center
China Lake, CA 93555
ATTN: Code 3925 1
Code 3175 1

Commander
Naval Veapons Center
Dahlgren, VA 22448
ATTN: Mr. K. Ferris 1

Commander
Naval Training Equipment
Orlando, FL 32813
ATTN: Code N-2224 1

Commander
Naval Air Test Center
Service Test Division
Aero Medical Branch
Patuxent River, MD 20670
ATTN: Mr. Fred Hoerner 1

Commander
Naval Avionics Facility
6000 E. 21st Street
Indianapolis, IN 46218
ATTN: Technical Library 1

Dean of Research Administration
Naval Postgraduate School
Monterey, CA 93940
ATTN: Dr. J. Powers 1

Commandant
U.S. Coast Guard Headquarters
400 7th Street, NW
Washington, DC 20591
ATTN: GDST/62 TRPT 1

Director
HQS Army Research Institute
1300 Wilson Boulevard
Arlington, VA 22209

Headquarters
U.S. Army
Washington, DC 20350
ATTN: DAMA-WSA 1

Commanding General
U.S. Army Electronics Command
Fort Monmouth, NJ 07703
ATTN: DRSEL-VL-E 1
DDRSEL-TL-BD 1
DRSEL-VL-I 1

Commanding General
U.S. Army Material Command
Washington, DC 20315
ATTN: DRCDR-HA 1

Director
U.S. Army Night Vision Lab
Fort Belvoir, VA 22060
ATTN: DRSEL-NV-SD 1

Commander
U.S. Army Research and Development Command
P.O. Box 209
St. Louis, MO 63166
ATTN: DRSAV-EV 1

Commander
U.S. Army Aviation Center
Ft. Rucker, AL 36362
ATTN: ATQZ-D-SGA 1

Director
Human Engineering Labs
Aberdeen Proving Grounds, MD 21105
ATTN: DRXRD-HEL 1

Headquarters Aeronautical Systems Division
Air Force Systems Command
Wright-Patterson AFB, OH 45433
ATTN: ASD/YRD 1
ASD/SD 1

Air Force Avionics Laboratory
Air Force Systems Command
Wright-Patterson AFB, OH 45433
ATTN: AFAL/AA 1
AFAL/CC 1
AFAL/RWI 1

Air Force Flight Dynamics Laboratory
Air Force Systems Command
Wright-Patterson AFB, OH 45433
ATTN: AFFDL/FG 1

Aero Medical Research Laboratory
Wright-Patterson AFB, OH 45433
ATTN: AMRL/HE 1

Air Force Office of Scientific
Research
1400 Wilson Boulevard
Arlington, VA 22209 1

Federal Aviation Agency
NAFEC Bldg. 10
Atlantic City, NJ 03405
ATTN: Mr. D. Elliott 1

Defense Advanced Research
Project Agency
1400 Willson Blvd.
Arlington, VA 22209
ATTN: Dr. Strom 1

National Aeronautical and
Space Administration
Langley Research Center
Mail Stop 1574
Hampton, VA 23665
ATTN: Mr. R. Morris 1

National Aeronautical and
Space Administration
Ames Research Center
Mail Stop 200-10
Moffitt Field, CA 94035
ATTN: Mr. J. Dusterberry 1

Institute for Defense Analysis
400 Army-Navy Drive
Arlington, VA 22204
ATTN: Mr. L. Biberman 1
Dr. A. Schnitzler 1